A METHODOLOGY FOR DESIGNING TONPILZ-TYPE TRANSDUCERS

A THESIS SUBMITTED TO
THE GRADUATE SCHOOL OF NATURAL AND APPLIED SCIENCES
OF
MIDDLE EAST TECHNICAL UNIVERSITY

BY

KERİM ÇEPNİ

IN PARTIAL FULFILLMENT OF THE REQUIREMENTS
FOR
THE DEGREE OF MASTER OF SCIENCE
IN
MECHANICAL ENGINEERING

SEPTEMBER 2011

Approval of the thesis:

A METHODOLOGY FOR DESIGNING TONPILZ-TYPE TRANSDUCERS

submitted by **KERİM ÇEPNİ** in partial fulfillment of the requirements for the degree of **Master of Science in Mechanical Engineering Department, Middle East Technical University** by,

Prof. Dr. Canan Özgen
Dean, Graduate School of **Natural and Applied Sciences** _____

Prof. Dr. Suha Oral
Head of Department, **Mechanical Engineering** _____

Assoc. Prof. Dr. Derek K. Baker
Supervisor, **Mechanical Engineering Dept., METU** _____

Prof. Dr. Mehmet Çalışkan
Co-supervisor, **Mechanical Engineering Dept., METU** _____

Examining Committee Members:

Prof. Dr. S. Kemal İder
Mechanical Engineering Dept., METU _____

Assoc. Prof. Dr. Derek K. Baker
Mechanical Engineering Dept., METU _____

Prof. Dr. Mehmet Çalışkan
Mechanical Engineering Dept., METU _____

Assist. Prof. Dr. Yiğit Yazıcıoğlu
Mechanical Engineering Dept., METU _____

Assist. Prof. Dr. Barış Bayram
Electrical and Electronics Engineering Dept., METU _____

Date: _____

I hereby declare that all information in this document has been obtained and presented in accordance with academic rules and ethical conduct. I also declare that, as required by these rules and conduct, I have fully cited and referenced all material and results that are not original to this work.

Name, Last Name: KERİM ÇEPNİ

Signature :

ABSTRACT

A METHODOLOGY FOR DESIGNING TONPILZ-TYPE TRANSDUCERS

Çepni, Kerim
M.Sc., Department of Mechanical Engineering
Supervisor : Assoc. Prof. Dr. Derek K. Baker
Co-Supervisor : Prof. Dr. Mehmet Çalışkan

September 2011, 116 pages

Tonpilz-type transducers are the most commonly used projectors in underwater acoustic applications. However, no complete design approach is available in the literature for such transducers. The present study aims to fill this gap in the literature by providing a systematic design approach for the Tonpilz-type transducers. The proposed methodology involves the use of three different analytical models and a finite element model of such transducers. Each model provides a different level of accuracy that is tightly correlated with the model's complexity and computational cost. By using these models sequentially starting with the simplest and fastest model to yield an initial design and concluding with the most detailed and accurate model to yield an optimized final design the overall design time is reduced and greater flexibility is given to the designer. An overview of each of these four models is given. The constructed models are benchmarked against published experimental data. The overall design methodology is demonstrated by systematically applying the four models to design a Tonpilz-type transducer. Possible improvements to the proposed methodology are discussed.

Keywords: Tonpilz, transducer, underwater acoustics, piezoelectric, finite element method

ÖZ

TONPİLZ-TÜRÜ ELEKTROAKUSTİK ÇEVİRİCİLER İÇİN BİR TASARIM METODOLOJİSİ

Çepni, Kerim
Yüksek Lisans, Makina Mühendisliği Bölümü
Tez Yöneticisi : Doç. Dr. Derek K. Baker
Ortak Tez Yöneticisi : Prof. Dr. Mehmet Çalışkan

Eylül 2011, 116 sayfa

Tonpilz-türü elektroakustik çeviriciler, su altı akustiği uygulamarında en yaygın olarak kullanılan vericilerdir. Buna rağmen, bu türdeki elektroakustik çeviricilerin tasarımına yol gösteren tam bir kaynak literatürde bulunmamaktadır. Bu çalışma, Tonpilz-türü elektroakustik çeviriciler için sistematik bir tasarım yolu sunarak literatürdeki bu açığı doldurmayı hedeflemektedir. Önerilen metodoloji, bu türdeki elektroakustik çeviricilerin üç analitik ve bir sonlu elemanlar modelini içermektedir. Her bir model, karmaşıklıkları ve hesap yükleri ile yakından ilgili olarak farklı doğruluk seviyeleri sunmaktadır. Bu modellerin, ilk tasarıma ulaşmak için en basit ve en hızlısı ile başlanacak ve optimize edilmiş son tasarıma ulaşmak için en detaylı ve en doğrusu ile sonlandırılacak şekilde sırasıyla kullanımı, tasarım için gereken toplam süreyi düşürmekte ve tasarımcıya büyük esneklik kazandırmaktadır. Bu dört model, genel olarak tanıtılmış ve açıklanmıştır. Yayınlanmış deneysel verilerle karşılaştırarak kurulan modellerin performansları değerlendirilmiştir. Tüm tasarım metodolojisini gösterim amaçlı, dört modeli sistematik bir şekilde kullanarak bir Tonpilz-türü elektroakustik çevirici tasarlanmıştır. Önerilen metodoloji için olası geliştirme yolları açıklanmıştır.

Anahtar Kelimeler: Tonpilz, elektroakustik çevirici, su altı akustiği, piezoelektrik, sonlu elemanlar metodu

To Mom and Dad

ACKNOWLEDGMENTS

First of all, I would like to express my sincere gratitude and appreciation to my supervisor Assoc. Prof. Dr. Derek K. Baker for his farsighted guidance, steady support, and extremely motivating encouragements throughout my little adventurous career full of unexpected events. I feel so lucky to have the chance of conducting my studies under his supervision despite having a thesis subject out of his areas of interest.

I would also like to express my sincere graditute to my co-supervisor Prof. Dr. Mehmet Çalışkan for his instructive comments and precious advice. The present study would have serious deficiencies without being enlightened by his knowledge and experience.

I would like to give my special thanks to my friend Hüseyin Kağan Oğuz for our countless in-depth discussions about the subject and his kind helps whenever needed. I would like to thank Prof. Dr. Hayrettin Köymen as well for his concise and insightful comments that enhanced the present study remarkably.

Additionally, I would like to thank my ex-company Meteksan Defence for introducing me to the subject of this study and providing opportunities to study on it.

And last but not the least, I am wholeheartedly grateful to my mom and dad for their endless love, support, and patience throughout my entire life as well as the thesis period.

TABLE OF CONTENTS

LIST OF TABLES

TABLES

LIST OF FIGURES

FIGURES

LIST OF SYMBOLS

$[C^S]$ clamped capacitance matrix, C/V

$[K]$ stiffness matrix, N/m

$[K^E]$ short circuit stiffness matrix, N/m

$[M]$ mass matrix, kg

$[N]$ transduction coefficient matrix, N/V

$[R]$ resistance matrix, Ns/m

β_{ij} $1/\varepsilon_{ij}$ (subscripts indicate axes), mV/C

Δf bandwidth of frequency response around resonance, 1/s

Δf_{SL} bandwidth of source level, 1/s

Δt_c change in thickness of the piezoceramic ring due to applied electric field, m

η_{ea} electroacoustic efficiency, %

η_{em} electromechanical efficiency, %

η_{ma} mechanoacoustic efficiency, %

κ_{th} tail-to-head ratio, m

λ^* reference wavelength, m

λ_m Lamé's first parameter

λ	wavelength, m
μ	Lamé's second parameter
ω	angular frequency, rad/s
ω_n	angular natural frequency, rad/s
ρc	specific acoustic impedance, Ns/m^3
ρ	density, kg/m^3
ρ_h	density of head mass, kg/m^3
ρ_t	density of mass, kg/m^3
$\tan\delta$	loss tangent
θ	angle referring to half of beam width, $^\circ$
υ	Poisson's ratio
ε_0	vacuum permittivity, C/mV
ε_{ij}	absolute permittivity (subscripts indicate axes), C/mV
ξ	displacement, m
$\{F\}$	force vector, N
$\{x\}$	displacement vector, m
$\{Q\}$	charge vector, C
$\{V\}$	voltage vector, V
A	area, m^2

a radius of active surface of head mass, m

A_{cs} area of planar surfaces of piezoceramic stack, m^2

A_c area of planar surfaces of piezoceramic stack, m^2

A_h active surfae area of head mass, m^2

B susceptance, S

BW beam width, °

c_{ij} elastic stiffness coefficient (subscripts indicate axes), Pa

c speed of sound, m/s

C_0 clamped capacitance of piezoceramic stack, C/V

C_0 free capacitance of piezoceramic stack, C/V

D_f directivity factor

d_{ij} piezoelectric strain constant (subscripts indicate axes), C/N

D_i electric displacement (subscript indicate axis), C/m^2

DI directivity index, dB

E_c modulus of elasticity of piezoceramic stack, Pa

e_{ij} piezoelectric stress constant (subscripts indicate axes), C/m^2

E_i electric field (subscript indicate axis), V/m

$e_{r.reactance}$ absolute percent relative error of radiation reactance, %

$e_{r.resistance}$ absolute percent relative error of radiation resistance, %

E_Y modulus of elasticity, Pa

F force, N

f frequency, 1/s

f_1, f_2 frequencies of half response, 1/s

F_{bot} force applied from bottom surface, N

F_e excitation force, N

f_{flex} first flexural resonance frequency of head mass, 1/s

F_{ir} force applied from inner circumferential surface, N

f_n natural resonance frequency, 1/s

F_{or} force applied from outer circumferential surface, N

f_{SL} frequency regarding peak value of source level, 1/s

F_{top} force applied from top surface, N

G conductance, S

g_{ij} piezoelectric stress constant (subscripts indicate axes), Vm/N

h_{ij} piezoelectric strain constant (subscripts indicate axes), V/m

I current, A

K stiffness, N/m

k wavenumber, rad/m

k_{33} electromechanical coupling coefficient

K_{cs} stiffness of piezoceramic stack, N/m

K_c stiffness of piezoceramic ring, N/m

K_e effective stiffness, N/m

K_g stiffness of glue, N/m

k_r wavenumber in radial direction, rad/m

K_s stiffness of stud, N/m

k_z wavenumber in axial direction, rad/m

ka Helmholtz number

L length, m

l_{cs} length of piezoceramic stack, m

l_c length of piezoceramic stack, m

l_{se} effective length of stud, m

l_t length of tail mass, m

M mass, kg

M_{cs} mass of piezoceramic stack, kg

M_c mass of piezoceramic stack, kg

M_e effective mass, kg

M_h mass of head mass, kg

M_r radiation reactance, Ns/m

M_t mass of tail mass, kg

N transduction coefficient, N/V

n number of piezoceramic rings

n_c number of piezoceramic rings

n_m a constant related with mesh

p pressure, Pa

p_{ref} plane wave acoustic intensity, W/m^2

p_{ref} reference pressure, Pa

p_{rms} root-mean-square pressure, Pa

Q_m mechanical quality factor

R electrical impedance, V/A

r distance, m

R_0 electrical resistance due to cables etc., V/A

r_{c_i} inner radius of piezoceramic stack, m

r_{c_mean} mean radius of piezoceramic stack, m

r_{c_o} outer radius of piezoceramic stack, m

r_{cs_i} inner radius of piezoceramic stack, m

r_{cs_o} outer radius of piezoceramic stack, m

R_e effective resistance, Ns/m

r_{ht_m} average value of r_h and r_{ht}, m

r_{ht} radius of rear surface of head mass, m

R_h radiation resistance, Ns/m

r_h radius of active surface of head mass, m

r_i inner radius, m

R_m mechanical resistance, Ns/m

r_m radius of acoustic medium that provide free field boundary condition, m

r_o outer radius, m

R_r radiation resistance, Ns/m

r_s radius of stud, m

r_t radius of tail mass, m

s_{ij} elastic compliance coefficient (subscripts indicate axes), m^2/N

S_i strain (subscript indicate axis)

SL_p peak value of source level, dB

t time, s

t_c thickness of piezoceramic ring, m

t_{flex} thickness regarding first flexural resonance frequency of head mass, m

t_h thickness of head mass, m

T_i stress (subscript indicate axis), Pa

TVR transmitting voltage response, dB

u velocity, m/s

u^* complex conjugate of velocity, m/s

u_0 normal velocity, m/s

u_{bot} velocity observed at bottom surface, m/s

u_h velocity of head mass, m/s

u_{ir} velocity observed at inner circumferential surface, m/s

u_{or} velocity observed at outer circumferential surface, m/s

u_{rms} root-mean-square velocity of head mass, m/s

u_{top} velocity observed at top surface, m/s

u_t velocity of tail mass, m/s

V voltage, V

V_{drive} driving voltage, V

W_a radiated power, W

W_e input electrical power, W

x displacement, m

x_h displacement of head mass, m

x_m maximum distance between two connected node in mesh, m

X_r radiation reactance, Ns/m

x_t	displacement of tail mass, m
Y	admittance, S
y	a constant related with mesh
Z	mechanical impedance, Ns/m
z	impedance coefficient, Ns/m
Z_r	radiation impedance, Ns/m
1-D	one dimensional
2-D	two dimensional
3-D	three dimensional
dB	decibel
DDF	double-degree-of-freedom
DOF	degree-of-freedom
FE	finite element
H_1	struve function of first kind of order 1
J_0	bessel function of first kind of order 0
J_1	bessel function of first kind of order 1
PZT	lead zirconate titanate
SDF	single-degree-of-freedom
SL	source level, dB

SPL sound pressure level, dB

Y_0 bessel function of second kind of order 0

Y_1 bessel function of second kind of order 1

CHAPTER 1

INTRODUCTION

1.1 Brief History of Underwater Acoustics

Aristotle pointed out that sound could be heard in water like in air [1], which might be the first documented statement about underwater acoustics in the history. About 18 centuries later, in 1490, the archetypal engineer Leonardo da Vinci wrote an outstanding disclosure about the subject to his notebook as follows:

"If you cause your ship to stop, and place the head of a long tube in the water and place the outer extremity to your ear, you will hear ships at a great distance from you." [2]

Although there were no signs of the directivity of the sound nor its sensitivity due to mismatch between air and water media, the statement covered all the basics of modern passive sonar systems such as generation, propagation and reception of sound, and even self-noise [3].

The first handling of the theory of sound came from Sir Isaac Newton, in 1687, in his *Mathematical Principles of Natural Philosophy* [3]. Then in 1877, Lord Rayleigh (John William Strut) addressed deeper aspects, such as the description of sound waves mathematically, in his book *Theory of Sound* which is accepted as the starting point of modern acoustics [1].

Meanwhile, experiments were also being conducted. In 1743, Abbé J. A. Nollet proved Aristotle's determination and reported hearing a pistol shot, whistle, bell, and shouts with his head underwater [1]. Another experiment, also being the first quantitative one, was from Daniel Colladon and Charles Sturm who measured the speed of sound in fresh water with great accuracy in 1826 [4]. A representative sketch of the corresponding experiment is shown in Figure 1.1.

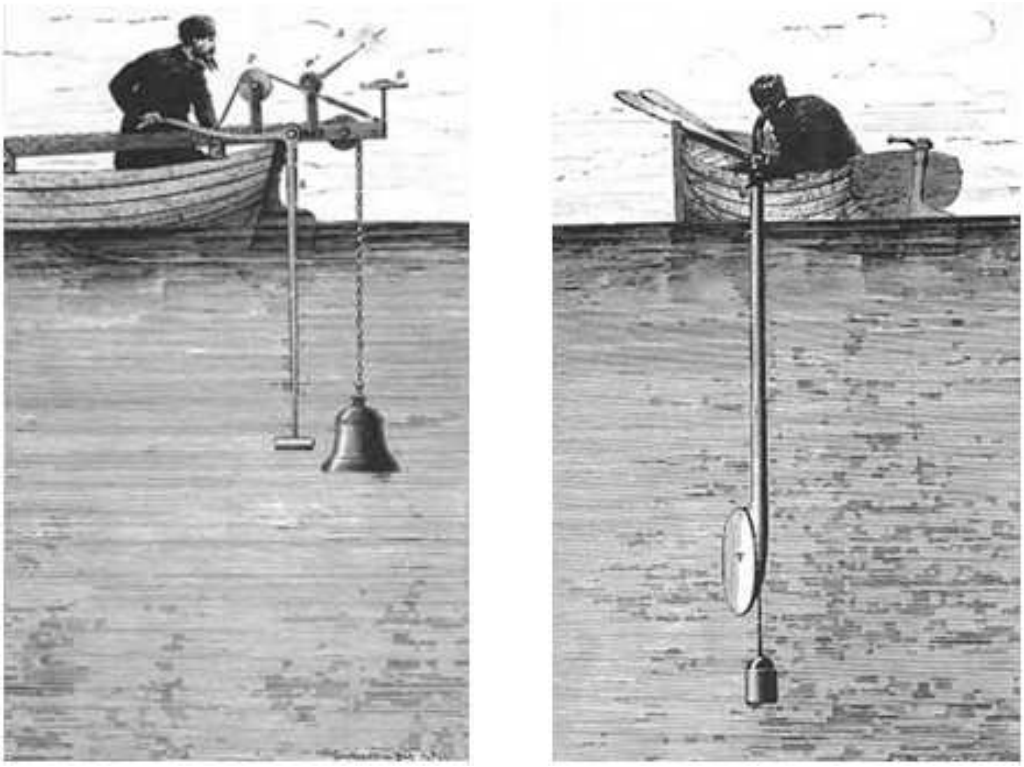

Figure 1.1: A representative sketch of the first quantitative experiment in underwater acoustics [5]

On the other hand, some inventions mainly related with transduction were having great impact on underwater acoustics. In the 1840's, magnetostriction was discovered by James Joule with the identification of the change in dimensions of a magnetic material under a magnetic field [6]. In 1880, it was Jacques and Pierre Curie brothers' time for another spectacular discovery, piezoelectricity [7].

In addition to these experimentations and inventions, practical applications were started to be demonstrated at about the end of 19^{th} century. The submarine bell was the first device which was basically used for measuring the distance from the vessels to the lightships using the idea behind the experiment of Colladon and Sturm [2, 3, 4]. Underwater acoustic devices working with Leonardo's basic idea, called SC devices, MB tubes and MV tubes were extensively used in World War I. However, self noise was a big problem with these devices which led to the development of towed systems such as the U-3, which was yet another passive listening device but was towed 300 to 500 ft behind instead of being mounted to ships and which were used through the end of World War I [3].

These passive sonar systems were pretty good at detecting sound sources such as submarines, but were not sufficient for accurate localization. A month after the tragedy of the Titanic in 1912, L.F. Richardson filed a patent about underwater echo ranging, which marked the beginning of active sonar history [2, 4]. In 1914, R. A. Fessenden designed and built the first high-power underwater electroacoustic transducer, a moving-coil transducer called a *Fessenden Oscillator*, which can both receive and transmit acoustic signals [3, 4]. It was used for submarine signaling and echo ranging while having other capabilities such as detecting an iceberg 2 miles away and the seafloor to a depth of 186 ft [1, 2, 4]. A few years later, in 1917, Langevin used the piezoelectric effect with a quartz-steel sandwich to develop the first underwater piezoelectric transducer. After further improvements, in 1918, echoes from a submarine could be heard at a distance of 1500 m for the first time [1, 2, 3, 4].

During the period between World War I and World War II, scientists were beginning to explore the fundamental concepts of underwater sound such as propagation and absorption. In 1919, H. Lichte published a scientific paper, which is the first paper on underwater sound, about the bending of sound ways due to temperature and salinity gradients in sea water [1, 2]. After the invention of bathythermographs in 1937, E. B. Stephenson discovered the “afternoon effect”, which was the main reason for transducer’s mysterious unreliability due to the temperature gradients in the water especially in the afternoons [1, 2, 3].

In the meantime, developing improved transducers were made possible by inventions in material science. For instance, after World War I, Rochella salt replaced quartz due to its stronger piezoelectric effect [2, 4]. In 1944, A. R. von Hippel discovered barium titanate ceramics which are superior to Rochelle salt. A decade later, even better piezoelectric properties were found in lead zirconate titanate ceramics, which are still being used extensively for underwater acoustic transducers [4].

In addition to the improvements in material science and a better understanding of sound behavior under water, developments in electronics in various subjects such as amplifying, processing and displaying sonar information led to the development of various underwater acoustic systems during World War II and afterwards. Acoustic homing torpedoes, acoustic mines, sonobuoys, scanning sonar sets, and wake detectors are examples of such systems that are still being used and developed today.

1.2 Overview of Sonar Applications and Transducer Types

When compared with the other radiation forms, acoustic radiation is best suited for underwater use since acoustic waves provide relatively negligible levels of attenuation in water. Therefore, underwater applications regarding exploration of the seas are heavily dominated with the acoustical phenomena. Hence, the engineering science of sonar is constituted by the use of acoustical phenomena within underwater applications [2].

The term *sonar* is actually an acronym for "SOund Navigation And Ranging" and involves two types which are named as *active sonar* and *passive sonar* [4]. Active sonar refers to emitting acoustic signals and receiving their echoes reflected back from the insonified objects whereas passive sonar refers to only listening to the water and sensing the acoustic waves generated by the objects inside the water. In both types, acoustic signals are used mainly for detecting and locating objects in the water. Due to their characteristic functions, projectors which are used for emitting the acoustic signals have a leading role in active sonar systems whereas hydrophones which listen to the medium have the same importance in passive sonar systems. Although most active sonar systems use the same transducers as both projectors and hydrophones due to their reciprocal transduction mechanisms, transducers which can only work as hydrophones are more common in passive sonar systems due to their specialized structures for reception [4]. Active sonar systems look superior to passive ones when comparing their capabilities. However, passive sonar systems also have advantages when operational requirements are considered. For instance, passive sonar systems allow the identification of targets by analyzing the noise they generate whereas the same situation is not applicable for active sonar systems since the received signal is not generated by the targets. Also, active sonar systems possess the risk of concealing their own locations while emitting acoustic signals, which is never a concern for passive sonar systems. That is why submarines mostly use their passive sonar systems in order to remain hidden under deep seas. However, they still need active sonar systems at least for moving safely which is only possible by detecting and avoiding obstacles.

According to their fields of use, sonar applications can be divided into three groups as naval, civilian, and scientific. Due to the competition in defense industries especially during World Wars I and II, naval investments played a large role in the advancement of sonar technologies which were applied to naval applications first and then expanded to other fields.

Naval sonar applications include but are not limited to anti-submarine warfare, homing torpedoes, sobonuoys, acoustic mines, minesweeping sonars, surveillance and security systems, hand-held sonars, and communication systems. Anti-submarine warfare sonars are typically included on surface vessels to protect against submarines. For this purpose, hull-mounted and towed sonars are mainly used. Hull-mounted sonars are capable of scanning the water both vertically and horizontally with their directional, high-power, long signals. On the other hand, towed arrays are capable of eliminating the shadow zone, which occurs due to thermal gradients related with changes in depth and hides submarines, as they can work in such depths. Also, towed arrays are less affected by the self noise of the surface vessel since they are operated from a considerable distance away from the surface vessels [2]. Homing torpedoes involve moderately high frequency sonars because of the limited available space and benefits regarding noise reduction and high directionality. Sonobuoys are expendable devices that contain hydrophones and radio transmitters and are used by aircrafts to locate submarines. A representative sketch of the working principles of sonobuoys is shown in Figure 1.2. Acoustic mines use hydrophones to initiate explosions after sensing the noise generated by target ships at a certain dominant frequency. However, this mechanism can be tricked by minesweeping sonars which mimic the noise generated by potential targets of the mine in order to save the actual targets against explosions [2].

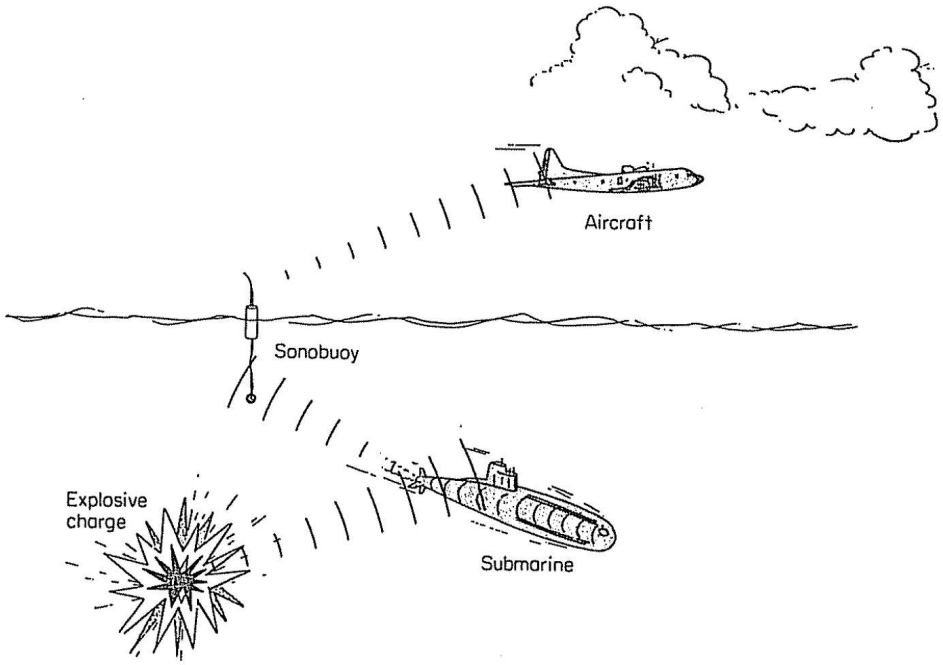

Figure 1.2: A representative sketch of the working principles of sonobuoys [2]

In addition to the naval applications, civilian and scientific sonar applications also have a significant share in underwater acoustics. Some of the devices used in such applications are bottom profilers, side scanners, fish finders, position markers, underwater telephones, remotely operated vehicle sonars, unmanned underwater vehicle sonars, biomass estimators, speedometers, ocean temperature sensors, and water wave measurement devices [2].

Sonar applications have a wide range of frequency ranging from about 1 Hz up to over 1 MHz. Either as hydrophones or projectors, the transducers are generally used in numbers up to 1000 or more as a group to form a planar, cylindrical, or spherical array depending on the operational requirements in order to enhance the capabilities available with a single transducer [4]. Pictures of a hull-mounted cylindrical array and a submarine spherical array which both consist of Tonpilz-type transducers are shown in Figure 1.2.

In addition to the Tonpilz-type transducers, various types of underwater acoustic transducers are also available. Transducers which can be used as projectors and typically also as hydrophones can be divided into 5 groups with respect to their shapes and working principles as ring and spherical transducers, piston transducers, transmission line transducers, flextensional transducers, and flexural transducers. On the other hand, transducers which can only be used as hydrophones can be divided into 4 groups as cylindrical and spherical hydrophones, planar hydrophones, bender hydrophones, and vector hydrophones. Among all these types, Tonpilz-type transducers are the most commonly used in underwater acoustics [4].

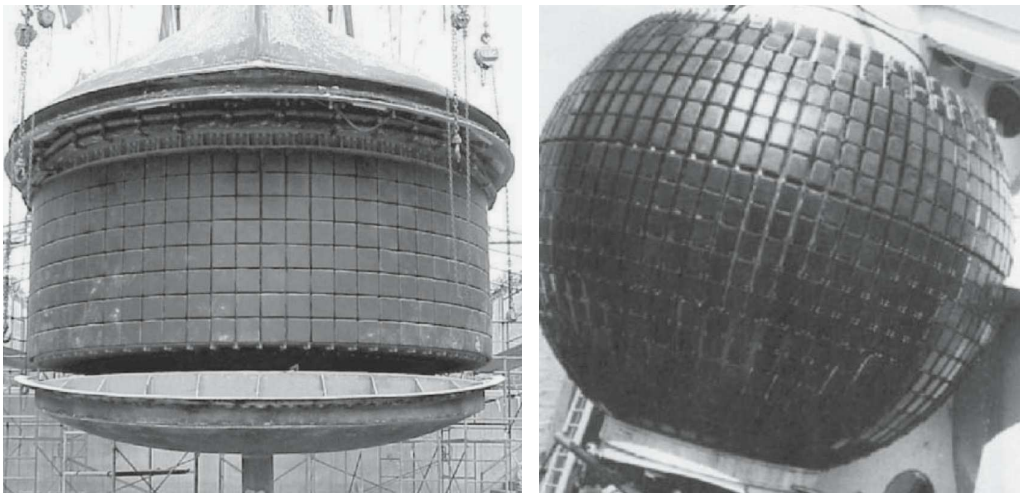

(a) (b)

Figure 1.3: Pictures of (a) a hull-mounted cylindrical array and (b) a submarine spherical array which both consist of Tonpilz-type transducers [4]

1.3 Basics of Underwater Acoustics

Acoustic waves can be described as the passage of pressure fluctuations through an elastic medium as the result of vibrational excitation imparted to the medium from an acoustic source. In addition to the source and medium, there should also be receivers, such as a human ear, microphones etc., to sense the pressure fluctuations which can then be used for various purposes. Hence, acoustics can be referred to as the study of acoustic waves and its various effects. Therefore, the scope of acoustics is very wide, ranging from fundamental physical acoustics to bioacoustics and psychoacoustics, and also includes technical fields such as noise control, sound recording and reproduction, design of concert halls, and finally transducer technology. [8, 9]

Acoustic waves are principally longitudinal waves in which the direction of the particle oscillation are in parallel with the direction of the wave propogation [8]. These waves, which refer to the periodic fluctuations of pressure around the thermodynamic equilibrium pressure along the direction of the wave propogation, can be defined in terms of the three characteristics frequency, wavelength, and pressure amplitude. Frequency, f, refers to the total number of fluctuations of the pressure per unit time. Its representation in radians is called the angular frequency, ω, and is expressed as follows:

$$\omega = 2\pi f \tag{1.1}$$

The wavelength, λ, depends on the propogation velocity of the acoustic wave, also called the sonic speed, c, which is a characteristic property of the medium. Although it is a function of temperature, pressure, and some other properties, the sonic speed in water is approximately 1500 m/s whereas in air it is around 343 m/s. The sonic speed inside solids can also be approximated with the following expression [8]:

$$c = \sqrt{\frac{E_Y}{\rho}} \tag{1.2}$$

where E_Y and ρ are the modulus of elasticity and density of the solid medium, respectively. Once the sonic speed is known, the wavelength for the wave propogation can readily be found in terms of the frequency as follows:

$$\lambda = \frac{c}{f} \tag{1.3}$$

Wavelength is the distance between the location of maximum pressure for two consecutive waves at any given instant. As related with the wavelength, the (angular) wavenumber, k, is also extensively used in underwater acoustics and is expressed as follows:

$$k = \frac{2\pi}{\lambda} \tag{1.4}$$

The last characteristic of acoustic waves, pressure amplitude of oscillation, is commonly presented in deciBel, dB, units which indicate their pressure levels with respect to a reference value instead of their actual values. DeciBel units, literally referring to one-tenth of the seldom used unit Bel, are especially useful in handling large values. The sound pressure level, SPL, which can be calculated at any location in the medium subjected to acoustic propogation, is defined as follows:

$$SPL = 10\log\left(\frac{p_{rms}^2}{p_{ref}^2}\right) = 20\log\left(\frac{p_{rms}}{p_{ref}}\right) \tag{1.5}$$

The reference pressure, p_{ref}, equals to 20 μPa in air acoustics, which is the threshold of audibility. However, in underwater acoustics, p_{ref} is defined as 1 μPa since audibility is usually not a concern as well as being not applicable for the whole frequency range considered [10].

The simplest acoustic waves are a key concept in acoustics and can be considered as the plane waves. In plane waves, at any given instant all acoustic variables have a common amplitude and phase at all points on any given plane perpendicular to the direction of the wave propogation. The intensity of plane waves, which corresponds to acoustic energy per unit area and is commonly used in underwater acoustics, can be expressed as follows:

$$I_r = \frac{p_{rms}^2}{\rho c} \tag{1.6}$$

where ρc is called as the specific or characteristic acoustic impedance of the medium, which correspond to the ratio between pressure and particle velocity in plane waves. In underwater acoustics, approximately 3500 times higher specific acoustic impedance is encountered than in air acoustics. Therefore, underwater acoustic transducers must be able to work under significantly higher stress levels. Also, environmental conditions are much more challenging in underwater acoustics due to corrosion, temperature extremes, and obstacle impact. Therefore, rugged structures and transduction mechanisms must be considered while designing underwater acoustic transducers [11].

1.4 Piezoelectricity

The word *piezoelectricity* is derived from the combination of the Greek words, *piezo* or *piezein* meaning “to press, to squeeze”, and *electric* or *elektron* meaning “amber”, an ancient gemstone which generates negative electrical charge when rubbed [12]. The term was first used by Hankel in 1881 [13], a year after the discovery of the piezoelectric phenomenon by the Curie brothers [14]. Further information about the discovery and history of piezoelectricity is available in the literature [15, 16, 17].

As the name implies, piezoelectricity can simply be described as “electricity by pressure” [18]. More formally, piezoelectricity is a phenomenon which addresses the proportional development of electrical displacement under the influence of mechanical stress in certain materials, called piezoelectric materials [19]. Energy conversion due to piezoelectricity is named as the piezoelectric effect and is divided into two groups, named as the direct piezoelectric effect and the converse (indirect, inverse) piezoelectric effect. In the direct piezoelectric effect, electric charge and voltage is generated by application of mechanical stress and pressure. In the converse piezoelectric effect, mechanical strain and displacement is obtained due to an applied electric field and voltage. A sketch of the direct and converse piezoelectric effects are shown in Figure 1.4. Up to a certain level of applied electric field or mechanical stress that depends on the material properties, piezoelectric effects are linear and also reciprocals of each other [4, 20].

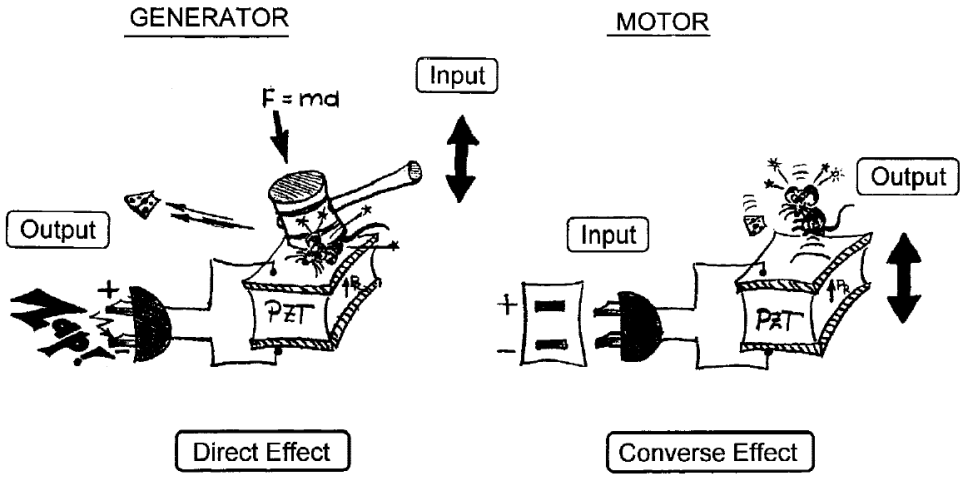

Figure 1.4: A sketch of the direct and converse piezoelectric effects [16]

The piezoelectric effects depend on the direction of the applied electric field and mechanical stress as well as the polarization direction of the piezoelectric material. For instance, when an electric field parallel to the polarization axis is applied to a piezoelectric bar, its length changes considerably only if it is polarized parallel to its length. Polarization is the process of aligning the randomly oriented electric dipoles in ferroelectric materials to make them useful in terms of piezoelectricity [4]. This is achieved by applying a strong electric field to the material near the Curie temperature, where polarization is easier due to temperature. However, above the Curie temperature polarization is impossible, since electric dipoles cannot be manipulated and become randomly oriented throughout the material. Therefore, after polarization, operating conditions around the Curie temperature must be avoided, in order not to lose the material's piezoelectric properties. In addition, high static pressure cycling, high alternating electric fields, and aging also affect polarization adversely [4]. Some naturally polarized non-ferroelectric materials, such as quartz and wurtzite, which cannot be polarized manually and also do not have problems due to the loss of polarization, also exhibit piezoelectric properties. Although they have excellent stability, better piezoelectric coefficients can be achieved with their ferroelectric counterparts [21]. For this reason, after the Second World War quartz lost its dominance in sonar applications to piezoelectric ceramics, also called as piezoceramics, which are still the most widely used materials in underwater transducer designs [4, 20]. In addition to having better piezoelectric properties, piezoceramics are also superior to natural piezoelectric crystals such as quartz, Rochelle salt, lithium sulphate etc., in terms of low cost, flexibility in size, and ease of manufacturability and reproducibility [20]. In the production of piezoceramics, firstly, randomly oriented crystallites are sintered together by being subjected to a high temperature. At this stage, the piezoelectric effects at the micro level cancel each other out at the macro level due to randomness, leading them to be useless in terms of piezoelectricity. Therefore, polarization is the second and probably the most important stage of production, as it allows the ceramic to attain its piezoelectric properties. During the polarization stage, maintaining the ceramic at a high electric field (such as 10 kV/cm) may lead to dielectric breakdowns due to internal flaws in the material whose probability increases with thickness. Therefore, thicknesses in the polarization axis more than 10 mm are not common [20]. Due to their brittle nature, piezoceramics are unreliable under tension. Therefore, it is necessary to keep piezoceramics under compression and avoid subjecting them to tensile stresses [22]. Also, to decrease the risk of depolarization, a good rule of thumb is not to exceed 75% of the Curie temperature after polarization [23].

At the end of the Second World War, the first piezoceramics, which were based on barium titanate ($BaTiO_3$) compositions, were discovered and used in various underwater applications. Then, these barium titanate based piezoceramics became obsolete after the discovery of lead zirconate titanate (PZT) based piezoceramics in 1954. Of all the ceramic materials, PZT ceramics are the most commonly used due to their high electro-mechanical coupling, suitable quality factor, and good frequency-temperature characteristics [24]. PZT ceramics are also one of the most studied piezoceramic materials due to their widespread application areas in science, industry, medicine, communications, transformation, and information technologies. However, the use of pure PZT is quite rare. Instead various compositions of PZT with different dopants and additives to achieve certain properties are more common and available commercially [25]. For instance, a composition called PZT-4, which is classified as Navy Type I, has resistance to depoling at high electric field or mechanical stress conditions, making it suitable for high-power applications. In constrast, PZT-5A (Navy Type II) has better charge sensitivity but cannot withstand high electric fields [26].

Mathematical representation of piezoelectric relations involves numerous position and time dependent parameters defined in tensor form, which can be counted as: strain, S; stress, T; electric displacement, D; and electric field, E. These parameters depend on each other and the following material constants: elastic stiffness coefficient, c; elastic compliance coefficient, s; piezoelectric coefficients, d, e, g, h; and dielectric constants, ε, β. These coefficients are material specific and the manner in which they vary with temperature changes with material. However, it is reasonable to assume adiabatic working conditions [27] and accordingly, define the governing matrix equations of piezoelectric materials as follows:

$$\begin{aligned} \left[S\right]_{1x6} &= \left[s^E\right]_{6x6}\left[T\right]_{1x6} + \left[d\right]^t_{3x6}\left[E\right]_{1x3} \\ \left[D\right]_{1x3} &= \left[d\right]_{6x3}\left[T\right]_{1x6} + \left[\varepsilon^T\right]_{3x3}\left[E\right]_{1x3} \end{aligned} \tag{1.7}$$

$$\begin{aligned} \left[T\right]_{1x6} &= \left[c^E\right]_{6x6}\left[S\right]_{1x6} - \left[e\right]^t_{3x6}\left[E\right]_{1x3} \\ \left[D\right]_{1x3} &= \left[e\right]_{6x3}\left[S\right]_{1x6} + \left[\varepsilon^S\right]_{3x3}\left[E\right]_{1x3} \end{aligned} \tag{1.8}$$

$$\begin{aligned} \left[S\right]_{1x6} &= \left[s^D\right]_{6x3}\left[T\right]_{1x6} + \left[g\right]^t_{3x6}\left[D\right]_{1x3} \\ \left[E\right]_{1x3} &= -\left[g\right]_{6x3}\left[T\right]_{1x6} + \left[\beta^T\right]_{3x3}\left[D\right]_{1x3} \end{aligned} \tag{1.9}$$

$$\left[T\right]_{1x6} = \left[c^D\right]_{6x3}\left[S\right]_{1x6} - \left[h\right]^t_{3x6}\left[D\right]_{1x3} \qquad (1.10)$$
$$\left[E\right]_{1x3} = -\left[h\right]_{6x3}\left[S\right]_{1x6} + \left[\beta^S\right]_{3x3}\left[D\right]_{1x3}$$

Here subscripts represent the dimensions of the matrices, capital letter superscripts represent the parameters kept constant while measuring the corresponding coefficients, and the superscript, *t*, represents the transpose of the corresponding matrix. All 4 sets of these equations are identical and are obtained by manipulating the coefficient matrices. Therefore, one may choose a set of equations according to a given application that requires certain independent variables.

As can be noted in Equations (1.7-1.10), piezoelectric coefficient matrices can be expressed in 4 different ways. However, since they all represent the same piezoelectric properties, they can be converted into each other. Mathematical representations of these coefficients can be expressed as follows:

$$d = \left(\frac{\partial S}{\partial E}\right)_T = \left(\frac{\partial D}{\partial T}\right)_E \qquad e = -\left(\frac{\partial T}{\partial E}\right)_S = \left(\frac{\partial D}{\partial S}\right)_T \qquad (1.11)$$
$$g = \left(\frac{\partial S}{\partial D}\right)_T = -\left(\frac{\partial E}{\partial T}\right)_D \qquad h = -\left(\frac{\partial T}{\partial D}\right)_S = -\left(\frac{\partial E}{\partial S}\right)_D$$

where T, E, S, or D are held constant while taking partial derivatives of S, D, T, or E, respectively. Although the number of coefficients looks large when the dimensions of the matrices presented in Equations (1.7-1.10) are considered, only 10 of the coefficients are independent for permanently polarized electrostrictive materials, such as PZT ceramics [4]. Therefore, most of the coefficients are either zero or identical to each other, which can be seen in the expanded form of Equation 1.7 as follows:

$$\begin{bmatrix} S_1 \\ S_2 \\ S_3 \\ S_4 \\ S_5 \\ S_6 \\ D_1 \\ D_2 \\ D_3 \end{bmatrix} = \begin{bmatrix} s_{11}^E & s_{12}^E & s_{13}^E & 0 & 0 & 0 & 0 & 0 & d_{31} \\ s_{12}^E & s_{11}^E & s_{13}^E & 0 & 0 & 0 & 0 & 0 & d_{31} \\ s_{13}^E & s_{13}^E & s_{33}^E & 0 & 0 & 0 & 0 & 0 & d_{33} \\ 0 & 0 & 0 & s_{44}^E & 0 & 0 & 0 & d_{15} & 0 \\ 0 & 0 & 0 & 0 & s_{44}^E & 0 & d_{15} & 0 & 0 \\ 0 & 0 & 0 & 0 & 0 & s_{66}^E & 0 & 0 & 0 \\ 0 & 0 & 0 & 0 & d_{15} & 0 & \varepsilon_{11}^T & 0 & 0 \\ 0 & 0 & 0 & d_{15} & 0 & 0 & 0 & \varepsilon_{11}^T & 0 \\ d_{31} & d_{31} & d_{33} & 0 & 0 & 0 & 0 & 0 & \varepsilon_{33}^T \end{bmatrix} \begin{bmatrix} T_1 \\ T_2 \\ T_3 \\ T_4 \\ T_5 \\ T_6 \\ E_1 \\ E_2 \\ E_3 \end{bmatrix} \qquad (1.12)$$

1.5 Overview of Tonpilz-Type Transducers

As an improvement to their ancestors, 42 years after the invention of Langevin transducers, Tonpilz-type transducers were invented in 1959 in their currently used state by Harry B. Miller [28, 29]. A picture of that invention in a disassembled state for better visibility of its constituents is shown in Figure 1.5 [28]. In contrast with the expectations at that time, Tonpilz-type transducers are currently the most widely used sonar projectors due to their simplicity, good performance, and low cost [30, 31]. In addition to their extensive use in naval sonar systems for more than 50 years, Tonpilz-type transducers are also used in industrial applications such as acoustic ranging devices and ultrasonic cleaners [32]. The word *Tonpilz*, which is a combination of two German words meaning "sound" and "mushroom", is attributed to these types of transducers due to their characteristic shape involving a large piston head and a slender driving portion behind the piston head [4, 33].

Like most of the other piston type transducers, Tonpilz-type transducers project sound in one direction and are suitable for assembling in large close-packed sonar arrays [4, 34]. When the superior capability of Tonpilz-type transducers in generating high acoustic power by compact means is used within sonar arrays, it is possible to obtain high intensity and highly directional acoustic waves which is extremely important in most sonar applications [4, 35].

Regarding their drive mechanisms, Tonpilz-type transducers can be divided into two groups as magnetostrictive and piezoelectric. Although their magnetostrictive counterparts can offer better performance in certain situations [4, 36], the ones with Navy Type I or III piezoceramics are much more common and are considered in the present work.

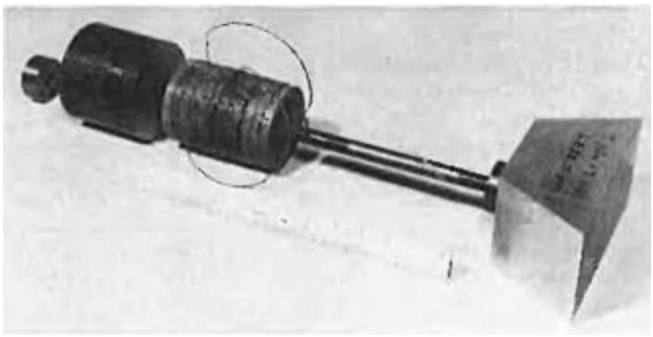

Figure 1.5: A picture of the first Tonpilz-type transducer built like in its current state with a disassembled presence for better visibility of its constituents [28]

Tonpilz-type transducers essentially consist of a 33-mode driven piezoceramic stack squeezed between a head mass and a tail mass by means of a stud [4, 20, 37]. This configuration allows the structure to have a longitudinal resonance at low to midrange frequencies, between 1-50 kHz, without requiring an excessively long piezoceramic stack [4, 20]. Although resonance frequency is avoided in most mechanical engineering designs due to displacement amplification, it is favorable in underwater acoustic transducers for the same reason which leads to higher sound pressure levels in the acoustic medium. A 3-D cross-sectional sketch of a typical Tonpilz-type transducer is shown in Figure 1.6 with its main parts identified [11]. In addition, a more detailed 2-D cross-sectional sketch of a typical Tonpilz-type transducer taken from a different source is shown in Figure 1.7 also with its parts identified [4].

The fundamental motion of the Tonpilz-type transducers is provided through application of an alternating voltage to the piezoceramic rings that in turn leads to consecutive elongations and contractions of the structure in the axial direction at the frequency of the applied voltage as a result of the piezoelectric effect. Hence, these alternating displacements of the piezoceramic stack are transmitted to the acoustic medium through the rubber boot covering the head mass and ultimately result in pressure fluctuations called acoustic waves in the water. Since the amplitude of the alternating displacements of the structure and hence the sound pressure level in the water is magnified at resonance, it is favorable to run these transducers close to their resonance frequencies by applying the alternating voltage accordingly.

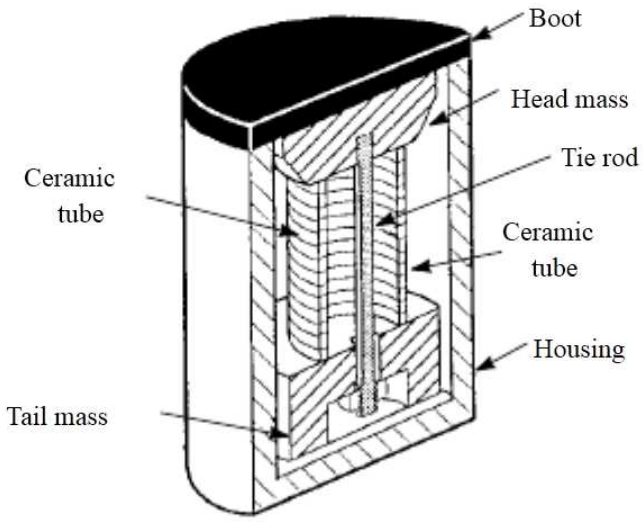

Figure 1.6: A 3-D cross-sectional sketch of a typical Tonpilz-type transducer [11]

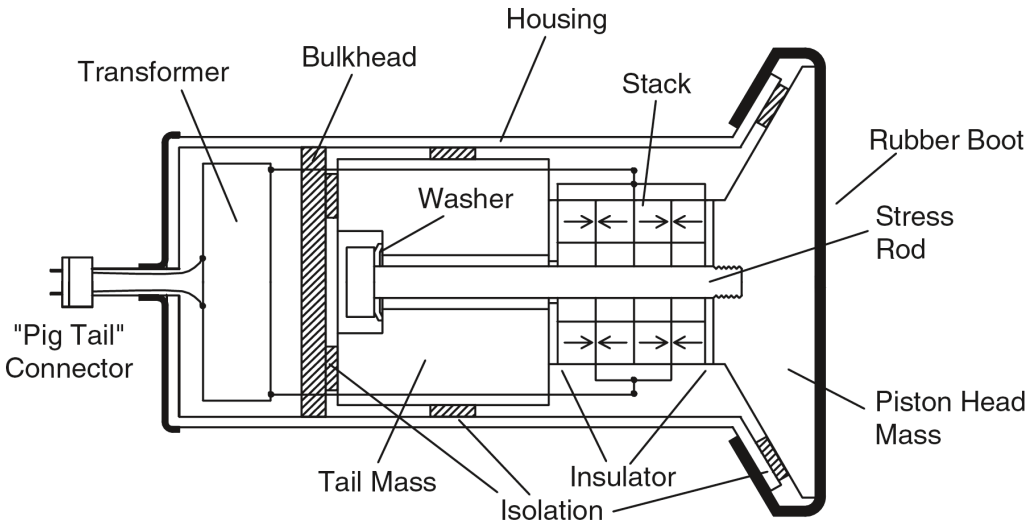

Figure 1.7: A detailed 2-D cross-sectional sketch of a typical Tonpilz-type transducer [4]

The piezoceramic stack can be considered as the most important part of the Tonpilz-type transducers as it is responsible for the generation of motion. The acoustical power obtained from the transducer is directly proportional with the volume of the piezoceramic rings existing in the stack [4]. A configuration of the 33-mode piezoceramic rings that is mechanically in series and electrically in parallel allows the application of the alternating voltage over the electrodes cemented on the parallel surfaces of the piezoceramic rings [20, 37]. As a practical requirement of this configuration, the consecutive piezoceramic rings must have opposite polarization directions as shown in Figure 1.7. In addition to the cements and electrodes, electrical insulators, which can also be used for tuning the resonance frequency to an extent in addition to their essential use for prohibiting the contact of piezoceramic rings with the head mass and tail mass, are the other passive elements in the piezoceramic stack. These passive elements degrade the electromechanical coupling coefficient of the Tonpilz-type transducers [4]. That is why the number of piezoceramic rings forming the stack should be kept as low as possible. For the same reason, in some designs, electrical insulators are not used, which as a result turns the head mass and tail mass into electrical ground.

The head mass has a critical importance in Tonpilz-type transducers as it directly takes the role of initiating the acoustic radiation. When the rubber boot is omitted, the surface in-contact with the acoustic medium of the head mass can be called as the active surface of the transducer. The active surface usually has a geometrical shape of either a circle or a square depending on the operational purposes of the transducer. In order to obtain as much acoustic power as

possible from the transducer, the area and the amplitude of the displacement normal to the acoustic medium of the active surface must be maximized. Therefore, the head mass should be as light as possible to increase the displacement amplitude and also as wide as possible to provide good acoustic matching with the water. However, decreasing the thickness while increasing the area lowers the flexural resonance frequency of the head mass, where half of the active surface moves out of phase with the other half, resulting in a null response in terms of acoustic radiation [4]. On the other hand, the ratio of the masses of the tail mass to the head mass has a tremendous effect on the acoustic radiation. In the ideal case where the tail mass has an infinite mass, the sound pressure level generated becomes 6 dB more than the case where the masses of the head mass and tail mass are equal to each other, as a result of the different velocities encountered by the head mass in both cases [4]. In order to have a lighter mass and also push the frequency of the flexural mode of the head mass away from the fundamental frequency of the transducer, a portion of the head mass is usually tapered away from the center to the edge which results in a characteristic conical shape for the head mass. With respect to the requirements, the material selected for the head mass should have a low density while also having a high stiffness. Aluminium is commonly used for the head mass as it satisfies these conditions.

The stud, which is also referred to as the stress rod or tie rod, has a key function in addition to keeping the transducer parts together. Since the piezoceramics are not reliable under tensile stresses, the stud prevents this situation by applying a steady compressive stress on the piezoceramics higher than the peak alternating stress occurring due to the applied alternating voltage [38, 39]. Therefore, the piezoceramics always work reliably under compression with the stud. This compressive effect is provided by means of a nut behind the tail mass. Instead of the nut and stud couple, a bolt can also be used as shown in Figure 1.7. The stud also degrades the motion of the transducer to an extent as it clamps the piezoceramic stack. Therefore, the stud must have as low a stiffness as possible to minimize this degrading effect while also having as high an ultimate tensile strength as possible to provide the steady compressive stress and also resist against fatigue failure which would occur due to the alternating stresses. Hence, high strength steels are commonly used as the material for the stud [4].

The tail mass can be seen as the least important part when compared with the previously introduced ones as its almost only function is being a counter weight to the head mass. However, it still has an influence on the resonance frequency of the transducer. To increase the radiated

power and bandwidth of the transducer, the mass of the tail mass should be as large as possible. Hence, the material selected for the tail mass must have a high density to satisfy this need with a reasonable volume. Steel is commonly used as the material for the tail mass. For high frequency designs where the volume needs to be small, tungsten is also used [4].

In addition to the core parts of the Tonpilz-type transducers introduced, in practice several supplementary parts are also required in order to realize the functioning of the transducer. For instance, the housing is needed for protecting the core parts against water, physical damage, and shock while also preventing a probable acoustical short circuit between the head mass and the other core parts of the transducer as it isolates every part except the head mass from the water [4, 11]. Also, the vibrating core assembly is located in the housing. In the ideal case, the core assembly should only be in contact with the water in order not to dissipate energy needlessly. This ideal case is approximated with the use of pressure-relief isolation materials such as foam rubber as shown in Figure 1.7. Depending on the operational conditions of the transducer, the mounting may involve rigid connections as well from the head mass, tail mass or even the piezoceramic stack [4]. However, in such kind of mountings, the efficiency of the transducer is prone to degradation. The acoustically transparent rubber boot in front of the head mass is mainly used to protect the head mass against corrosion and prevent in-gress of water into the housing. Depending on the material used for the rubber boot, which is usually neoprene, butyl rubber or urethane [4, 33], and its thickness, the acoustical properties of the transducer such as the bandwidth change. Although the initial efficiency of the transducer may not be high depending on the material and assembly details, the transducer efficiency can decrease even further with the use of rubber boot since it restricts the movement of the head mass to an extent. Any air pockets between the rubber boot and the active surface of the head mass must be avoided as it would reduce the acoustic loading and hence the radiated power of the transducer [4]. As the last supplementary parts, a water-proof connector and a transformer, which is also referred to as the electrical matching circuit, are required in the Tonpilz-type transducers. Actually, it is possible to run the transducer without the matching circuit but it may not be electrically feasible. Thus, the matching circuit is involved in the design for both adjusting the voltage supplied to the transducer and matching the electrical impedances of the transducer and the electrical source. Since the occurrence of the supplementary parts show significant differences depending on the operational needs, these parts are not considered while modeling Tonpilz-type transducers throughout the present work.

1.5.1 Performance Metrics of Tonpilz-type Transducers

The three most important performance metrics of the Tonpilz-type transducers are the resonance frequency, source level and bandwidth [40, 41]. Among these, the resonance frequency is usually the only performance characteristic that needs to exactly match the design requirements [20]. The conductance response of the transducer is the most reliable indicator of the resonance frequency. The conductance, being an electrical term, can best be defined with Ohm's Law as follows:

$$I = \frac{V}{R} = VY = V\,(G + iB) \tag{1.13}$$

where I is the current, V is the voltage, R is the impedance, Y is the admittance, G is the conductance, and B is the susceptance. Therefore, the conductance is the real part of the reciprocal of the impedance. It directly reflects the motional characteristics of the transducer. Hence, the frequency where the peak value for the conductance occurs corresponds to the resonance frequency of the transducer [20]. Although the resonance frequency addresses the largest motional response, peak sound pressure level in the water generated by the transducer may not be at the resonance frequency due to the frequency dependent terms affecting the sound pressure level, namely, the efficiency and the directionality of the transducer. There are two efficiencies applicable to electroacoustic transducers, namely, the electromechanical and mechanoacoustic efficiencies. The overall efficiency of the transducer is the product of these efficiencies and is named as the electroacoustic efficiency, η_{ea}. In addition to frequency, the electroacoustic efficiency is also dependent on the physical conditions of the transducer, which are difficult to quantify. More detailed information regarding the efficiency terms for the Tonpilz-type transducers is given in Section 2.2.

On the other hand, the directionality of an electroacoustic transducer can be quantified with two closely related but different terms named as the directivity index and beam width. The acoustic axis of the transducer should be defined before introducing these terms. To reiterate, the surface in-contact with the acoustic medium of the head mass can be called the active surface of the transducer from which the acoustic radiation initiates. The axis which is normal to the active surface and passes through its center point is called the acoustic axis of the transducer. The directivity factor, D_f, of a transducer corresponds to the ratio of the transmitted acoustic intensity of the transducer along its acoustic axis to the intensity which would occur at the acoustic axis if the transducer was a monopole and radiating the same amount of

acoustic power [20]. The directivity index, DI, is simply the dB-scale representation of the directivity factor. For simple geometries, analytical representations for the directivity factor are available under certain assumptions. The formulation for the directivity factor of a Tonpilz-type transducer with a circular active surface vibrating in a rigid baffle with the assumption of uniform oscillation velocity is as follows [4]:

$$D_f = \frac{(ka)^2}{[1 - J_1(2ka)/ka]} \tag{1.14}$$

where k is the wavenumber and a is the radius of the circular active surface considered. Once the directivity factor is known, the directivity index can readily be found with the following expression:

$$DI = 10\log(D_f) \tag{1.15}$$

After the definitions of the efficiency and directivity index, one can determine the sound pressure level generated in the water with respect to the input electrical power, W_e, to the transducer. The sound pressure level can be represented by two terms according to the working conditions of the transducer. These terms are the transmitting voltage response, TVR, and the source level, SL. Both represent the dB-scale ratio of the intensity at the acoustic axis 1 m away from the active surface generated by the transducer to the intensity of an ideal plane wave leading to a pressure of 1 μPa at the same point [20]. However, the alternating voltage applied to the transducer must have a magnitude of 1 volt for the TVR whereas there is no such limit for the SL. Hence, the SL can be defined in terms of the TVR depending on the linearity of the response of the transducer under varying driving voltage. The TVR can be expressed in terms of the efficiency, directivity index, and input electrical power as follows by using Equation 1.6 and assuming $\rho c = 1.5 \times 10^6\ kg\ m^{-2}\ s^{-1}$ for water [20]:

$$TVR = 10\log\left[\frac{(\rho c W_e/4\pi)}{(1\,\mu\text{Pa})^2}\right] + DI + 10\log(\eta_{ea})$$

$$TVR = 10\log\left(\frac{W_e}{1\text{ watt}}\right) + DI + 10\log(\eta_{ea}) + 170.8\text{ dB} \tag{1.16}$$

To reiterate, the input electrical power, W_e, must be calculated for a driving voltage of 1 volt in Equation 1.16. The SL should be considered for different driving voltages, V_{drive}. The SL is expressed in terms of the TVR depending on the linearity of the transducer as follows:

$$SL = TVR + 20\log\left(\frac{V_{drive}}{1\text{ volt}}\right) \tag{1.17}$$

Instead of using Equations 1.16 - 1.17, a more accurate and effective way of determining the TVR or SL is directly measuring the pressure 1 m away from the transducer on its acoustic axis and then calculating the dB-scale ratio of the corresponding intensity with the intensity regarding the reference frequency, 1 μPa. Such an approach is also applicable for the FE analysis in which the acoustic medium is modeled.

Although it is safe and practically easy to measure the TVR due to the low driving voltage, the same is not valid for the SL due to physical limitations. In other words, a driving voltage beyond the physical limits can either not be realized or does not result in the expected SL values. Therefore, the SL at the driving limits of the transducer is a better measure of the performance when compared to the TVR as it reflects the capabilities of the transducer better. The limitations for the SL, also called as the power limitations, can be divided into four groups as electrical, mechanical, thermal and acoustic. Electrical breakdown or depoling of the piezoceramics is the possible electrical limitations to the driving voltage [20]. Mechanical limitations include the failure of the piezoceramic stack or the stud due to the alternating stresses with respect to the driving voltage during operation. The heating mechanisms within the transducer, such as those due to the dielectric and hysteresis losses of the piezoceramics, and frictional and other kinds of mechanical losses within the transducer, can result in the piezoceramic reaching the Curie temperature for the piezoceramics, which leads to depolarization, above a certain driving voltage. Lastly, even though the transducer can safely work without suffering from the previously explained limitations, acoustic radiation may not be at the expected levels due to the cavitational limits of the acoustic medium. In other words, if the transducer tries to generate the acoustic power which corresponds to the amplitude of the alternating pressure in the water being higher than the hydrostatic pressure, the transducer basically fails to generate that much acoustic power and instead wastes the available power by making water vapor bubbles in the water. In short, the power limitations for the Tonpilz-type transducers must be considered while designing such transducers in order not to face unexpected results.

Hence, the peak value and the bandwidth for the maximum SL with respect to the power limitations can be considered as the most important performance metrics of the Tonpilz-type transducers after the resonance frequency. The bandwidth of the SL corresponds to the absolute difference between the frequencies at which the values of the SL are 3 dB less than the peak value of the SL.

In addition to the three most important performance metrics, beam width, which was the second term mentioned related with the directionality of the transducer, can also have critical importance depending on the operational requirements. Beam width is a dB-scale measure of angular response of the transducer in which the intensity measured on the acoustic axis of the transducer is correlated with the intensities measured on the other axes which are not normal to the active surface but pass through the center of the active surface. When a spherical coordinate system, in which the center of the active surface is placed at the origin, is considered, the beam pattern of the transducer can be obtained by correlating the far field intensities measured for points on axes having different inclination and azimuth angles than the acoustic axis with the intensity obtained on the acoustic axis at the same radial distance. Although the beam pattern has a 3-D representation, for transducers having axisymmetric geometries a 2-D representation is sufficient. Such a beam pattern is shown in Figure 4.8. When the acoustic axis is considered to have 0° inclination and azimuth angles, the beam width is determined considering the inclination and azimuth angles of the axes whose points of interest have 3 dB less intensity than the measurement point on the acoustic axis. Hence, the absolute difference of the corresponding inclination and azimuth angles is the beam width. For axisymmetric transducers, the differences in inclination and azimuth angles are equal to each other. Therefore, determining the beam pattern for constant inclination angle at 0° is sufficient to obtain the 3-D beam pattern of the transducer just by rotating the existing 2-D beam pattern around the acoustic axis.

Hence, although the directivity index and beam width are both related with the directionality of the transducer, their definitions are completely different. However, a narrow beam width corresponds to a high directivity index and a wide beam width corresponds to a low directivity index. Depending on the operational requirements, directivity index of a single transducer may not be sufficiently high. In such cases, an array consisting of a number of transducers is commonly used to boost the directivity index as well as the SL.

In this section, only the performance metrics considered throughout the present work is introduced. For instance, the electromechanical coupling coefficient is not considered even though it is a good indicator of performance. In addition, although the Tonpilz-type transducers are able to operate both as a projector and a receiver, performance metrics related with the receiving characteristics, such as the receiving voltage sensitivity, are not considered. Information related with these performance metrics and other metrics is available in the literature [4, 20].

1.5.2 Survey of Studies Regarding Tonpilz-Type Transducers

Due to the large number of design parameters involved in Tonpilz-type transducers, finding a balanced optimum among these parameters with respect to the performance requirements is not an easy task [11]. Also, the influences of the design parameters on the performance metrics are not independent of each other [40]. Even worse, the design requirements usually contradict with each other [33]. For instance, providing both a high SL and a wide bandwidth is probably the greatest challenge in Tonpilz-type transducer design. On the other hand, design constraints and physical limitations further increase the difficulties in design procedures. For example, lowering the mass of the head mass by decreasing its thickness to get a higher SL without sacrificing the beam width appears logical but it may lead to a flexural mode of the head mass around the fundamental resonance frequency of the transducer that would completely ruin the design. As another example, increasing the mass of the tail mass in order to get a higher SL and a wider bandwidth leads to a heavier transducer which usually is not favorable [4]. In addition to overcoming all these challenges, all the design parameters existing in the Tonpilz-type transducers must be in harmony to satisfy the most important design requirement, the fundamental resonance frequency. Hence, although a Tonpilz-type transducer looks simple as it is only an assembly of a few basic parts, seeking an optimum among numerous contradictory requirements and conditions make design procedures very hard.

The studies regarding Tonpilz-type transducers are mostly about introducing new methods for improving certain performance metrics, especially the bandwidth. Among such studies, an improvement in the bandwidth by using a special geometry of the head mass involving a cavity inside is presented by Chhith *et al.* [35]. A similar method involving a hole in the active surface of the head mass for improving the bandwidth is introduced by Xiping *et al.* [31]. In parallel, Saijyou *et al.* [34] investigate a Tonpilz-type transducer with a head mass involving a hollow section inside and a bending piezoelectric resonator disk on its active surface to improve the bandwidth. In the study of Brosnan *et al.* [29], a higher SL and a wider bandwidth are achieved by using a piezoelectric material manufactured with a new technique. In the studies of Roh *et al.* [40] and Pei *et al.* [41], piezocomposite stacks with the modes 2-2 and 1-3, respectively, are used as the active material for the same Tonpilz-type transducer instead of the same-sized piezoceramic stacks and improvements in both the SL and bandwidth are observed. The danger of the flexural mode of the head mass is turned into

a benefit by widening the bandwidth by fine tuning the frequency of the flexural mode with respect to the fundamental resonance frequency in the studies of Hawkins *et al.* [42], Yao *et al.* [30], and Rajapan [43] for the Tonpilz-type transducer having different sizes and fundamental resonance frequencies. Lastly, Crombrugge *et al.* [44] show a method for increasing the bandwidth for the Tonpilz-type transducers by using up to three different matching layers with different thicknesses and material properties between the head mass and water.

Although few in number, different optimization techniques used with particular parametric models of Tonpilz-type transducers are introduced in some studies. The study of McCammon *et al.* [33] involves a technique called nonlinear goal programming, which is used for optimizing various properties involving the resonance frequency, the length, and the weight of the transducer. The same optimization technique is also used within the study of Crombrugge *et al.* [44]. Another optimization technique named as statistical multiple regression analysis method is used within the studies of both Roh *et al.* [40], Pei *et al.* [41], and Chhith *et al.* [35] for maximizing the TVR without sacrificing the bandwidth through optimization of the dimensional parameters of the Tonpilz-type transducers considered in each study.

In each mentioned study, only a single modeling technique is used for designing Tonpilz-type transducers. Finite element modeling has the biggest share among all the modeling techniques [30, 35, 40, 41, 42, 43]. Also, a considerable number of the studies involve 1-D distributed models of the Tonpilz-type transducers [31, 33, 34, 44]. These modeling techniques are usually validated with experiments [30, 31, 33, 34, 42, 43]. On the other hand, only a few studies introduce improvements to existing modeling techniques, such as the study of Kim *et al.* [45] about a new simulation technique for FE models. Also, the studies of Mančić *et al.* [46] and Iula *et al.* [47] brought two unique 2-D distributed models to the literature.

Even though various modeling techniques are used in different studies, only a single study is spotted in the literature that compares the accuracies of different modeling techniques. The study conducted by Teng *et al.* [48] investigates the accuracies of just a 1-D distributed model and a FE model with respect to experimental measurements. Another gap in the literature is related with studies showing design approaches for the Tonpilz-type transducers. In this respect, the study of Chen *et al.* [37] is unique, which describes a method for designing the transducer from scratch, but only with a limited accuracy since the approach only involves a lumped-parameter model.

1.6 Thesis Overview

1.6.1 Objectives

The main purpose of the present work is to fill a gap in the literature by providing a systematic design approach for the Tonpilz-type transducers which are extensively used in underwater acoustic applications. Objectives considered in order to fulfill or support the main purpose are listed from the most to the least important as follows:

- Propose a methodology for designing Tonpilz-type transducers which involves the systematic use of four different types of validated analytical and numerical models;
- Verify the validity of the proposed methodology with a sample design procedure;
- Evaluate the accuracies of the models used throughout the methodology with respect to the experimental results available in the literature and make a comparison between the models;
- Constitute an original finite element model of the Tonpilz-type transducers suitable for parametric studies;
- Validate the acoustic field in the finite element model;
- Combine the principle equations available in the literature regarding the Tonpilz-type transducers for building an original analytical model of the Tonpilz-type transducers suitable for parametric studies;
- Build two analytical models available in the literature in accordance with parametric studies;
- Identify the key points and important issues which can be encountered while designing Tonpilz-type transducers;
- Suggest possible improvements to the proposed methodology.

1.6.2 Scope

Due to the interdisciplinary nature of the Tonpilz-type transducer which combines underwater acoustics, structural mechanics, electronics, material sciences, thermodynamics and so on, the boundaries of the present work must be clearly defined to avoid getting lost within the details of any discipline.

The methodology introduced with the present work is only applicable to Tonpilz-type transducers which have transduction mechanisms based on piezoelectricity. In addition, only the projector characteristics of the Tonpilz-type transducers are considered.

Since the main purpose of the present work is to propose a design methodology, various complexities within common Tonpilz-type transducers are simplified as much as possible while still capturing the significant characteristics of such transducers. In addition, the sample design procedure conducted using the methodology is kept as simple as possible as it is presented only for illustrative purposes. Lastly, since the models used in the methodology are adapted from models available in the literature and the development of these models is not the primary novel contribution of the present work, the basic principles of each model are discussed but for brevity the reader is referred to the literature for details.

1.6.3 Organization

In Chapter 1, the Tonpilz-type transducers are identified and discussed after introducing general information about underwater acoustics and piezoelectricity.

In Chapter 2, four different models for the Tonpilz-type transducers are introduced and references are provided for readers interested in learning about the details of these models.

In Chapter 3, the models introduced in Chapter 2 are benchmarked with respect to experimental data and their performances are compared with each other.

In Chapter 4, the proposed design methology for the Tonpilz-type transducers are introduced and a sample design procedure is conducted with respect to the methodology.

In Chapter 5, the benefits and weaknesses of the methodology are discussed and possible ways for improving the methodology are discussed.

CHAPTER 2

MODELING TECHNIQUES

2.1 Simple Lumped-Parameter Model

Lumped models are the simplest ones for modeling electroacoustic transducers. Although it is possible to increase the level of detail by increasing the degrees of freedom of these models, these more complex models may not produce more accurate results due to their fundamental nature which ignores important details and contain significant approximations for the sake of simplicity. However, lumped models are still very useful as a starting point in transducer design and they may offer results appropriate for use in more advanced models. Essentially, lumped models rely on the assumption of having physical components of the transducer with dimensions less than one quarter of the wavelength in the corresponding material within the frequency band of interest. In the most basic lumped model of a Tonpilz-type transducer, the device is analogous to the simple mass-spring system shown in Figure 2.1. In this analogy, the head mass is analogous to an ideal rigid mass whereas the piezoceramic stack is analogous to an ideal massless spring. The other transducer parts such as tail mass, pre-stress stud, insulators, glues etc. are basically ignored. Although the driving force of the transducer, F_e, and the energy dissipation element, R_e, are drawn in the figure, they may be neglected in the so-called simplest lumped model.

In this section, a lumped model is developed by combining similar models available in the literature [4, 20]. The aim of this model is to provide the rough dimensions of the main transducer parts based on an inputted resonant frequency and bandwidth. Fine tuning of the dimensions, and hence the final design, can be made using more detailed models presented in the following sections. Therefore, accuracy is not critical for this model.

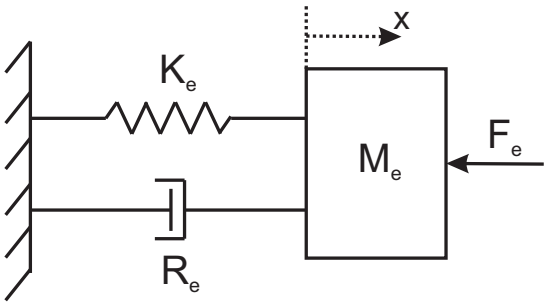

Figure 2.1: Sketch of a single-degree-of-freedom mass-spring system

In Figure 2.1, K_e is an ideal massless spring element, R_e is an ideal massless damping or resistance element, M_e is an ideal rigid mass and F_e is an excitation to the system. This system has a single-degree-of-freedom, hereafter referred to as SDF for conciseness, since it consists of a single mass which only has a translational degree-of-freedom along the x-axis. The equation of motion for the system is written as follows:

$$M_e \frac{\mathrm{d}^2 x}{\mathrm{d}t^2} + R_e \frac{\mathrm{d}x}{\mathrm{d}t} + K_e x = F_e \tag{2.1}$$

$$M_e \frac{\mathrm{d}u}{\mathrm{d}t} + R_e u + K_e \int u \mathrm{d}t = F_e \tag{2.2}$$

where $u = dx/dt$. When the impedance analogy between the mechanical terms and the electrical terms are considered with respect to Equation 2.2, it is possible to express the SDF mass-spring system shown in Figure 2.1 with the electrical equivalent circuit shown in Figure 2.2. Mechanical terms with their electrical analogues in the impedance analogy are shown in Table 2.1.

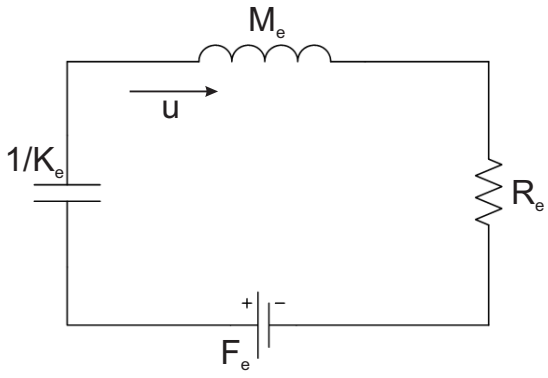

Figure 2.2: Electrical equivalent circuit of the single-degree-of-freedom mass-spring system shown in Figure 2.1

Table 2.1: Mechanical Terms with Their Electrical Analogues in the Impedance Analogy

Mechanical Terms	Electrical Analogues
Force	Voltage
Velocity	Current
Mass	Inductance
Damper	Resistance
Compliance (1/Stiffness)	Capacitance

Angular natural frequency, ω_n, and natural frequency, f_n, for the SDF mass-spring system shown in Figure 2.1 can be expressed as follows:

$$\omega_n = \sqrt{\frac{K_e}{M_e}} \tag{2.3}$$

$$f_n = \frac{\omega_n}{2\pi} = \frac{1}{2\pi}\sqrt{\frac{K_e}{M_e}} \tag{2.4}$$

The displacement response of the SDF mass-spring system shown in Figure 2.1 for the spring-controlled, damper-controlled and mass-controlled conditions of the excitation frequency, ω, are as follows, respectively [49]:

$$x \simeq \left(\frac{F_e}{K_e}\right)\sin\omega t \qquad [\omega \ll \omega_n] \tag{2.5}$$

$$x = -\frac{F_e \cos\omega_n t}{R_e\omega_n} \qquad [\omega = \omega_n] \tag{2.6}$$

$$x \simeq \frac{F_e}{M_e\omega^2}\sin\omega t \qquad [\omega \gg \omega_n] \tag{2.7}$$

When the amplitudes of displacements are considered, the amplitude at the angular resonance frequency can be expressed in terms of the amplitude well-below resonance using Equations 2.3 and 2.6 as follows:

$$|x|_{\omega=\omega_n} = \frac{F_e}{R_e\omega_n} = \frac{F_e\omega_n}{R_e}\frac{1}{\omega_n^2} = \frac{F_e\omega_n}{R_e}\frac{M_e}{K_e} = \left(\frac{F_e}{K_e}\right)\frac{\omega_n M_e}{R_e} = \left(\frac{F_e}{K_e}\right)Q_m \tag{2.8}$$

$$Q_m = \frac{\omega_n M_e}{R_e} \tag{2.9}$$

where Q_m is called the *mechanical quality factor* or the *mechanical storage factor* [4]. In addition to its definition as an amplification factor for displacement at resonance frequency, Q_m has another definition related with the bandwidth of the frequency response at resonance. It can be formulated as follows:

$$Q_m = \frac{f_n}{f_1 - f_2} = \frac{f_n}{\Delta f} \tag{2.10}$$

where f_1 and f_2 are the frequencies where the frequency response is half the value of the response at the resonance frequency. Therefore, Δf is the bandwidth of the frequency response around resonance.

The advantage of this modeling technique is that it can explicitly provide dimensions of the main transducer parts with respect to a set of required performance parameters. However, with the mass-spring model shown in Figure 2.1, only the dimensions of the head mass and piezoceramic stack can be given. With a little effort, it can also be possible to obtain rough dimensions for the tail mass while still using the same mass-spring model. For this purpose, a double-degree-of-freedom, hereafter referred to as DDF for conciseness, mass-spring system, which has the head mass and tail mass as separate masses, can be used and then reduced into a SDF system with a few approximations, in order to use the equations derived for the simpler case. The corresponding DDF mass-spring system is shown in Figure 2.3.

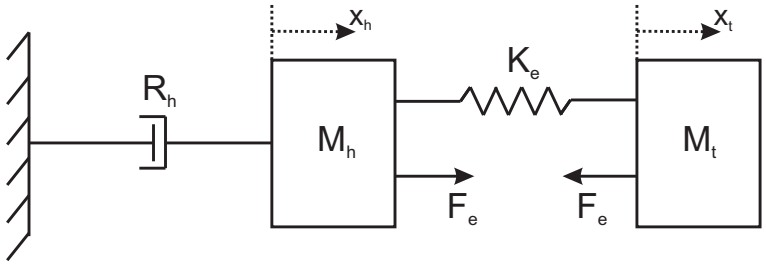

Figure 2.3: Sketch of the double-degree-of-freedom mass-spring system, including head mass, M_h, and tail mass, M_t, separately

The equations of motion for the DDF mass-spring system shown in Figure 2.3 can be expressed as follows:

$$M_h \frac{\mathrm{d}^2 \mathrm{x_h}}{\mathrm{d}t^2} = F_e + (x_t - x_h)K_e - R_h \frac{\mathrm{d}x_h}{\mathrm{d}t} \qquad M_h \frac{\mathrm{d}u_h}{\mathrm{d}t} = F_e + K_e \int (u_t - u_h)\mathrm{d}t - R_h u_h \tag{2.11}$$

$$M_t \frac{\mathrm{d}^2 \mathrm{x_t}}{\mathrm{d}t^2} = -F_e - (x_t - x_h)K_e \qquad M_t \frac{\mathrm{d}u_t}{\mathrm{d}t} = -F_e - K_e \int (u_t - u_h)\mathrm{d}t \tag{2.12}$$

The electrical equivalent circuit of the DDF mass-spring system with respect to Equations 2.11 and 2.12 is shown in Figure 2.4.

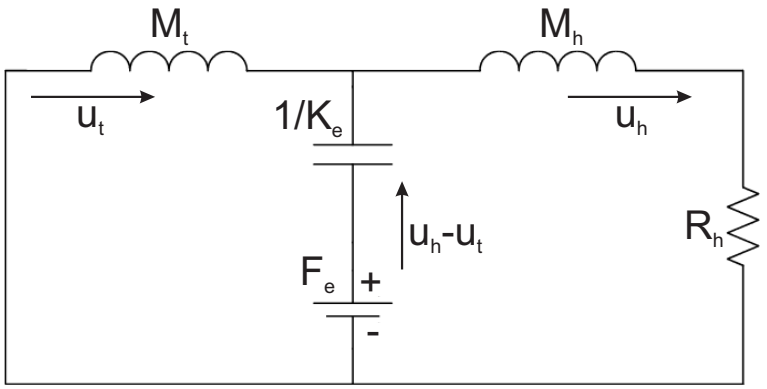

Figure 2.4: Electrical equivalent circuit of the double-degree-of-freedom mass-spring system shown in Figure 2.3

In Figure 2.3, the term R_h represents the radiation resistance (See Appendix A for further information about radiation impedance) due to the interaction between the head mass and the acoustic medium. There is no such term for the tail mass since acoustic radiation to the acoustic medium occurs only from the head mass and the tail mass vibrates in air or in a pressure release environment which provides negligible loss resistance in Tonpilz transducers. The electrical equivalent circuit of the DDF mass-spring system can be converted into the SDF electrical equivalent circuit shown in Figure 2.2 with the approximation, $R_h \ll \omega(M_h + M_t)$ [4]. Then, the effective mass, M_e, and the effective damper, R_e, shown in Figure 2.1 can be expressed as follows:

$$M_e = \frac{M_h M_t}{M_h + M_t} \qquad\qquad R_e \approx \frac{R_h}{(1 + M_h/M_t)^2} \tag{2.13}$$

According to Equation 2.13, the definitions of Q_m and ω_n represented in Equations 2.9 and 2.3, respectively, can be expanded as follows:

$$Q_m = \frac{\omega_n M_e}{R_e} = \omega_n \left(\frac{M_h M_t}{M_h + M_t}\right)\left[\frac{(M_h + M_t)^2}{M_t^2 R_h}\right]$$

$$= K_e^{0.5}\left(\frac{M_h + M_t}{M_h M_t}\right)^{0.5}\left[\frac{M_h M_t (M_h + M_t)}{M_t^2 R_h}\right] = \frac{(K_e M_h)^{0.5}}{R_h}\left(1 + \frac{M_h}{M_t}\right)^{1.5} \tag{2.14}$$

$$\omega_n = \sqrt{K_e\left(\frac{M_h + M_t}{M_h M_t}\right)} \tag{2.15}$$

In addition to Equations 2.14 and 2.15, the tail-to-head mass ratio, κ_{th}, is used to solve for the three unknowns: K_e, M_h, and M_t.

$$\kappa_{th} = M_t/M_h \tag{2.16}$$

Typically the designer has some freedom in specifying the tail-to-head mass ratio. Any value between 1 and 10 is reasonable [20], and typical values range between 2 and 4 [4]. The value basically represents the ratio of the vibration velocities of the head mass to the tail mass. Hence, the higher the tail-to-head mass ratio, the higher the vibration velocity of the head mass, which results in higher radiated acoustic power. However, above a certain value, weight might be a concern depending on the design constraints.

Hence, the unknowns K_e, M_h, and M_t can be found by solving Equations 2.14 - 2.16, simultaneously. However, radiation resistance, R_h, has to be known before solving Equation 2.14. In order to fix R_h, the shape and active surface dimensions of the head mass have to be determined first, and subsequently the radiation resistance can be found. The shape of the active surface of the head mass is often determined based on the application of the transducer. For instance, for a circular shaped head mass vibrating in a rigid baffle with a certain resonance frequency and active surface diameter, Figure A.1, which shows the analytical results for a circular piston in a rigid baffle, can be used to find the radiation resistance. Based on the operational scenarios of the transducer, the shape of the active surface of the head mass can be found. For instance, square-shaped head masses are popular in array applications for maximizing the active surface of the array by closely packing the active surfaces of the head masses. Circular or custom shaped head masses are used to achieve other goals. Also, directivity requirements of the transducer must be considered while determining the shape and the dimensions of the active surface of the head mass. The beam width requirement of the transducer can be used to find the necessary dimensions of the active surface of the head mass with respect to a pre-defined resonance frequency. For instance, for a circular piston vibrating in a rigid baffle, the following formulation can be used to determine the beam width of the transducer [4]:

$$p(r,\theta) = j\rho c k u_0 a^2 \frac{e^{-jkr}}{r} \frac{J_1(ka\sin\theta)}{ka\sin\theta} \tag{2.17}$$

where, θ is the angle relative to the acoustic axis of the transducer of the point where the pressure calculation is made, in the acoustic medium, r is the distance between the point in the medium and the acoustic center of the transducer, u_0 is the normal velocity of the piston with respect to the medium, k is the wavenumber, a is the radius of the circular piston, and ρ and c are the density and the sonic speed of the acoustic medium, respectively. If there is no directivity requirement, the dimension of the active surface can be determined with respect to the radiation resistance. Basically, the higher the radiation resistance, the higher the acoustic

power transmitted to the acoustic medium. To reiterate, while determining a dimension it should be noted that the dimensions of the transducers parts should be lower than one quarter of the wavelength in the corresponding material for lumped modeling. Then, the dimensions can be fine-tuned to any value needed by design requirements with more advanced models.

At this level of modeling, avoiding complex shapes for the transducer parts is best. Therefore, the geometric definition of the head mass can be completed with the addition of thickness to its active surface dimensions. However, to define the thickness, the material type has to be determined first. For high acoustic radiated power, a head mass with low weight relative to the tail mass is needed. Therefore, materials with low density such as aluminium, beryllium alloy AlBeMet, and magnesium with densities of 2700 kg/m^3, 2100 kg/m^3, 1770 kg/m^3, respectively, can be selected [4]. Hence, after selecting the material, the thickness of the head mass, t_h, can be found with the following expression:

$$t_h = M_h / A_h \rho_h \tag{2.18}$$

where A_h is the area of the active surface and ρ_h is the density of the material of the head mass. However, the thickness determined using Equation 2.18 needs to be much higher than the thickness which would result with the flexural mode of the head mass, which is explained in detail in Section 3.4. The formulation for the first flexural resonance frequency of the head mass in terms of its radius, a, sonic speed, c, and Poisson's ratio, υ, is as follows [4]:

$$f_{flex} = \frac{1.65 c t_{flex}}{4a^2 \sqrt{(1-\upsilon^2)}} \tag{2.19}$$

The flexural mode of the head mass must be at a significantly higher frequency than the resonance frequency of the transducer in order not to influence the function of the transducer based on its longitudinal mode. If the thickness determined using Equation 2.18 is lower than the one required in Equation 2.19, Equations 2.14 - 2.16 must be reiterated for the unknowns K_e, M_h, and M_t with a lower radius for the head mass. After the material and thickness of the head mass are defined, the dimensions of the piezoceramic stack are found. First, the material of the piezoceramics has to be selected. After selecting the material, knowing the value of K_e, which is equal to the stiffness of the piezoceramic stack in this model, one can find the ratio between the area, A_c, and length, l_c, of the piezoceramic stack as follows:

$$K_e = \frac{E_c A_c}{l_c} \qquad\qquad \frac{A_c}{l_c} = \frac{K_e}{E_c} \tag{2.20}$$

On the other hand, a practical value for the ratio of area of the active surface to area of piezoceramic stack, A_h/A_c, can be taken as [4]:

$$A_h/A_c = 5 \tag{2.21}$$

Hence, the length and area of the piezoceramic stack can be found using Equations 2.20 and 2.21. Only the inner and outer radii of the piezoceramic stack are left unknown. The inner and outer radii are assumed to scale with respect to a mean radius, which is defined with respect to the active surface, in a way that vibration of the piezoceramic stack has the least chance to excite the flexural modes of the head mass. For this purpose, the mean radius, r_{c_mean}, is defined as follows:

$$r_{c\_mean} = \sqrt{A_h/4\pi} \tag{2.22}$$

Hence, the inner radius, r_{c_i}, and the outer radius, r_{c_o}, are found as follows:

$$A_c = \pi\left[(r_{c\_mean} + \Delta r_c)^2 - (r_{c\_mean} - \Delta r_c)^2\right] \tag{2.23}$$

$$r_{c\_o} = r_{c\_mean} + \Delta r_c \tag{2.24}$$

$$r_{c\_i} = r_{c\_mean} - \Delta r_c \tag{2.25}$$

The dimensions of the tail mass are the remaining outputs of this method. When compared with the head mass and the piezoceramic stack, the tail mass may be considered as the simplest element in a Tonpilz-type transducer since it is not involved in acoustic radiation like the head mass or in a drive mechanism like the piezoceramic stack. It is there just to provide the required mass. Its geometry is modeled as a cylinder, which has a radius more than the outer radius of the piezoceramic stack and less than one quarter of the wavelength with respect to its material. Therefore, the material for the tail mass should also be selected before defining its dimensions. In order to reduce its volume, a material with high density such as steel and tungsten should be used for the tail mass. After defining the radius, r_t, and the material of the tail mass, the last dimension left, namely the length of the tail mass, l_t, is found as follows:

$$l_t = \frac{M_t}{\rho_t \pi r_t^2} \tag{2.26}$$

where ρ_t is the density of the material selected for the tail mass.

2.2 Lumped-Parameter Electrical Equivalent Circuit Model

Electrical equivalent circuits are powerful tools for gaining insight into the working principles of acoustic transducers as well as for designing acoustic transducers to certain specifications. Different electrical equivalent circuits with different levels of detail can be built for the same transducer. This modeling technique of electromechanical transducers has been studied for a long time and such models have been available in the literature for more than half a century [50, 51, 52, 53]. Since the focus of this research is on developing a design methodology for Tonpilz-type transducers rather than on developing novel modeling techniques, and since many very good equivalent circuit models already exist in the existing literature, a novel equivalent circuit model is not developed for this work. Rather the model by Sherman and Butler [4] is used, which is introduced in this section. The investigated model is based on the lumped-parameter representation of the transducer parts as ideal masses, springs, and dampers. The basis for this model is exactly the same as the one in the Simple Lumped-Parameter Model introduced in Section 2.1. However, a few additional transducer parts are included in this model, such as the stud, the mass of the piezoceramic stack, and the glue between the piezoceramic rings. Also, several electrical terms are included in the model. The schematic representation of the modeled transducer is shown in Figure 2.5. The electrical equivalent circuit adapted from Sherman and Butler is depicted in Figure 2.6. The model requires the physical dimensions and the material constants of the transducer parts as the inputs. Depending on these inputs, various outputs including electrical admittance and radiated acoustic power can be attained. The electrical equivalent circuit can be solved with the aid of electrical circuit software in the frequency domain. Hence, the frequency response of the transducer can be obtained accordingly.

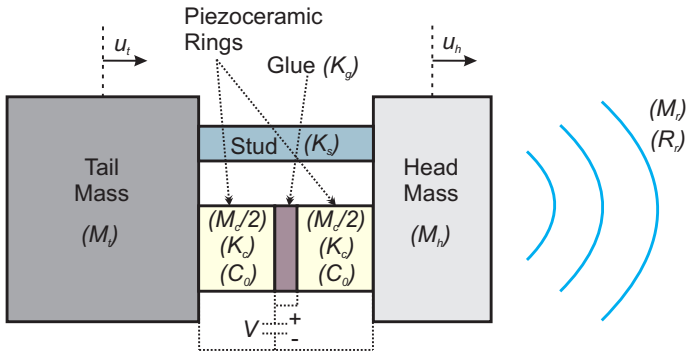

Figure 2.5: Schematic view of the modeled transducer (Adapted from [4])

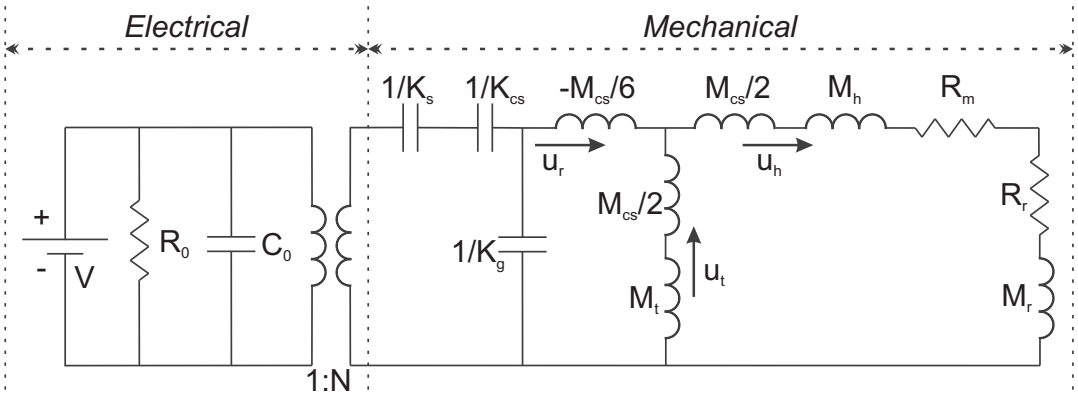

Figure 2.6: Electrical equivalent circuit of the transducer shown in Figure 2.5 (Adapted from [4])

The term N is called the *transduction coefficient* or *transformation ratio* [4, 20]. It defines the relationship between the applied electrical voltage, V, and the force generated, F, due to this voltage. It is mathematically represented as $N = F/V$. It has to be defined in terms of material constants and dimensional parameters in order to be used in the equivalent circuit shown in Figure 2.6. Such a definition for the lumped and 1-D case can be derived using the definition of d_{33} in Equation (1.11) as follows:

$$N = \frac{F}{V} = \frac{K_c \Delta t_c}{E t_c} = \frac{(A_c/t_c s_{33}^E)(S\, t_c)}{E t_c} = \frac{S}{E}\frac{A_c}{s_{33}^E t_c} = \frac{d_{33} A_c}{s_{33}^E t_c} \tag{2.27}$$

where E is the electric field applied through the thickness, S is the strain through the thickness, K_c is the short-circuit (E=0) stiffness, t_c is thickness, Δt_c is change in thickness due to the applied electric field, and A_c is the cross-sectional area of the piezoceramic rings constituting the stack.

The terms R_r and M_r in Figure 2.6 represent the radiation resistance and reactance, respectively. They are functions of both the wavelength and the geometrical shape of the transducer. For this level of modeling, in which the vibration velocity of the head mass is assumed to be uniform, simple analytical representations of these terms can be used. One of these models is introduced in Appendix A.2. However, in reality, the velocity of the head mass deviates from uniformity based on the mode shapes of the transducer.

The terms M_h, M_t, and M_c represent the masses of the head mass, the tail mass, and the piezoceramic stack, respectively. As depicted in Figure 2.6, the mass of the piezoceramic stack is divided into two parts and attached to both the head mass and the tail mass with series

connections. Also, the radiation impedance terms R_r, and M_r are connected serially to the head mass since the acoustic radiation to the medium is achieved by means of the head mass. In other words, the same velocity of vibration, u_h, is applicable to the head mass and the radiation impedance terms. The anti-phase motions of the head mass and the tail mass can be seen with the directions of the currents u_h and u_t (the velocity of vibration of the tail mass) in the equivalent circuit. Also, the parallel arrangement of the terms M_h and M_t means that the forces acting on the head mass and the tail mass are equal to each other.

The terms K_s, K_{cs}, and K_g represent the stiffnesses of the stud, piezoceramic stack (when E=0), and glue between the piezoceramic rings, respectively. The series arrangement of the terms $1/K_s$ and $1/K_{cs}$ in the equivalent circuit means that the displacements of the ideal springs representing the stud and the piezoceramic stack are equal to each other. Inherently, the forces required for these displacements are proportional with the magnitudes of their stiffnesses. In other and mechanically more meaningful words, a portion of the force generated by the piezoelectric effect is used to ensure the same displacement for the stud as for the piezoceramic stack. Therefore, the stiffer the stud, the more force required for its displacement. That is why the stiffness of the stud should be kept as low as possible in order not to affect the motion of the transducer adversely. Typical values for the ratio K_{cs}/K_s range between 5 and 15 [20]. After the part of the force used for the motions of the stud and the piezoelectric stack, the remaining force left from the piezoelectric effect equals to the force required to displace the glue as well as the total force required for the inertias of the masses, the radiation loading, and the loads due to mechanical dissipation during the acoustic radiation.

The term, C_0, is defined as the *clamped capacitance*. In this definition, *clamped* refers to the condition in which the strain parallel to the applied electric field is kept constant as zero. In other words, the motion of the piezoceramic is restricted in the clamped condition. With a similar approach, the free capacitance, C_f, can be defined as the capacitance in which the stress at the boundaries where the electric field is applied is kept constant as zero. In other words, the motion of the piezoceramic is not restricted in the free condition. The relationship between C_f and C_0 for the lumped & 1-D case is defined as follows:

$$\frac{C_0}{C_f} = 1 - k_{33}^2 \tag{2.28}$$

In Equation (2.28), the term k is called the *electromechanical coupling coefficient*. It can be defined as the ratio of the transduced mechanical energy to the input electrical energy or

vice versa [54]. Therefore, materials with high k shows better piezoelectric properties. In the corresponding notation, subscripts refer to the corresponding axes of the directions of the electric field and the strain in the material. The mathematical representations for C_f and k_{33}^2 for the lumped & 1-D case are as follows:

$$C_f = \frac{n\varepsilon_{33}^T A_c}{t_c} \tag{2.29}$$

$$k_{33} = \frac{d_{33}}{\sqrt{s_{33}^E \varepsilon_{33}^T}} \tag{2.30}$$

The term R_m represents the internal mechanical resistance of the transducer. Basically, it depends on the assembly details and increases with frequency [4]. For better acoustical radiation, it should be as low as possible when compared with the radiation resistance, R_r. Their relationship determines the mechanoacoustical efficiency, which typically ranges between 60% and 90%, with the following formulation [4]:

$$\eta_{ma} = \frac{R_r}{R_r + R_m} \tag{2.31}$$

The term R_0 represents the electrical resistance of the transducer due to the piezoceramic rings, which are electrically considered as capacitors. Therefore, it is the shunt resistance of these capacitors responsible for the electrical leakage. When the resistances due to cables etc. are ignored, the electromechanical efficiency, η_{em}, can be directly related with this term. The mathematical representation of R_0 can be expressed as follows:

$$R_0 = (\omega C_f \tan\delta)^{-1} \tag{2.32}$$

R_0 and R_m are the only dissipative elements in the electrical equivalent circuit shown in Figure 2.6. At mechanical resonance and with the exception of the term C_0 all capacitive elements in the electrical equivalent circuit tend to vanish, which leads to the effective usage of the electrical source in terms of acoustic radiation. Even better effectiveness can be achieved by tuning out the electrical capacitive term, C_0, at resonance with a suitable electrical circuitry located between the source and the transducer. The meanings of capacitive and dissipative elements should not be mixed though. Capacitive elements determine the relationship between the required and the used amounts of power drawn from the source whereas dissipative elements, which are considered in the calculations of efficiencies, determine the relationship between the total power used and the power used for the desired outcome.

2.3 Matrix Model

Matrix models can be labeled as the most advanced analytical tools for the design, analysis and evaluation of electroacoustic transducers. Before moving into them deeply, it is better to go over their evolution. In fact, matrix models are just simpler and easier representations of the distributed models that originate from lumped-parameter models. Let us consider the long rod with length, L, and cross-sectional area, A, divided into sections with lengths, Δx, as shown in Figure 2.7(a) and assume that the diameter of the rod is very small compared to its length. Therefore, the rod can have a 1-D lumped-parameter representation with ideal masses and springs for the x-direction as shown in Figure 2.7(b).

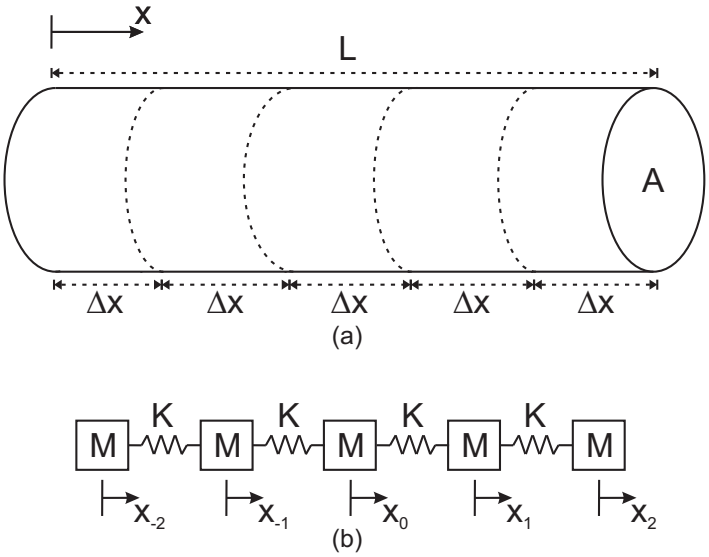

Figure 2.7: (a) A sketch of a long rod, and (b) its 1-D lumped-parameter representation with ideal masses and springs

In Figure 2.7(b), $M = \rho A \Delta x$ is the mass of each section, and $K = E_Y A/\Delta x$ is the stiffness of the ideal springs connecting the adjacent masses serially, where ρ is density and E_Y is the modulus of elasticity for the rod material. Also, x_i for i=[-2, 2] represents the displacements of the corresponding masses along the x-axis. Accordingly, the equation of motion for the lumped mass with the displacement vector, x_0, can be written as follows:

$$M\frac{\partial^2 \xi_0}{\partial t^2} = K(\xi_1 - \xi_0) - K(\xi_0 - \xi_{-1})$$

$$\frac{\partial^2 \xi_0}{\partial t^2} = \frac{E_Y}{\rho}\frac{(\xi_1 - \xi_0)/\Delta x - (\xi_0 - \xi_{-1})/\Delta x}{\Delta x} \tag{2.33}$$

If the number of sections in Figure 2.7(a) approaches to infinity, which also corresponds to $\Delta x \rightarrow 0$, one can reach to the famous 1-D wave equation, applicable for the whole rod, using Equation 2.33 as follows:

$$\frac{\partial^2 \xi}{\partial t^2} = c^2 \frac{\partial^2 \xi}{\partial x^2} \tag{2.34}$$

where $c = \sqrt{E_Y/\rho}$ is the sonic speed, more formally the speed of the longitudinal waves, inside the rod. Hence, the wave equation is derived with an approach based on lumped elements. Actually, the word *distributed* in the term "distributed models" symbolizes the continuous distribution of ideal masses and springs all through the material [4]. The general solution of the 1-D wave equation for displacement can be expressed in a complex sinusoidal form as follows:

$$\xi(x,t) = Xe^{-i(kx-\omega t)} + Ye^{i(kx+\omega t)} \tag{2.35}$$

where ω is the angular frequency and $k = \omega/c$ is the Helmholtz number. The time independent solutions for the particle velocity, $u(x)$, and the force, $F(x) = AE_Y(\partial\xi/\partial x)$, can be expressed with respect to Equation 2.35 as follows:

$$u(x) = i\omega\left[Xe^{-ikx} + Ye^{ikx}\right] \tag{2.36}$$

$$F(x) = -ikAE_Y\left[Xe^{-ikx} - Ye^{ikx}\right] \tag{2.37}$$

where X and Y are the constants to be determined with respect to the boundary conditions. Hence, the relationship between the mechanical impedances ($Z = F/u$) at x =0, Z_0, and at x =L, Z_L, also known as the transmission line equation, can be expressed using Equations 2.36 and 2.37, as follows [4]:

$$Z_0 = \frac{\rho cA\left[Z_L + i\rho cA\tan(kL)\right]}{\rho cA + iZ_L\tan(kL)} \tag{2.38}$$

The same relation in Equation 2.38 can be expressed in matrix form as well in terms of the forces F_0 and F_L and the velocities u_0 and u_0 at locations x =0 and x =L, respectively, in the long rod shown in Figure 2.7(a) as follows:

$$\begin{bmatrix} F_0 \\ F_L \end{bmatrix} = \begin{bmatrix} z_a & -z_b \\ z_b & -z_a \end{bmatrix} \begin{bmatrix} u_0 \\ u_L \end{bmatrix} \tag{2.39}$$

where

$$z_a = -i\rho cA\cot(kL) \qquad\qquad z_b = -i\rho cA\sin(kL)$$

Hence, the 1-D matrix model of a long rod is obtained, which can also be used in order to analyze systems including numerous such rods of different materials connected serially to each other. Such serial connections of 3 long bars, for which 1-D modeling is acceptable due to suitable cross dimensions, are shown in Figure 2.8(a). Also, forces, F, and velocities, u, at the boundaries are shown in Figure 2.8(b) for each bar.

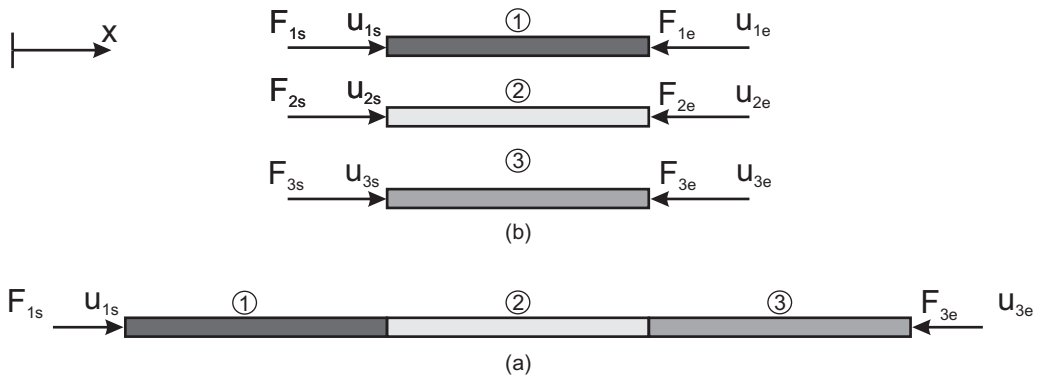

Figure 2.8: Sketches of (b) the 3 bars with different materials and boundary conditions, and (a) the assembly constituted by serial connection of these bars

As shown in Figure 2.8(b), the bars labeled as ①, ②, and ③ have serial connections with each other. The frequency response of the whole assembly at its two boundaries in terms of the forces and the velocities can be found by simultaneous solution of the following equations regarding to both the individual bars and their boundary conditions:

$$\begin{bmatrix} F_{1s} \\ F_{1e} \end{bmatrix} = \begin{bmatrix} z_{1a} & -z_{1b} \\ z_{1b} & -z_{1a} \end{bmatrix} \begin{bmatrix} u_{1s} \\ u_{1e} \end{bmatrix} \qquad \begin{bmatrix} F_{2s} \\ F_{2e} \end{bmatrix} = \begin{bmatrix} z_{2a} & -z_{2b} \\ z_{2b} & -z_{2a} \end{bmatrix} \begin{bmatrix} u_{2s} \\ u_{2e} \end{bmatrix} \qquad \begin{bmatrix} F_{3s} \\ F_{3e} \end{bmatrix} = \begin{bmatrix} z_{3a} & -z_{3b} \\ z_{3b} & -z_{3a} \end{bmatrix} \begin{bmatrix} u_{3s} \\ u_{3e} \end{bmatrix}$$

$$F_{1e} = F_{2s} \qquad F_{2e} = F_{3s}$$

$$u_{1e} = u_{2s} \qquad u_{2e} = u_{3s}$$

It is also possible to obtain matrix models for piezoelectric materials, simply by constituting their coefficient matrix with respect to the governing equations related with piezoelectricity. In addition to the mechanical ports considered for isotropic metals, an electrical port is also involved in the matrix models of piezoelectric materials in order to represent the voltage and the current. Therefore, systems comprising of both kinds of materials, such as Tonpilz-type transducers, can be modeled by identifying the correct boundary conditions between connecting materials and solving the corresponding matrix equations accordingly.

However, for longitudinally oscillating transducers, such as Tonpilz-types, 1-D modeling can only provide reasonable results if the lateral dimensions of the transducer are less than one quarter of the longitudinal oscillation's wavelength in the corresponding materials constituting the transducer [55]. However, even with such conditions, radial modes of the transducer still affect the longitudinal modes and decrease the accuracy of 1-D models. Especially, the radial modes of the piezoceramic rings in Tonpilz-type transducers have a strong influence on the longitudinal modes of the whole structure [56]. In addition, representing parallel components in an assembly, such as the stud being parallel to the piezoceramic stack in Tonpilz-type transducers, is not possible with 1-D transmission line models. Therefore, 3-D (actually 2-D axisymmetric) analytical models have been developed in order to take both the radial and the longitudinal modes into account and obtain more accurate results. In general, these 3-D analytical models can be divided into two groups as equivalent circuit models and matrix models. Actually, both kinds of these models are based on the same coupled differential wave equations but only their representations are different. The studies of Lin [57, 58, 59] and the study of Feng *et al.* [60] can be shown as examples involving equivalent circuit models of piezoelectric materials with different geometries. On the other hand, the studies of Iula *et al.* involve the first-time modeling of a transducer constituted by their 3-D matrix model of a piezoelectric cylindrical disk [47, 61, 62]. As an improvement to these, the studies of Mančić offer 3-D matrix models of both piezoelectric and isotropic materials for the geometries of cylindrical ring and disk [46, 56, 63]. In this section, Mančić's model [56] is presented as the representative matrix model, which is also used in the following chapters.

In Mančić's matrix model, the piezoceramic ring is modeled as a transfer function involving 5 inputs which lead to 5 outputs. The model can also be considered as a 5-port network element. The model is applicable to piezoceramic rings or disks polarized parallel to their thickness direction. The inputs of the model are the forces acting on the 4 contour surfaces, namely top, bottom, inner circumferential, and outer circumferential surfaces, and the voltage difference between the planar surfaces which leads to an electric field parallel to the thickness. Hence, the outputs are the velocities of the corresponding 4 contour surfaces and the current between the planar surfaces. In fact, the inputs and the outputs can be switched but the velocities and the currents are usually the unknowns in practice. The geometry considered in the model with the model parameters and dimensions are shown in Figure 2.9(a). Also, the 5-port network element representation of the piezoceramic ring modeled is shown in Figure 2.9(b).

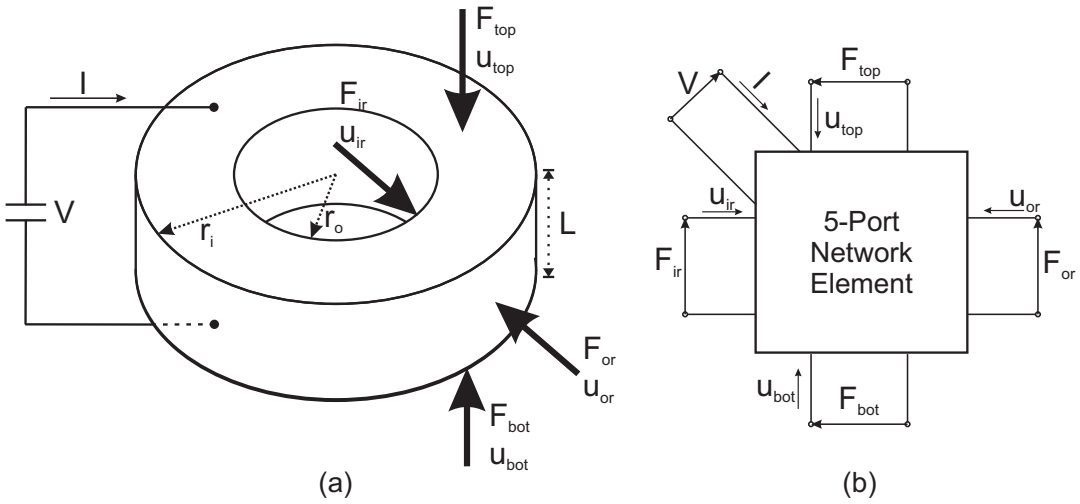

Figure 2.9: (a) Model parameters & dimensions, and (b) 5-port network element representation of the piezoceramic ring subjected to the matrix model (Adapted from [56])

The model is obtained by approximate solution of two coupled wave differential equations, resembling oscillations in axial and radial directions, with two orthogonal wave functions in a cylindrical coordinate system. Therefore, only the motions in the axial and radial directions are considered in the model, which actually makes the model 2-D. However, due to axial symmetry, it can be considered as a 3-D model despite the exclusion of the torsion and shearing stresses, which are actually negligible in the motion of Tonpilz-type transducers. The forces acting on the 4 contour surfaces, the voltage difference between the planar surfaces, the velocities and the current are assumed to be uniformly distributed over the corresponding surfaces. In addition, electric fields in the radial and circumferential directions are taken as zero since they can be assumed negligible in these directions. Also, the material is modeled as ideal, and therefore without any losses. Since any output in the model is dependent on all the inputs, the model is capable of coupling axial and radial modes. It is possible to connect numerous network elements from their corresponding ports to mathematically represent the structures created by assembling different types of materials, and investigate their mechanical and electrical responses. Also, acoustic impedances of the surroundings can be applied as loads from the corresponding ports to the modeled structures. For instance, radiation impedance can be applied as a loading from the port corresponding to the active surface of the head mass of a Tonpilz-type transducer, which leads to the calculations regarding acoustic radiation. The mathematical representation of the matrix model for piezoceramic rings and disks with the corresponding constants are as follows:

$$\begin{bmatrix} F_{ir} \\ F_{or} \\ F_{top} \\ F_{bot} \\ V \end{bmatrix} = \begin{bmatrix} z_{11} & z_{12} & z_{13} & z_{13} & z_{15} \\ z_{21} & z_{22} & z_{23} & z_{23} & z_{25} \\ z_{13} & z_{23} & z_{33} & z_{34} & z_{35} \\ z_{13} & z_{23} & z_{34} & z_{33} & z_{35} \\ z_{15} & z_{25} & z_{35} & z_{35} & z_{55} \end{bmatrix} \begin{bmatrix} u_{ir} \\ u_{or} \\ u_{top} \\ u_{bot} \\ I \end{bmatrix} \tag{2.40}$$

$$z_{11} = \frac{-2\pi L}{j\omega}\left\{c_{12}^{D} - c_{11}^{D}\left[1 - k_r r_i(A_1 J_0(k_r r_i) + B_1 Y_0(k_r r_i))\right]\right\}$$

$$z_{22} = \frac{2\pi L}{j\omega}\left\{c_{12}^{D} - c_{11}^{D}\left[1 + k_r r_o(A_2 J_0(k_r r_o) + B_2 Y_0(k_r r_o))\right]\right\}$$

$$z_{12} = \frac{-2\pi k_r r_i L c_{11}^{D}}{j\omega}\left[A_2 J_0(k_r r_i) + B_2 Y_0(k_r r_i)\right]$$

$$z_{21} = \frac{-2\pi k_r r_o L c_{11}^{D}}{j\omega}\left[A_1 J_0(k_r r_o) + B_1 Y_0(k_r r_o)\right]$$

$$z_{13} = \frac{2\pi r_i c_{13}^{D}}{j\omega} \qquad z_{15} = \frac{2\pi r_i L h_{31}}{j\omega\pi(r_o^2 - r_i^2)} \tag{2.41}$$

$$z_{23} = \frac{2\pi r_o c_{13}^{D}}{j\omega} \qquad z_{25} = \frac{2\pi r_i L h_{31}}{j\omega\pi(r_o^2 - r_i^2)}$$

$$z_{33} = \frac{c_{33}^{D} k_z \pi(r_o^2 - r_i^2)}{j\omega\tan(k_z L)} \qquad z_{34} = \frac{c_{33}^{D} k_z \pi(r_o^2 - r_i^2)}{j\omega\sin(k_z L)}$$

$$z_{35} = \frac{h_{33}}{j\omega} \qquad z_{55} = \frac{L}{j\omega\varepsilon_{33}^{S}\pi(r_o^2 - r_i^2)}$$

$$A_1 = \frac{Y_1(k_r r_o)}{J_1(k_r r_i)Y_1(k_r r_o) - J_1(k_r r_o)Y_1(k_r r_i)} \qquad A_2 = \frac{Y_1(k_r r_i)}{J_1(k_r r_i)Y_1(k_r r_o) - J_1(k_r r_o)Y_1(k_r r_i)}$$

$$B_1 = \frac{J_1(k_r r_o)}{J_1(k_r r_o)Y_1(k_r r_i) - J_1(k_r r_i)Y_1(k_r r_o)} \qquad B_2 = \frac{J_1(k_r r_i)}{J_1(k_r r_o)Y_1(k_r r_i) - J_1(k_r r_i)Y_1(k_r r_o)}$$

$$k_r = \frac{\omega}{\sqrt{c_{11}^{D}/\rho}} \qquad k_z = \frac{\omega}{\sqrt{c_{33}^{D}/\rho}} \tag{2.42}$$

where, k_r and k_z are the wavenumbers defined with respect to the sonic speeds in the radial and axial directions, respectively.

The same model is applicable for isotropic metals as well by the exclusion of the electrical port. Also, due to isotropy, the stiffness coefficients, c_{ij}, can be expressed in terms of the Lame's coefficients, λ_m and μ, which are functions of Poisson's ratio, υ, and the modulus of elasticity, E_Y. Also, Helmholtz numbers for radial and longitudinal directions are the same. The mathematical representation of the matrix model for isotropic metal rings and disks with the corresponding constants are as follows:

$$\begin{bmatrix} F_{ir} \\ F_{or} \\ F_{top} \\ F_{bot} \end{bmatrix} = \begin{bmatrix} z_{11} & z_{12} & z_{13} & z_{13} \\ z_{21} & z_{22} & z_{23} & z_{23} \\ z_{13} & z_{23} & z_{33} & z_{34} \\ z_{13} & z_{23} & z_{34} & z_{33} \end{bmatrix} \begin{bmatrix} u_{ir} \\ u_{or} \\ u_{top} \\ u_{bot} \end{bmatrix} \tag{2.43}$$

$$z_{11} = \frac{-2\pi L}{j\omega} \{c_{12} - c_{11} [1 - kr_i(A_1 J_0(kr_i) + B_1 Y_0(kr_i)]\}$$

$$z_{22} = \frac{2\pi L}{j\omega} \{c_{12} - c_{11} [1 + kr_o(A_2 J_0(kr_o) + B_2 Y_0(kr_o)]\}$$

$$z_{12} = \frac{-2\pi kr_i L c_1}{j\omega} [A_2 J_0(kr_i) + B_2 Y_0(kr_i)]$$

$$z_{21} = \frac{-2\pi kr_o L c_1}{j\omega} [A_1 J_0(kr_o) + B_1 Y_0(kr_o)]$$

$$z_{13} = \frac{2\pi r_i c_{12}}{j\omega} \qquad z_{23} = \frac{2\pi r_o c_{12}}{j\omega}$$

$$z_{33} = \frac{c_{11} k\pi (r_o^2 - r_i^2)}{j\omega \tan(kL)} \qquad z_{34} = \frac{c_{11} k\pi (r_o^2 - r_i^2)}{j\omega \sin(kL)}$$

$$c_{12} = c_{13} = \lambda_m \qquad c_{11} = c_{33} = \lambda_m + 2\mu$$

$$\lambda_m = \frac{\upsilon E_Y}{(1+\upsilon)(1-2\upsilon)} \qquad \mu = \frac{E_Y}{2(1+\upsilon)}$$

$$k = k_r = k_z = \frac{\omega}{\sqrt{c_{11}/\rho}}$$

where the constants, A_1, A_2, B_1, and $B2$ are the same as the ones presented for the matrix model of piezoelectric rings and disks.

Hence, one can model structures consisting of different kinds of materials connected together either in parallel or serially, such as Tonpilz-type transducers, by using Mančić's 3-D matrix model and analyze their frequency responses accordingly.

2.4 Finite Element Model

The finite element (FE) method has been used for solving a wide range of engineering and scientific problems after its introduction by Turner et. al. in 1956 [64]. In the FE method, approximate results are obtained numerically with respect to the governing partial differential equations for the problem domains subjected to general boundary conditions [65]. The fundamental idea on which FE method is based is the *discretization* of the problem domain into a finite number of *elements* and then the combination of the discrete solutions for these elements is obtained in order to achieve the solution for the whole problem [66]. In general, analytical approaches can only offer solutions, though usually exact and continuous, for problems which involve significant simplifications and assumptions. Even a small amount of complexity in the problem domain can make obtaining an analytical solution extremely difficult. For instance, even though Tonpilz transducers with head masses having a square-shaped active surface have been used extensively in underwater applications for more than half a century, no analytical model has been published for such head masses. On the other hand, the discretization in the FE method allows solution to large and complex problems by reducing them to smaller and simpler problems in a systematic manner. However, FE method can only provide approximate solutions, with an accuracy changing in parallel with the intensity of discretization.

The FE method consists of 3 major steps: 1) preprocessing; 2) solution; and 3) postprocessing. Preprocessing is the stage where the problem is defined in the numerical environment. Preprocessing mainly involves the definitions of geometry, material properties, element types to be used for discretization, element connectivities (mesh), and boundary conditions including constraints and loadings with respect to the investigated problem. Preprocessing can be considered as the most important stage in FE modeling, since wrongly defined problems can only lead to incorrect results, which is best described by the phrase: *"Garbage In, Garbage Out"* [67]. The model is ready for solution after the preprocessing. Solution is the stage where the governing algebraic equations in matrix form for each element are assembled and solved simultaneously for the unknowns, namely the degrees-of-freedom of the elements such as displacement, pressure, and voltage. Then, the derived variables based on the unknowns, such as stress, and electric charge, are computed by back substitution. In postprocessing, which is the final stage in a FE analysis, the results obtained in the solution stage can be sorted, printed, plotted, animated, or manipulated to obtain even more information about the problem. [68]

Rapid developments in computer technology enabled a FE method revolution for the design, analysis and evaluation of electroacoustic transducers [4]. From these perspectives, the FE method is the most powerful modeling technique available today when compared with the techniques introduced in Sections 2.1 - 2.3, since it can provide more information than the other techniques. Detailed information, such as the stress distribution throughout the analyzed structure, is readily available within the FE solutions. In addition, structures that are more complex than the ones suitable for analysis with the other techniques, including irregular boundaries, can be handled with the FE method [69]. However, all these benefits come with a major cost that is the time required for preparation and computation. Also, sometimes it can be challenging to prepare a FE model realistically due to crowded structural variables like in the case of flextensional transducers [70]. Nevertheless, due to its significant advantages, the FE method has been used extensively for scientific and engineering purposes in the analysis of electroacoustic transducers, such as Tonpilz-type transducers [42, 45, 71, 72, 73].

By its very nature, FE method can be placed somewhere between the lumped-parameter and matrix models explained in the previous sections. In FE models, the structure being investigated is divided into lumped sections as shown in Figure 2.7 but unlike distributed models, the number of these sections is kept at a finite level. Therefore, Figure 2.7 can be considered as a FE model which has 5 elements corresponding to 5 sections. In the FE method, such discretization is made through a very systematic fashion by means of various types of elements. Every element consists of a number of nodes which vary with the element's type. All numerical calculations are based on the nodes, and the relation between the nodes are described within the governing algebraic equations of the corresponding element depending on the element's type. Therefore, all the masses, loads, motions etc. are associated with the nodes in a FE model. The elements and nodes of a 2-D FE model for an arbitrary Tonpilz transducer are shown in Figure 2.10. The quality of element connectivities, also referred to as the mesh, of a FE model directly determines the quality of a FE model. Completely different results can be obtained for the same structure modeled with different meshes. Therefore, the mesh of a FE model should be in accordance with the properties of the elements used in order to accurately reflect reality.

In addition to the mesh, the number of elements used in a FE model is directly related with the accuracy of the solution. In general, the larger the number of elements, the closer the nodes in the mathematical representation of the structure, the better the approximation of the

continuum in the structure, and hence the higher the accuracy for the FE model. However, care must be taken while increasing the number of elements, since an excessively large number of elements may decrease the accuracy of the model due to accumulation of numerical errors. Additionally, the time required for computation always gets longer as the number of elements increases in FE models.

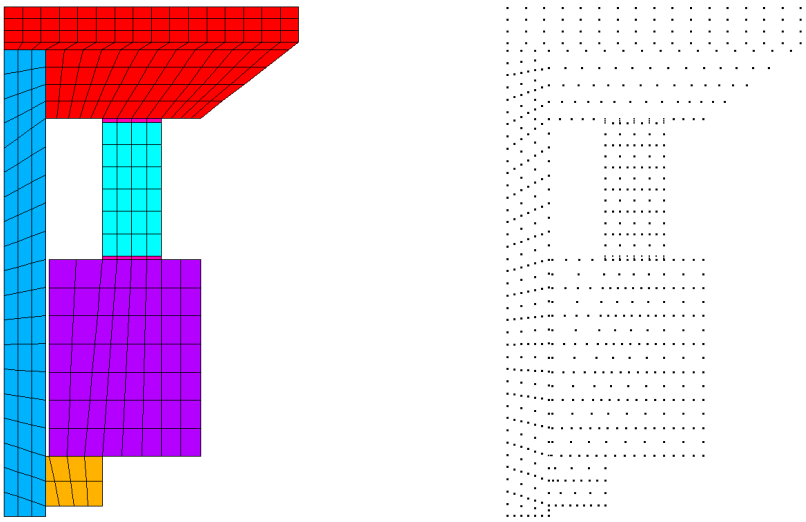

Figure 2.10: (a) Elements (different colors for different materials), and (b) nodes of a 2-D finite element model for an arbitrary Tonpilz transducer

In addition to the number of elements, the accuracy of the results obtained is also directly related with the accuracy of the material properties defined in a FE model [73]. Incorrect application of the material properties always yields wrong results. The required material constants differ with respect to the analysis type. In order to run a harmonic response analysis involving a piezoacoustic transducer coupled with an acoustic medium, which is the subject of the present work, definitions of the isotropic metals, piezoceramics and acoustic medium are needed. For the isotropic metals, three material properties, namely, modulus of elasticity, Poisson's ratio, and density are sufficient. For the piezoceramics, stiffness matrix, piezoelectric matrix, and dielectric matrix, all defined with respect to the polarization direction, are required in addition to the density. On the other hand, the sonic speed and density are the only material properties required for modeling of the acoustic medium. All the material properties used in the FE models presented in this work can be found in Appendix B.

The FE model presented in this section and used in the following sections is built with the FE software package ANSYS, which is also used in several studies available in the literature [42, 69, 70, 73]. A generic representation of the FE models of the Tonpilz-type transducers used in the present work is shown in Figure 2.11. The list of other software packages capable of modeling electroacoustic transducers include, but is not limited to, ATILA, COMSOL, and PZFlex. Several types of analysis are available within these FE packages. For the investigation of Tonpilz-type tranducers, harmonic response analysis of the transducers are conducted within ANSYS. In such an analysis, the steady-state response of the transducer subjected to an alternating voltage can be computed for the frequency band of interest. In the solution stage of the FE analysis, a combined matrix equation which includes all the governing equations, such as the equation of motion for the displacement degree-of-freedom (DOF), regarding the DOF's of each node is solved. For the harmonic response analysis, the following matrix equation in the sinosuidal form is solved for each node representing the isotropic metals within the transducer:

$$\left[[K] - \omega^2[M]\right]\{x\} = \{F\} \tag{2.44}$$

where $[K]$ is the stiffness matrix, [M] is the mass matrix, $\{x\}$ is the mechanical displacement vector, and $\{F\}$ is the force vector. For the nodes representing the acoustic medium, the governing equation is in a similar form with Equation 2.44 with the major difference being that pressure and not displacement is the DOF of interest. The coupling of the fluid and structural elements is provided within the elements located at the fluid-structure interface by means of a coupling matrix in the numerical calculations for these nodes. For the piezoelectric materials, the coupling of the mechanical and electrical terms is achieved by the solution of the following coupled matrix equations for the corresponding DOF's associated with the nodes representing such materials:

$$\begin{bmatrix} \left[K^E\right] + j\omega\,[R] - \omega^2\,[M] & -[N] \\ [N]^t & \left[C^S\right] \end{bmatrix} \begin{Bmatrix} \{x\} \\ \{V\} \end{Bmatrix} = \begin{Bmatrix} \{F\} \\ \{Q\} \end{Bmatrix} \tag{2.45}$$

where $[K^E]$ is the short-circuit (E=0) stiffness matrix, $[R]$ is the resistance matrix based on the acoustic radiation, [N] is the transduction coefficient matrix, $\left[C^S\right]$ is the clamped capacitance matrix, $\{V\}$ is the voltage vector, and $\{Q\}$ is the charge vector [4]. More detailed information regarding the theory of FE method is available in diverse sources in the literature [45, 65, 66, 68, 74].

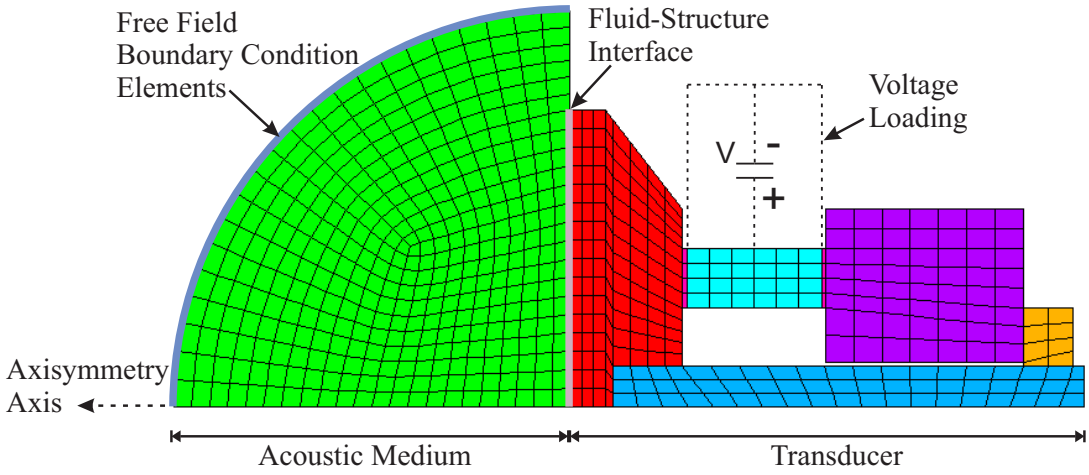

Figure 2.11: A generic representation of the finite element models built for the investigation of Tonpilz-type transducers for the present work

Several rules, assumptions and specifications are applicable for all the FE models built within ANSYS throughout the present work. Since the aim is presenting a methodology, Tonpilz-type transducers with complex shapes are avoided. Only the transducers whose 3-D structure can be simulated with a 2-D axissymmetric FE model are considered. Therefore, all the element types used in the FE models are 2-D and capable of providing means for an axis-symmetric analysis. The acoustic medium is defined by FLUID29 elements, which involve pressure and displacement DOF's. However, the displacement DOF's are only applicable for the nodes existing at the fluid-structure interface shown in Figure 2.11. The free-field boundary condition at the outer circumference of the acoustic medium is modeled by FLUID129 elements which practically absorb the incident acoustic waves and eliminate their reflection back through the acoustic medium. All isotropic metals except the head mass are defined by PLANE82 elements which provide a total of 8 nodes including mid-nodes. To avoid problems at the fluid-structure interface due to midnodes, the head mass is modeled by PLANE42 elements which only have 4 nodes. In addition to the 2 displacement DOF's for the 2 principle axes for all the structural nodes, elements representing the piezoceramics, PLANE223, also provide a DOF for voltage. Alternating voltage is applied by means of the voltage DOF of the nodes existing at the planar surfaces of the piezoceramic rings and electromechanical coupling is provided by the PLANE223 elements. Lastly, as a reasonable assumption for Tonpilz-type transducers, all the transducer parts are glued to each other. Hence, one can obtain direct (pressure, displacement, voltage) or derived (acoustic power, electrical admittance) frequency responses of Tonpilz-type transducers by the FE model introduced in this section.

CHAPTER 3

VALIDATION OF MODELING TECHNIQUES

In order to test the validity of the models introduced in Chapter 2, in-water measurements for the Tonpilz-type transducer with 50 kHz resonance frequency presented in the PhD dissertation of Bayliss are used [75]. A photograph of the transducer taken from Bayliss' study, and a view of its model built in the present work with the same viewing angle are shown in Figure 3.1. As mentioned in Bayliss' dissertation, the design of the transducer belongs to J. R. Dunn [76]. However, since the physical dimensions and the properties of the constituting materials of the transducer are taken from Bayliss' dissertation, the transducer is referred to as "Bayliss' 50 kHz Tonpilz" throughout the present work. While modeling the transducer, slight simplifications are made in the physical dimensions. The material properties for the transducer are shown in Appendix B. All the physical dimensions with the corresponding simplifications for the modeled transducer are presented in Appendix C.

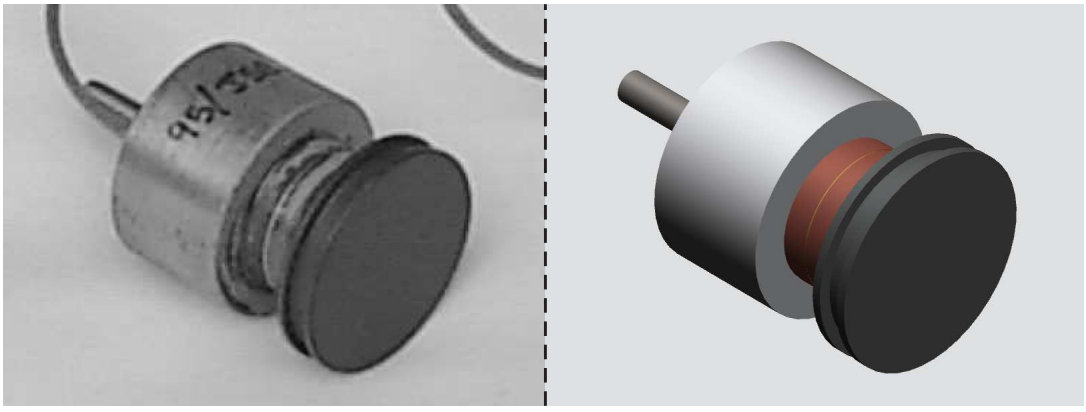

Figure 3.1: Bayliss' 50 kHz Tonpilz: (a) real [75], and (b) model

Of all the available measurement data in Bayliss' dissertation, only in-water conductance, G, and transmitting voltage response, TVR, measurements are considered for benchmarking the models built with respect to the modeling techniques introduced in Chapter 2. Conductance, which is an electrical term, is probably the best metric representing the motional response of an electroacoustic transducer working under constant voltage. Under such a condition, the peaks in the conductance plot at certain frequencies correspond to the resonances at these frequencies for the transducer [20]. On the other hand, TVR results of the models are also checked, since TVR can be considered as the most important final output of an electroacoustic transducer. In order to make the figures presenting the measurement data in Bayliss' dissertation more useful, these figures were digitized with the software Engauge Digitizer [77]. In-water measurement results of the conductance and TVR for Bayliss' 50 kHz Tonpilz are shown in Figure 3.2 and Figure 3.3, respectively [75]. The measurement results for the conductance look continuous due to the sufficiently large number of data points collected, but TVR measurements were made only at a smaller number of frequencies, resulting with a slight non-uniform trend in the TVR graph shown in Figure 3.3. In addition, in-water measurement testing conditions such as the mounting of the transducer and acoustic medium properties contribute to the non-smooth trends of both the conductance and TVR measurement results.

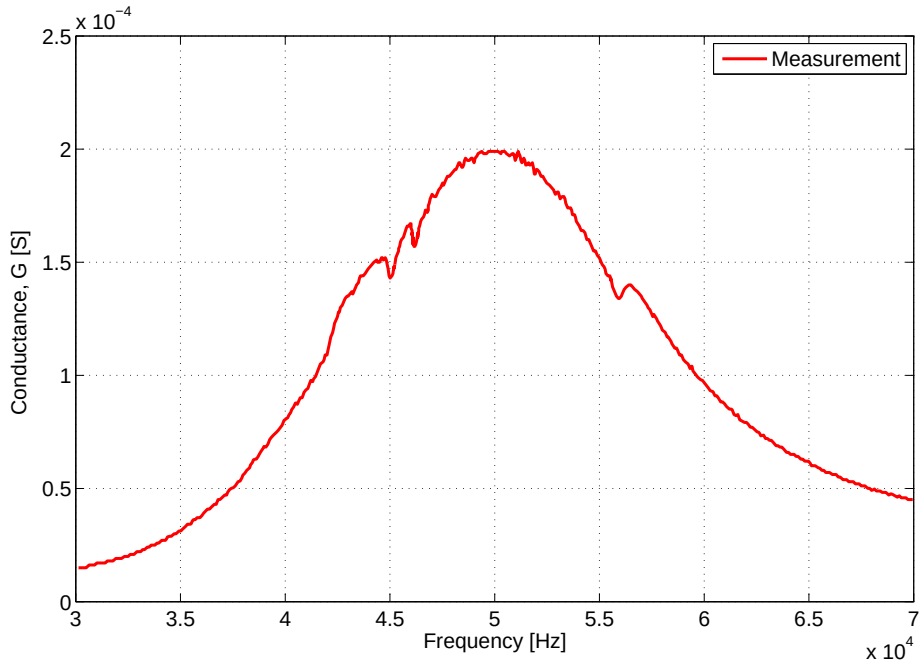

Figure 3.2: In-water conductance measurement results for the Bayliss' 50 kHz Tonpilz

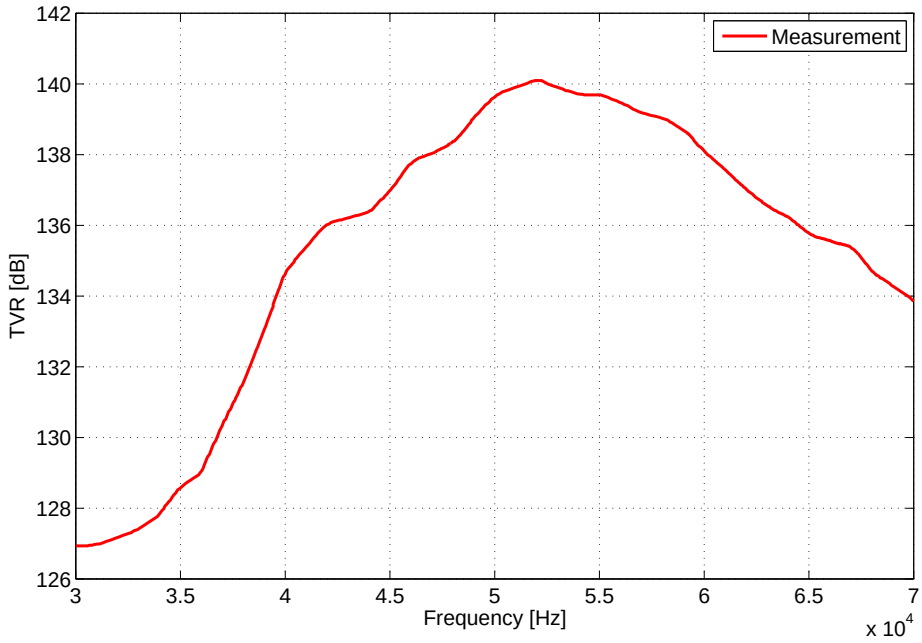

Figure 3.3: In-water TVR measurement results for the Bayliss' 50 kHz Tonpilz

For the in-water measurements, the transducer was put into a suitable housing by Bayliss for which only the active surface of the transducer was in contact with the water. The electrical components of the transducer were isolated from the water by means of an o-ring which prevents the in-gress of water in to the housing. The rigid baffle condition can be assumed when modeling the transducer due to the extended planar surface of the housing near the active surface of the transducer.

3.1 Validation of the Simple Lumped-Parameter Model

In contrast with the other models, the Simple Lumped-Parameter Model introduced in Section 2.1 is specifically developed to yield an initial approximation of the physical dimensions for the design of Tonpilz-type transducers based on a desired performance criteria. With respect to the intended use of the model, the resonance frequency, f_n, and the mechanical quality factor, Q_m, are sufficient for the model to provide rough physical dimensions as outputs for the transducer parts. Since the exact physical dimensions as well as the performance metrics of the Bayliss' 50 kHz are known, two methods can be used for testing the validity of the

Simple Lumped-Parameter Model. First, the desired performance metrics can be used in order to obtain physical dimensions which can then be compared with the actual dimensions of the transducer. Second, the actual dimensions of the Bayliss' 50 kHz Tonpilz can be used with the governing equations of the model in order to obtain the estimated performance metrics, which can then be compared with the actual performance metrics of the transducer. Due to the large number of physical dimensions and the differences in the geometrical shapes of the actual and modeled transducer parts, such as the head mass which has a semi-conical shape in the actual transducer whereas it is defined as a cylinder in the model, the second benchmarking method is preferred. When this second benchmarking method is used, it is also possible to compare the accuracy of the model with the other models, since they all provide performance metrics with respect to the pre-defined physical dimensions and material properties. Hence, in order to run the Simple Lumped-Parameter Model in reverse, masses of the head mass, M_h, and tail mass, M_t, and stiffness of the piezoceramic stack, K_{cs}, are needed. The corresponding values for the head mass and tail mass for Bayliss' 50 kHz Tonpilz are tabulated in Table 3.1.

Table 3.1: Data regarding the Head Mass and Tail Mass of Bayliss' 50 kHz Tonpilz

Transducer Part	Volume [mm^3]	Density [kg/m^3]	Mass [kg]
Head Mass	2826	2710	7.66E-3
Tail Mass	6567	7700	50.57E-3

Hence, the effective mass for Bayliss' 50 kHz Tonpilz is determined using Equation 2.13 as follows:

$$M_e = \frac{M_h M_t}{M_h + M_t} = 6.651 \times 10^{-3}\ kg$$

The effective stiffness, K_e, is determined considering the serial arrangement of the piezoceramic rings using the corresponding data in Appendices B and C as follows:

$$K_e = \frac{A_c}{n_c s_{33}^E t_c} = 1.083 \times 10^9\ N/m$$

where n_c corresponds to the number of piezoceramic rings in the piezoceramic stack. Hence, the estimated resonance frequency of the Bayliss' 50 kHz Tonpilz with respect to the Simple Lumped-Parameter Model is determined using Equation 2.4 as follows:

$$f_n = \frac{\omega_n}{2\pi} = \frac{1}{2\pi}\sqrt{\frac{K_e}{M_e}} = 64.2\ kHz$$

In order to determine the mechanical quality factor for the model, the radiation resistance must be known first. The radiation resistance, R_h, at the estimated resonance frequency with respect to the active surface radius of the Bayliss' 50 kHz Tonpilz, while considering the acoustic medium as water, is determined using Equation A.2 as follows:

$$R_h = Re(Z_r) = \rho c A\left(1 - \frac{J_1(2ka)}{ka}\right) = 764.9\ kg/s \qquad where \quad k = \frac{2\pi f_n}{c}$$

After having the radiation resistance for the corresponding resonance frequency, the estimated mechanical quality factor of the Bayliss' 50 kHz Tonpilz with respect to the Simple Lumped-Parameter Model is determined using Equation 2.14 as follows:

$$Q_m = \frac{(K_e M_h)^{0.5}}{R_h}\left(1 + \frac{M_h}{M_t}\right)^{1.5} = 4.65$$

Since conductance is the direct indicator of the motional response of the transducer, the resonance frequency and mechanical quality factor for the Bayliss' 50 kHz Tonpilz are determined with respect to the conductance measurements. The measurement and the Simple Lumped-Parameter Model results regarding the resonance frequency and mechanical quality factor of the Bayliss' 50 kHz Tonpilz are presented in Table 3.2. Absolute percent relative errors of the model results with respect to the measurement are also given in Table 3.2.

Table 3.2: The Measurement and the Simple Lumped-Parameter Model Results regarding the Resonance Frequency and Mechanical Quality Factor for the Bayliss' 50 kHz Tonpilz

Performance Metric	Measurement	Simulation	Relative Error [%]
Resonance Frequency (f_n)	50 kHz	64.2 kHz	28.4
Mechanical Quality Factor (Q_m)	2.74	4.65	69.7

Since the lateral dimensions of the Bayliss' 50 kHz Tonpilz are comparable with its longitudinal dimensions, the model's relative error is as high as 28.4% with respect to f_n. Even though the model contains a significant number of simplifying assumptions, the predicted Q_m is also of the correct magnitude but has a greater error than f_n. Overall, the accuracy of the model for the Bayliss' 50 kHz Tonpilz is acceptable and within expectations. Similar accuracies can be expected for any Tonpilz-type transducer, and better accuracies may be possible for transducers having negligible lateral dimensions with respect to their longitudinal dimensions. Therefore, the Simple Lumped-Parameter Model introduced in Section 2.1 can be used as a starting point for designing Tonpilz-type transducers.

3.2 Validation of the Lumped-Parameter Electrical Equivalent Circuit Model

The Lumped-Parameter Electrical Equivalent Circuit Model introduced in Section 2.2 can be used to predict both the conductance and TVR for the frequency band of interest, which are used for benchmarking the model. Since the model is built as an electrical circuit, it is straightforward to obtain conductance results. However, certain assumptions have to be made in order to obtain TVR results. First, it is assumed that the head mass of the transducer is vibrating with a spatially uniform velocity, like a piston. Therefore, any flexural motion with the head mass is neglected. Second, it is assumed that plane wave acoustic intensity is applicable 1 m away from the transducer, which is a very reasonable assumption for Bayliss' 50 kHz Tonpilz. Hence, Equation 1.16 introduced in Section 1.5.1 with η_{ea}=100% as discussed below is used in order to obtain the TVR results.

$$TVR = 10\log(W_a) + DI + 170.8\,dB \tag{3.1}$$

where W_a is the radiated acoustic power in watts and DI is the directivity index. The formulation of DI introduced in Equation 1.15 for the case of a cylindrical piston radiating in a rigid baffle, which is applicable to the Bayliss' 50 kHz Tonpilz due to the uniform velocity assumption, can be used in Equation 3.1. The radiated acoustic power can be calculated by the following formulation [4] using Equation A.2 for the radiation resistance, R_r, and the current at R_r's branch in the electrical circuit shown in Figure 2.6 which refers to the oscillation velocity of the head mass according to the impedance analogy:

$$W_a = |u_{rms}|^2 R_r \tag{3.2}$$

In order to run the model, all the parameters existing in the electrical equivalent circuit shown in Figure 2.6 have to be fixed first. Since it is not possible to determine the efficiencies accurately, especially the mechanoacoustic efficiency, the model is assumed to be ideal without any electrical or mechanical losses (i.e., η_{ea}=100%). Therefore, the power dissipation is only due to the acoustic radiation, which practically leads R_0 and R_m in Figure 2.6 to be zero. The values of the terms representing the masses of the head mass and tail mass, which are M_h and M_t, respectively, in Figure 2.6, are taken from Table 3.1, since they are identical with the ones used for the validation of the Simple Lumped-Parameter Model in Section 3.1. The same situation is also applicable for the stiffness of the piezoceramic stack, that is $K_{cs} = 1.083 \times 10^9\ N/m$ as

used in Section 3.1. The stiffnesses for the glue between the piezoceramic rings and the stud are estimated as $K_g = 5.456 \times 10^9\, N/m$ and $K_s = 6.919 \times 10^7\, N/m$, respectively, with respect to the physical dimensions in Appendix C and the material properties in Appendix B. Similarly, the mass of the piezoceramic stack is estimated as $M_{cs} = 4.53 \times 10^{-3}\, kg$. The transduction coefficient for the piezoceramics, N, is determined using Equation 2.27 as follows:

$$N = \frac{d_{33} A_c}{s_{33}^E t_c} = 0.626\, N/V$$

The last parameter to be determined in Figure 2.6 is the clamped capacitance of the piezoceramic stack, C_0, which is determined by combining Equations 2.28 and 2.29 as follows:

$$C_0 = \frac{n \varepsilon_{33}^T A_c}{t_c} \left(1 - k_{33}^2\right) = 3.942 \times 10^{-10}\, F$$

Hence, the model is run for the frequency range [30, 70] kHz with a step size of 0.05 kHz. The in-water conductance and TVR results of the Lumped-Parameter Electrical Equivalent Circuit Model of Bayliss' 50 kHz Tonpilz are shown in Figures 3.4 and 3.5, respectively, with the measurement results. The resonance frequency and mechanical quality factor, which are based on the conductance results shown in Figure 3.4, are given in Table 3.3 with the absolute percent relative errors with respect to the measured values.

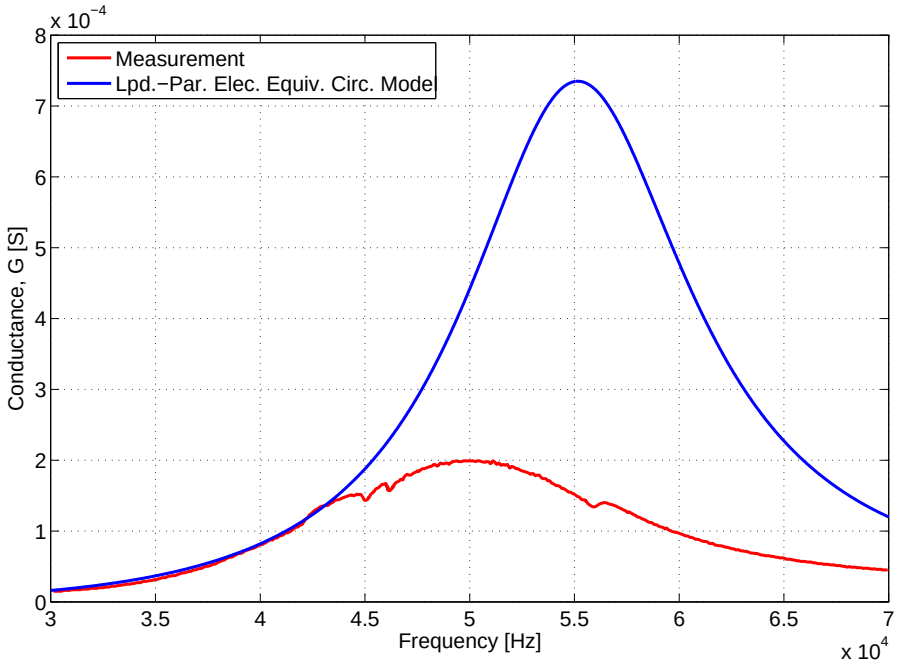

Figure 3.4: Lumped-Parameter Electrical Equivalent Circuit Model and measurement results for in-water conductance of the Bayliss' 50 kHz Tonpilz

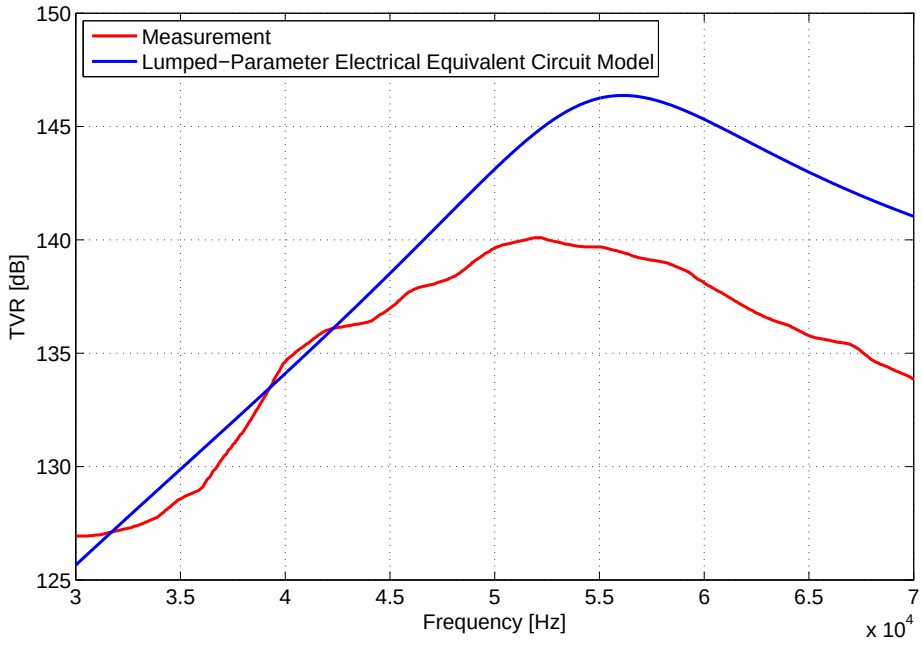

Figure 3.5: Lumped-Parameter Electrical Equivalent Circuit Model and measurement results for in-water TVR of the Bayliss' 50 kHz Tonpilz

According to the results, the inclusion of the stiffnesses of the stud and glue and the mass of the piezoceramic stack in the model result in significantly better accuracy for the estimated resonance frequency when compared with the Simple Lumped-Parameter model. The reasons for the differences in the peak values of both conductance and TVR are due to not considering the electrical and mechanical dissipation terms and assuming uniform velocity for the head mass within the model as well as limitations in the overall capability of the model. The shift of about 2 kHz in the TVR result when compared with the conductance result for both the experiment and simulation is related to the directivity index which increases with frequency. Therefore, even though the transducer has a resonance frequency at 50 kHz, it provides a better sound pressure level around 52 kHz.

Table 3.3: The Measurement and the Lumped-Parameter Electrical Equivalent Circuit Model Results regarding the Resonance Frequency and Mechanical Quality Factor for Bayliss' 50 kHz Tonpilz

Performance Metric	Measurement	Simulation	Relative Error [%]
Resonance Frequency (f_n)	50 kHz	55.2 kHz	10.4
Mechanical Quality Factor (Q_m)	2.74	4.29	56.6

3.3 Validation of the Matrix Model

Both the in-water conductance and TVR results can be obtained with the Matrix Model with the same approach used for the Lumped-Parameter Electrical Equivalent Circuit Model in Section 3.2. However, the Matrix Model is much more detailed than the Lumped-Parameter Electrical Equivalent Circuit Model since all the parts constituting the transducer are considered with their dimensions and more detailed material properties are used. As is also discussed in Section 2.3, the geometry of all the transducer parts are represented with network elements shaped as full or hollow cylinders in the Matrix Model. Then, these elements are connected to each other axially, radially, or both axially and radially in order to fulfill the boundary conditions of the corresponding transducer parts. Therefore, the whole transducer is represented with the network elements through the proper connections of the elements.

In order to connect the elements, the transducer parts which have geometrical shapes other than full or hollow cylinders also need to be represented with such shaped elements. Such representation is achieved either by simplifying the corresponding geometries into the available element geometries, or by representing these transducer parts as a combination of the available element geometries.

For instance, the head mass of Bayliss' 50 kHz Tonpilz has a complex geometry, which cannot be represented in terms of full or hollow cylinders. Therefore, it is simplified into a geometry which can be represented as a combination of a full cylinder and a hollow cylinder. The simplification is made in a way that the total mass, thickness, and the active surface dimensions of the head mass are kept identical in both the actual and modeled versions of the head mass.

On the other hand, the geometry of the tail mass is represented as a combination of 4 hollow cylinders with the necessary connections and without any simplification in the Matrix Model of Bayliss' 50 kHz Tonpilz. The reason for dividing the tail mass into 4 regions is to increase the accuracy of the element connections in the model. Exactly the same reason is applicable for representing the stud with 5 full cylinders. The cross-sectional view of the Bayliss' 50 kHz Tonpilz and its representation in the Matrix Model are shown in Figure 3.6. The transducer is represented with a total of 15 network elements which are labeled with the corresponding numbers shown in Figure 3.6(b).

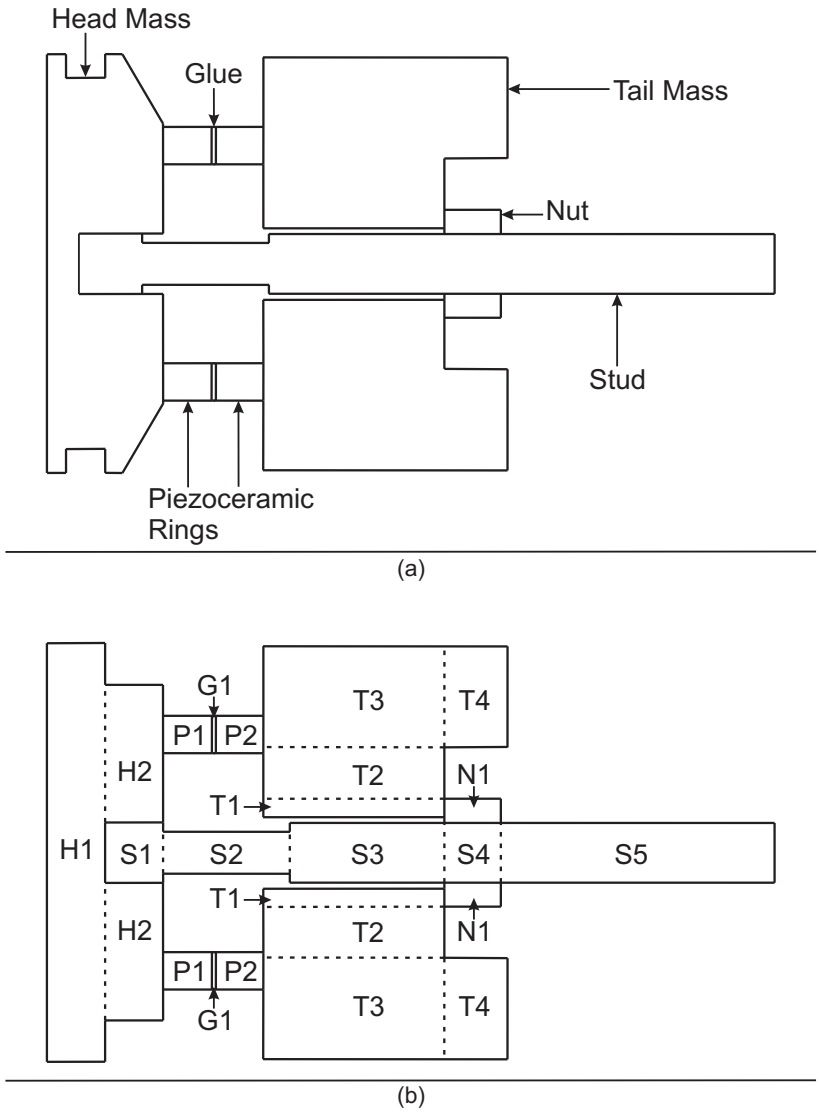

Figure 3.6: (a) Cross-sectional view of the Bayliss' 50 kHz Tonpilz and (b) its representation in the Matrix Model

In Figure 3.6, the thicknesses of the glue and the gap between the stud and tail mass are exaggerated for easier visualization. Other than that, both the cross-sectional view and its representation in the Matrix Model are depicted as having proportionally scaled-down dimensions of the Bayliss' 50 kHz Tonpilz. The connections between the network elements in the Matrix Model can be seen in Figure 3.6(b). The actual Matrix Model with the corresponding network elements is depicted in Figure 3.7(a). To reiterate, the 5-port network element representation of a piezoceramic ring that is introduced in Section 2.3 is shown in Figure 3.7(b). Also, the orientation of the transducer as well as the corresponding constituent network elements according to which the Matrix Model is built are shown in Figure 3.7(c).

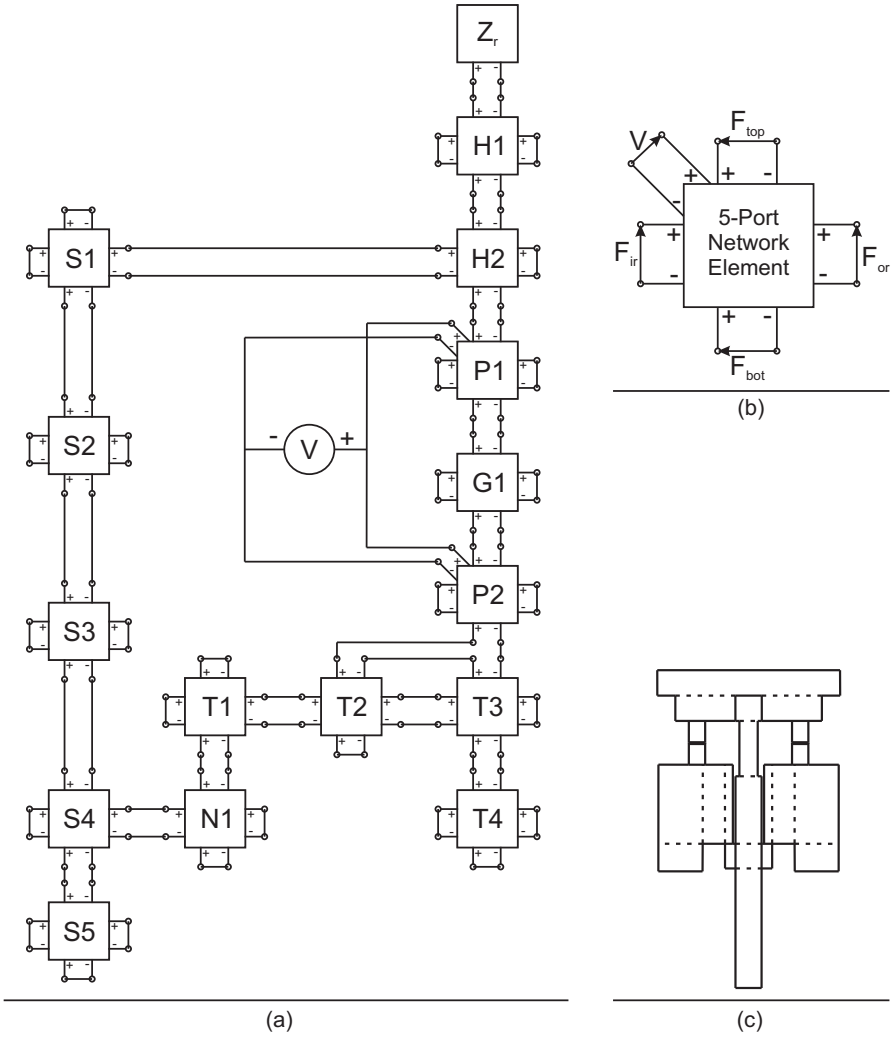

Figure 3.7: (a) The Matrix Model of Bayliss' 50 kHz Tonpilz with (b) the representation of a sample network element and (c) the orientation of the modeled transducer

The applied voltage and radiation impedance of the acoustic medium are assumed to be the only boundary conditions for Bayliss' 50 kHz Tonpilz in the model. Since all the surfaces except the active surface of the head mass are in-contact with air which has negligible acoustic impedance when compared with water, this assumption is reasonable. Therefore, all the ports representing the transducer boundaries except the electrical ports of the piezoceramic rings and the mechanical port representing the active surface of the head mass are short-circuited, which corresponds to a stress-free state. The radiation impedance is represented by the network element labeled as Z_r and it is modeled using Equation A.2 which is applicable for the case of uniform velocity of the head mass in a rigid baffle. Z_r is connected to the network element representing the head mass from the port which corresponds to the active surface.

For the transducer parts whose geometry are modeled by full cylinders such as the stud, a value very close to zero is used as the inner diameter needed by the corresponding network element. As an improvement over the 1-D transmission line models, the ports at the top of the network elements labeled $T2$ and $T3$ are connected to the bottom port of the network element $P2$ since it reflects the physics of the transducer better. This connection means that the sum of the forces acting towards the top surfaces of the elements T2 and T3 is equal to the force acting on the bottom surface of the element $P2$. However, such a representation cannot be valid for all similar connections. Even though the same situation would appear to be applicable between the elements $H2$, $S1$, and $H1$ with respect to Figure 3.6, such a representation would conflict with the physics of the transducer. Therefore, care must be taken while making the connections between the network elements.

The in-water conductance and TVR results of the Matrix Model of the Bayliss' 50 kHz Tonpilz with a step size of 0.05 kHz are shown in Figures 3.8 and 3.9, respectively, with the measurement results. The resonance frequency and mechanical quality factor, which are based on the conductance results shown in Figure 3.8, are given in Table 3.4 with the absolute percent relative errors with respect to the measured results.

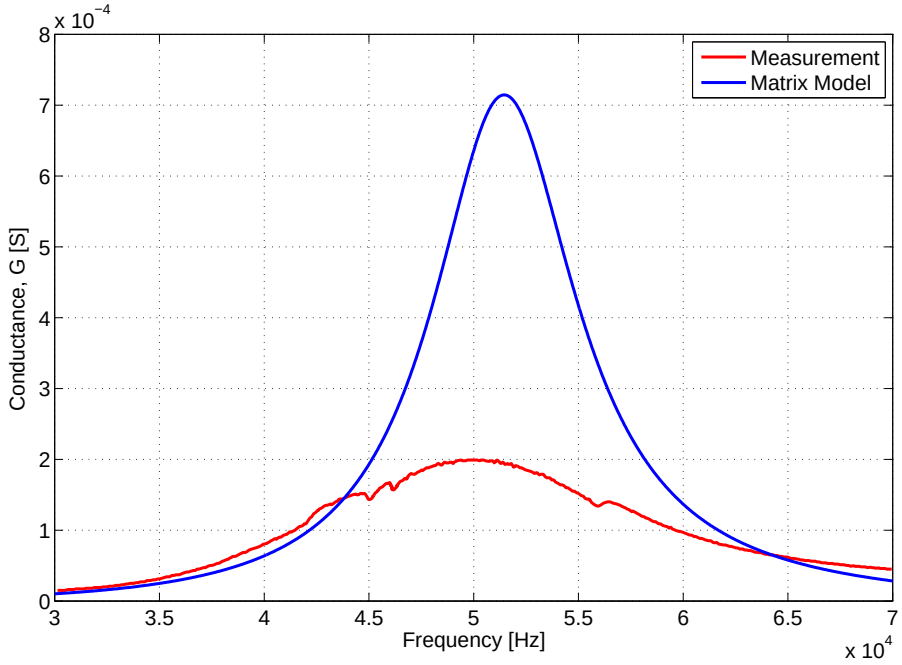

Figure 3.8: The Matrix Model and measurement results for in-water conductance of the Bayliss' 50 kHz Tonpilz

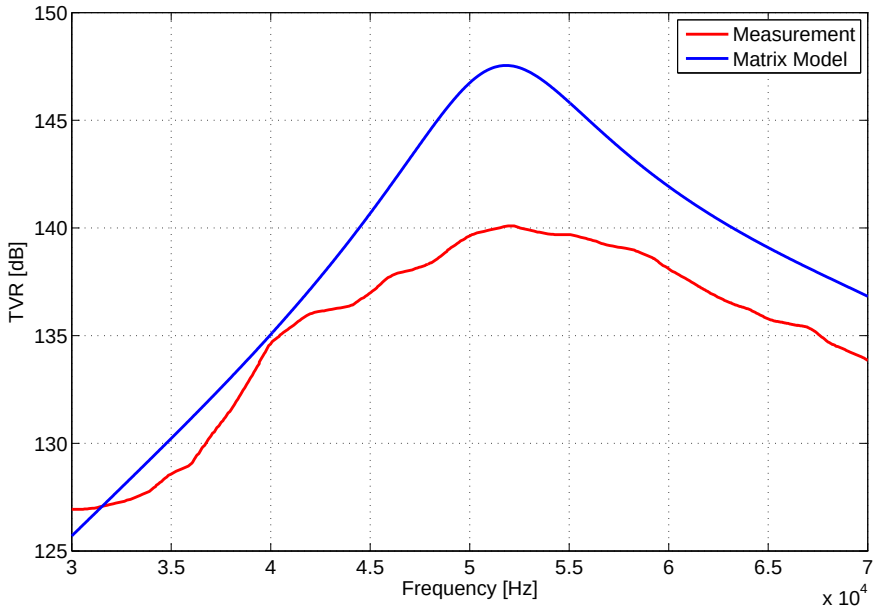

Figure 3.9: The Matrix Model and measurement results for in-water TVR of the Bayliss' 50 kHz Tonpilz

According to the results shown in Figures 3.8 and 3.9, and in Table 3.4, a detailed application of the dimensional and material properties of the transducer leads to a greater accuracy in the estimated resonance frequency despite the remaining simplifications within the model. This increase in accuracy can be attributed to the 2-D nature of the model that considers both the axial and radial modes of the Bayliss' 50 kHz Tonpilz, which actually has comparable axial and radial dimensions. In addition, the trends of the results obtained by the model are in accordance with the measurements, except for the high differences around resonance which can be related with the ideal working conditions considered in the model. However, a relatively worse accuracy is obtained for the mechanical quality factor when compared with the models validated in the previous sections which can be related with in-depth assumptions within the Matrix Model.

Table 3.4: The Measurement and the Matrix Model Results regarding the Resonance Frequency and Mechanical Quality Factor for Bayliss' 50 kHz Tonpilz

Performance Metric	Measurement	Simulation	Relative Error [%]
Resonance Frequency (f_n)	50 kHz	51.5 kHz	3
Mechanical Quality Factor (Q_m)	2.74	6.24	127.7

3.4 Validation of the Finite Element Model

Unlike the other models of the Bayliss' 50 kHz presented in the previous sections, the FE Model does not involve major geometrical simplifications. For instance, the conical shape of the head mass and the o-ring slot on the head mass are included in the FE Model. However, the representation of the hexagonal nut as a hollow cylinder and the non-existence of the electrodes and the narrow cylindrical hole at the tail mass for the cables connected to the electrodes are minor simplifications implemented in the FE Model in order to ensure axisymmetry. The FE Model of Bayliss 50 kHz Tonpilz is shown in Figure 3.10. In the figure, different materials are represented by different colors. Also, the transducer parts and the acoustic medium with their corresponding element types used for modeling in ANSYS are shown in Figure 3.10. As for the Matrix Model of Bayliss' 50 kHz Tonpilz, in the FE Model the transducer is assumed to be working in a rigid baffle and all of its surfaces except the one in-contact with the acoustic medium are in-contact with a vacuum. In accordance with the other modeling techniques introduced, the transducer parts are assumed to be rigidly connected to each other in the FE Model.

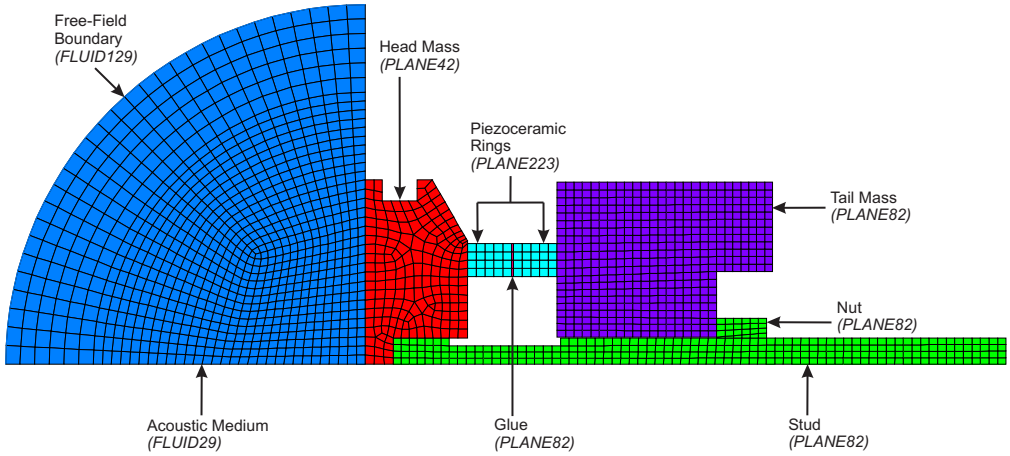

Figure 3.10: The FE Model of the Bayliss' 50 kHz Tonpilz

As for the other modeling techniques introduced in the previous sections, the FE Model is also capable of providing the in-water conductance and TVR results which are used for benchmarking the model's accuracy. Although the conductance result is obtained with exactly the same procedure conducted in the Lumped-Parameter Electrical Equivalent Circuit Model and the Matrix Model, the TVR result is obtained differently. Instead of using Equation 3.1 to

calculate TVR with respect to the radiated power and directivity index, TVR is directly obtained by reading the already calculated pressure values of the nodes representing the acoustic medium in the FE solution. The superiority of having the acoustic medium in the FE Model also provides a means for obtaining performance metrics of the transducer related with the acoustic medium such as beam width and directivity index. The steady-state pressure distribution in the water in front of the Bayliss' 50 kHz Tonpilz working at 50 kHz obtained by the FE Model is shown in Figure 3.11. In the figure, the radius of the acoustic medium is increased 10 times more than the one shown in Figure 3.10 for better visualization of the pressure fluctuation generated by the transducer.

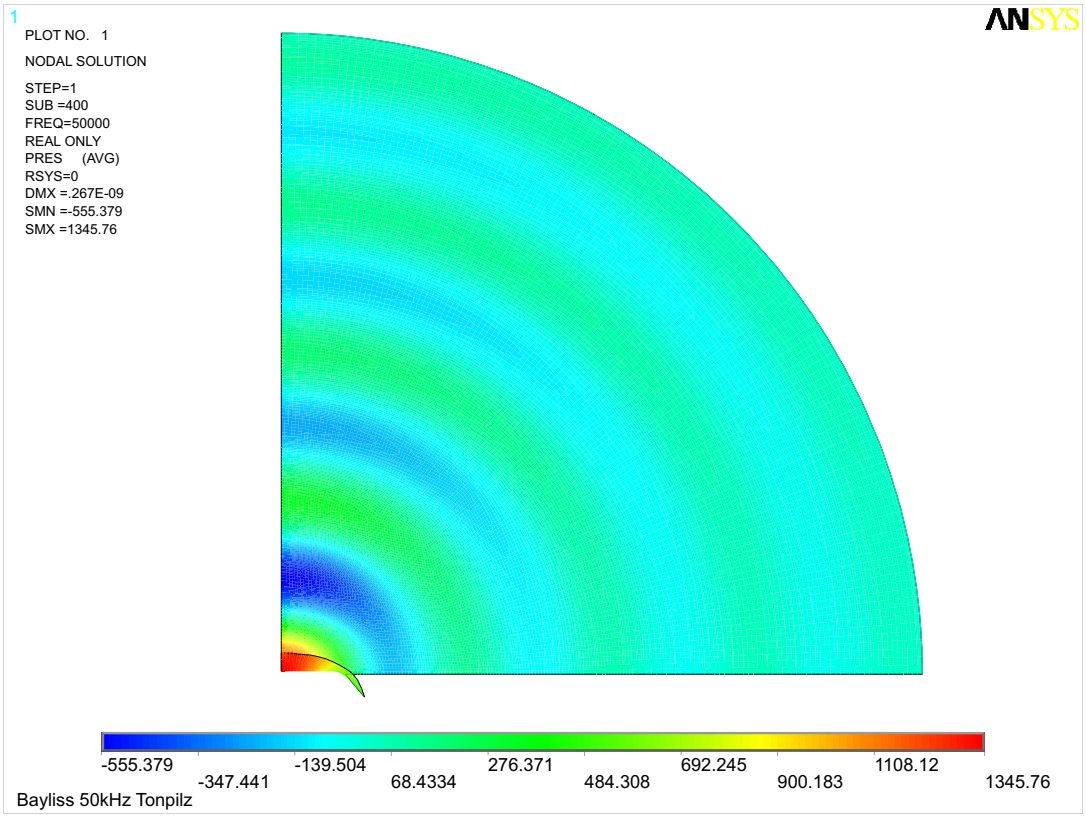

Figure 3.11: The steady-state pressure distribution in the water in front of the Bayliss' 50 kHz Tonpilz working at 50 kHz obtained by the FE Model (The values in the contour legend are in Pascals)

Hence, the in-water conductance and TVR results of the FE Model for Bayliss' 50 kHz Tonpilz with a step size of 0.05kHz are shown in Figures 3.12 and 3.13, respectively, with the measurement results. The resonance frequency and mechanical quality factor, which are based on the conductance results shown in Figure 3.12, are given in Table 3.5 with the absolute percent relative errors with respect to the measured results.

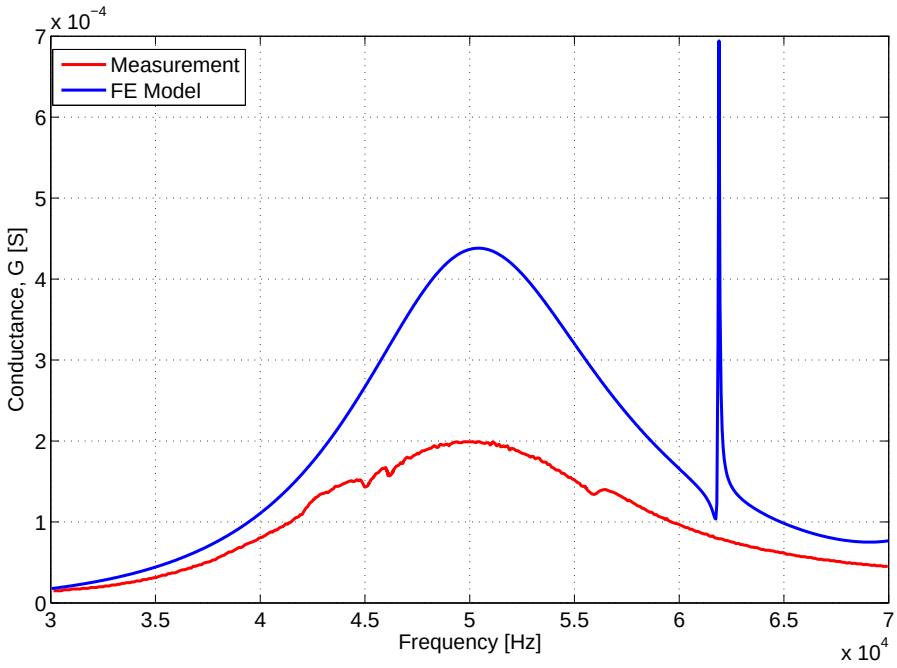

Figure 3.12: The FE Model and measurement results for in-water conductance of the Bayliss' 50 kHz Tonpilz

As expected, the most accurate results are obtained with the FE Model due to the most realistic nature of the FE Model when compared with the modeling techniques validated in the previous sections. The accuracy of 0.8% for the estimated resonance frequency with respect to the measurement clearly show that the FE modeling technique is appropriate for fine-tuning resonance frequencies while designing Tonpilz-type transducers. The mechanical quality factor is also much closer to the measured value when compared with the values obtained with the other validated models. Although the 29.5% relative error for the mechanical quality factor may look quite high, it is expected since the dissipative terms which determine the efficiency of the transducer are not involved in the model. Therefore, such an accuracy with the mechanical quality factor indicates a good representation of the behaviour of the transducer. It can also be seen through the trends of the model results shown in Figures 3.12 and 3.13 with respect to the measurement results. The ideal working conditions considered in the model is also the reason for the results obtained with the model being higher than the measurement results. Even though the material properties and physical dimensions are defined exactly in the ideal environment of the FE Model, such an ideality is not applicable for the actual transducer due to the deficiencies involved in the production and manufacturing stages of the materials, the assembly of the transducer, and the mounting of the transducer to the water-proof housing.

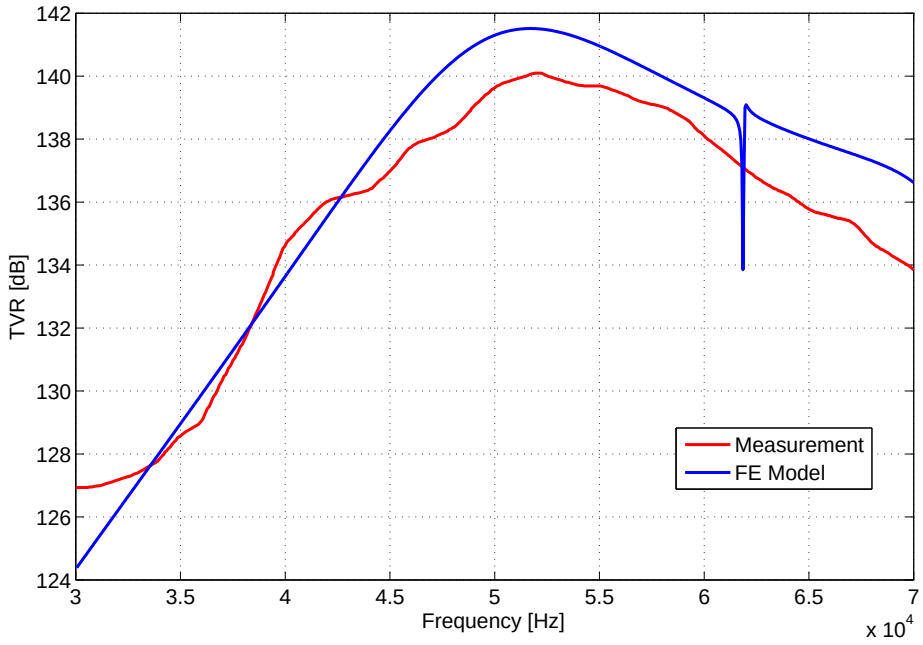

Figure 3.13: The FE Model and measurement results for in-water TVR of the Bayliss' 50 kHz Tonpilz

Although the FE Model results are in good agreement with the measurement results, an unexpected peak for the conductance and trough for the TVR in the FE model results is noticed at 61.9 kHz which do not exist in the measurement results. In order to identify the reasons for the peak and trough, the steady-state displacement profile of the transducer at 61.9 kHz, which is also shown in Figure 3.14, is obtained within the FE Model. As is clearly seen in the figure, 61.9 kHz corresponds to the longitudinal mode of the stud. Therefore, some portions of the stud undergo a displacement 3 orders of magnitude higher than the displacements occurring in the head mass, tail mass and piezoceramic stack. Since such a significant amount of energy is consumed for the motion of the stud, the transducer cannot effectively achieve its main function of generating acoustic waves. The reason why the peak is not seen in the measurements should be related with the mounting details of the transducer.

Table 3.5: The Measurement and the FE Model Results for the Resonance Frequency and Mechanical Quality Factor for the Bayliss' 50 kHz Tonpilz

Performance Metric	Measurement	Simulation	Relative Error [%]
Resonance Frequency (f_n)	50 kHz	50.4 kHz	0.8
Mechanical Quality Factor (Q_m)	2.74	3.55	29.5

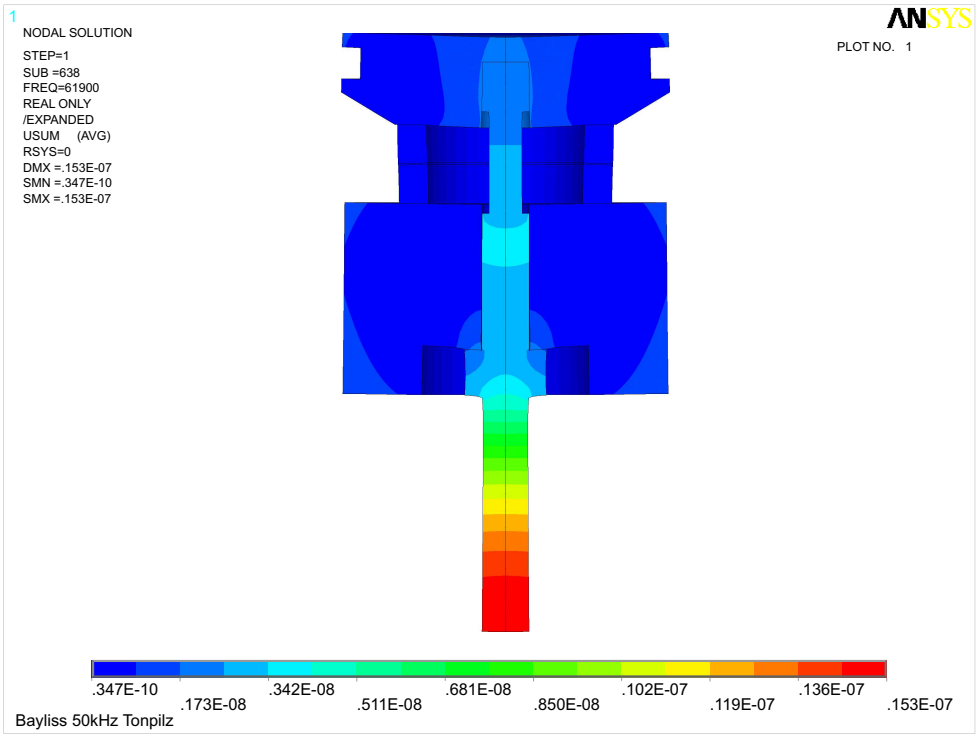

Figure 3.14: The displacement profile of the Bayliss' 50 kHz Tonpilz operating at 61.9 kHz (The values in the contour legend are in meters)

Hence, in addition to their outstanding accuracies, FE models are also capable of representing the motional behaviours of the transducers being analyzed. As a result of this capability, the reason for the 2 kHz shift with respect to the resonance frequency in the peak value of the TVR is completely understood. In Section 3.2, the reason is hypothesized to be related with the increase in the directivity index due to the increase in frequency. This statement is actually true, especially when the head mass is assumed to be oscillating with a uniform velocity. However, in reality the head mass cannot have a uniform velocity and TVR is directly related with the motion of the head mass. The deformed and undeformed shapes of the transducer at the frequencies 50.4 kHz and 52 kHz are shown in Figure 3.15. As is seen in the figure, the transducer undergoes a flapping mode for the head mass at 50.4 kHz, which corresponds to out-of-phase motion of the edges and the center of the head mass. Although exceptions exist [30], the flapping mode of the head mass is usually avoided in Tonpilz-type transducers as it reduces the average velocity of the head mass and hence causes a reduction in TVR levels which would possibly occur with a non-flapping head mass [78]. Therefore, even though 50.4 kHz is the resonance frequency of the FE Model, a better TVR level is obtained at 52 kHz due to the in-phase motion of the head mass as can be seen in Figure 3.15(b).

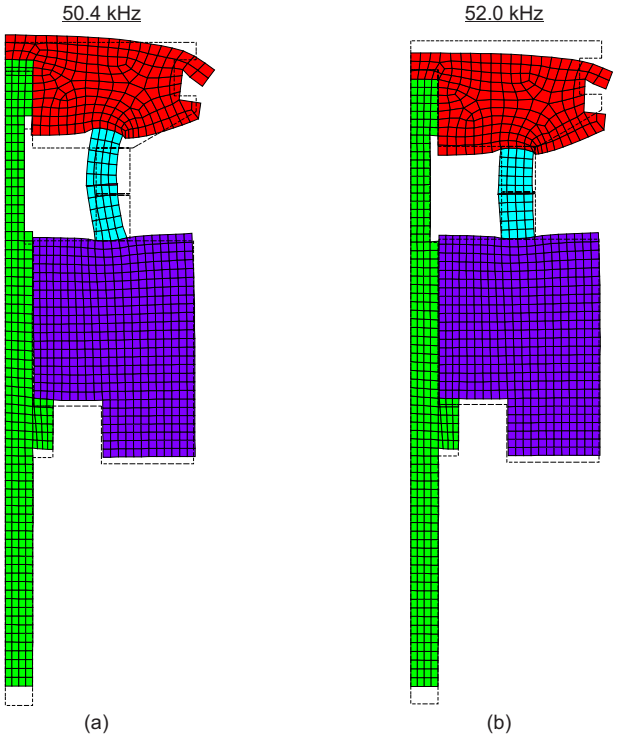

Figure 3.15: The deformed (in color) and undeformed (in dotted lines) shapes of the Bayliss' 50 kHz Tonpilz obtained with the FE model at (a) 50.4 kHz and (b) 52 kHz

3.5 Comparison of the Results Obtained with Different Modeling Techniques

For the sake of simplicity in comparing the results obtained with the different modeling techniques for the Bayliss' 50 kHz Tonpilz, the in-water conductance and TVR results shown in Sections 3.2 - 3.4 separately are shown together in Figures 3.16 and 3.17, respectively. In addition, the estimated resonance frequencies obtained with different models are presented in Table 3.6 with the corresponding computation times and absolute percent relative errors with respect to the measured resonance frequency.

The conductance results shown in Figure 3.16 are mainly considered for determining the estimated resonance frequencies with the corresponding models. The results are in good agreement with the expectations. The accuracies in the estimated resonance frequencies get better in parallel with the increase in the level of complexity within the models. Since efficiency is not considered in any of the models, having two or even three times higher values for conductance is also as expected. Also, the peak conductance values obtained with the Lumped-Parameter Equivalent Circuit Model and the Matrix Model are significantly higher

than the measured value as shown in Figure 3.16. However, it should be noted that the only resistive term in these models is the radiation impedance which is modeled by assuming a uniform vibration velocity of the head mass. However, this assumption is clearly refuted by the FE Model results about the motion of the head mass as shown in Figure 3.15. Therefore, in order to obtain more accurate and reliable results both in terms of the peak values and the corresponding frequencies, FE models are suggested.

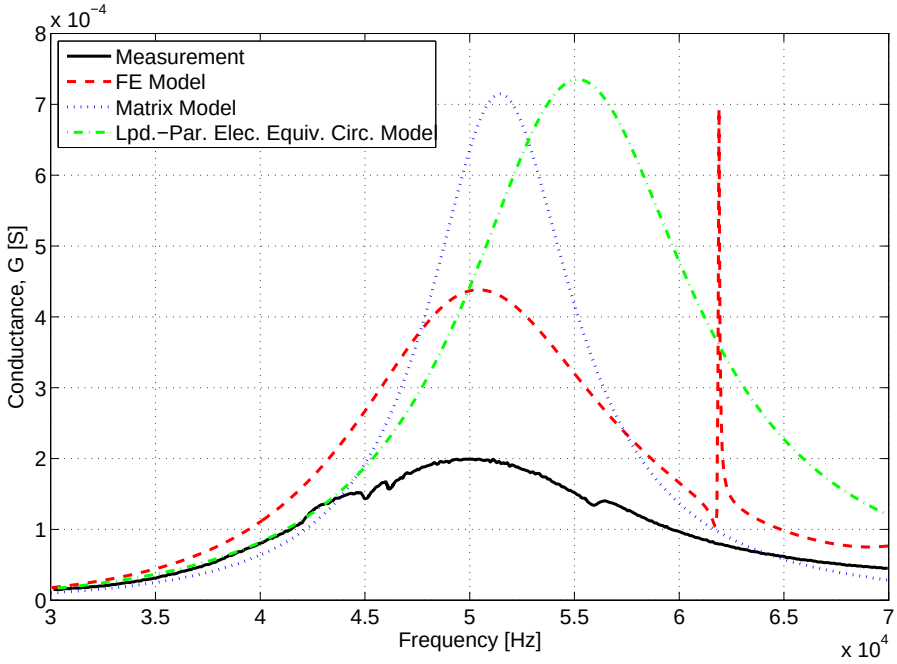

Figure 3.16: The modeling and measurement results for in-water conductance of the Bayliss' 50 kHz Tonpilz

However, computation times given in Table 3.6 should also be considered while comparing the accuracies of the models. For instance, while the FE Model's accuracy is 13 times better than the Lumped-Parameter Electrical Equivalent Circuit Model, its computation time is also 165 times longer. This increased computational cost would be even higher for the same accuracy for transducers which cannot be modeled axisymmetrically.

The accuracies of the TVR results obtained with the different models are also as expected. All the modeling results are higher than the measurement results due to the ideal conditions considered in the models. Having peak TVR values with the lumped-parameter models around 4-5 dB more than the FE Model is also related with the assumption of uniform oscillation velocity of the head mass as well as the lower levels of detail considered in the lumped-

parameter models. The same situation is also applicable for conductance results. On the other hand, the accuracy of the FE Model is extremely good in terms of both the estimation of the resonance center frequency of TVR and its value. The electromechanical efficiency of the Bayliss' 50 kHz Tonpilz is reported to be 63% in the dissertation of Bayliss [75]. This efficiency corresponds to a 2 dB reduction in the values of TVR due to the electrical and mechanical losses. Actually, the difference between the peak values of TVR obtained by the FE Model and measurement is also around 2 dB. Therefore, almost exact results are obtained with the FE Model of the Bayliss' 50 kHz Tonpilz with respect to the measurements. The other modeling techniques are also effective in the analysis of Tonpilz-type transducers, especially when their computation times and levels of complexity are considered.

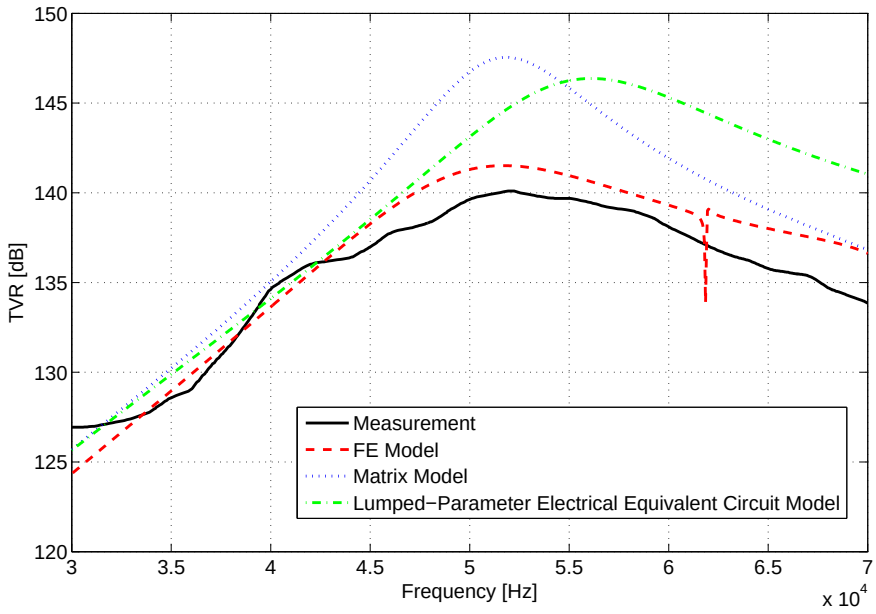

Figure 3.17: The modeling and measurement results for in-water TVR of the Bayliss' 50 kHz Tonpilz

Table 3.6: The Accuracies of the Models in terms of Resonance Frequencies with respect to the Measurement and Computation Times Required by the Models

	Resonance Freq. [kHz]	Rel. Error [%]	Comp. Time [s]
Simple Lumped Model	64.2 kHz	28.4	-
Equiv. Circuit Model	55.2 kHz	10.4	1.7
Matrix Model	51.5 kHz	3.0	44.7
FE Model	50.4 kHz	0.8	279.9

CHAPTER 4

DESIGN METHODOLOGY

4.1 Statement of the Proposed Methodology

In Chapter 2, several design techniques for Tonpilz-type transducers are introduced and then, the validity of these techniques is confirmed in Chapter 3. It is both stated and experienced that these techniques have various advantages and disadvantages relative to each other. Therefore, a design methodology involving all these techniques in a way which maximizes the advantages while minimizing the disadvantages regarding each technique is proposed in this section. The computational expenses of the modeling techniques are proportional with the accuracies offered by them. Depending on the complexity of the modeled transducer, the modeling techniques usually offers accuracies ranging between 1-30%. However, for the same transducer an accurate solution may take days to obtain with the FE Model whereas an approximate solution can be obtained instantly with the Simple Lumped-Parameter Model. Therefore, it is reasonable to combine the fast-paced nature of the simpler models for an initial design with the accuracy of the slower ones for a final design within a larger design methodology.

The schematic representation of the proposed design methodology for the Tonpilz-type transducers is shown in Figure 4.1. The methodology is separated into three sequential stages defined as definitions, initial design, and design optimization. First, the geometrical shape, dimensional parameters and materials of the transducer are defined with respect to the design criteria. Then, rough dimensions regarding the design criteria are determined with the Simple Lumped-Parameter Model, which cannot be done explicitly with the other models. Subsequently, in the design optimization stage, the dimensions obtained from the previous models are tuned iteratively with an optimization algorithm, by parameter sweeping with each model,

and/or through experimental work. The methodology allows the designer to avoid wasting time in the infinite design domain with the accurate but slow models while looking for an optimum. Instead, in the end, the methodology provides fairly reasonable initial values with the simpler and faster models relative to the most accurate one, which ultimately provides basis for prototype experiments. However, since the level of detail within the models increase while approaching towards the final design, an unexpected result due to the limited capabilities of the previous models can occur with the current model. Therefore, the results regarding the parameters coming from the previous model must be checked first for unreasonable results. In case of any such situation, it is best to turn back to the previous model(s) and reiterate the optimization procedure with respect to the feedback obtained from the subsequent model(s).

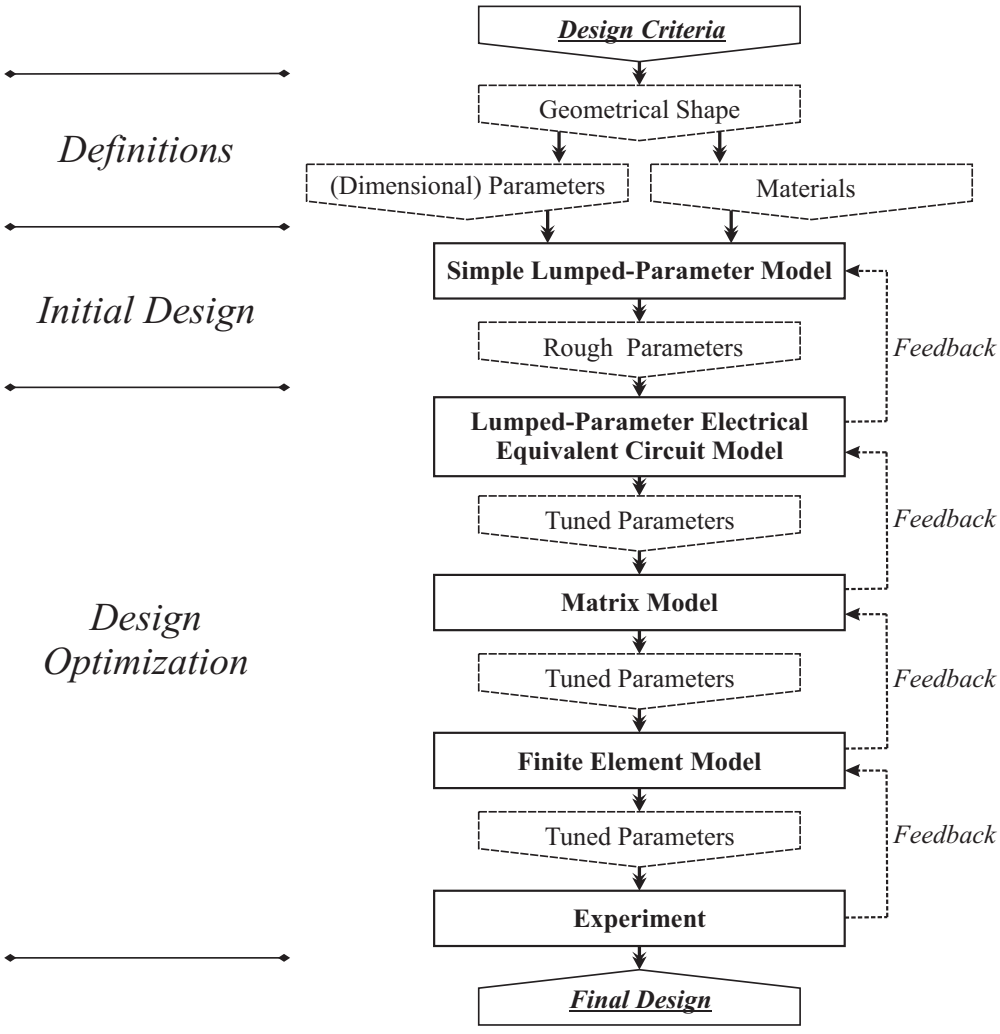

Figure 4.1: Schematic representation of the proposed design methodology for the Tonpilz-type transducers

4.2 Sample Transducer Design with the Proposed Methodology

In order to illustrate the effectiveness of the proposed methodology, a sample design procedure is conducted in this section. Instead of focusing on the detailed capabilities of each modeling technique or making extended optimization runs with them, attention is paid on the application of the proposed methodology. Also, since the proposed methodology is mainly based on parametric studies with the models introduced in Chapter 2 and the validity of these models are already verified in Chapter 3, the sample design procedure is finalized after obtaining optimum dimensions for the transducer using the FE Model with respect to the design criteria.

4.2.1 Statement of Design Criteria

The requirements within the design criteria are kept at a minimum due to the illustrative purposes of the sample design procedure. Nevertheless, the most important performance metrics of the Tonpilz-type transducers are still considered. The design criteria are mainly based on the source level, SL, performance of the transducer being designed. The primary requirement is to have the peak value of the SL at frequencies between 14.85 and 15.15 kHz. The secondary requirement is to have a bandwidth of 5 kHz for the SL. As the third requirement, the peak value of the SL is required be as high as possible while not being less than 204 dB. In addition to these requirements, the transducer is required to have a beam width narrower than 120°. For clarity, the design criteria listed with respect to the order of priority is presented in Table 4.1. On the other hand, no constraints are defined. Therefore, a transducer with any geometrical shape resembling the Tonpilz-type transducers without any physical limitations can be considered throughout the sample design procedure.

Table 4.1: The Design Criteria regarding the Sample Design Procedure

1.	Frequency of the Peak SL, f_{SL} [kHz]	14.85 < ... < 15.15
2.	Bandwidth of SL, Δf_{SL} [kHz]	5 < ...
3.	Peak SL, SL_p [dB]	204 < ...
4.	Beam Width, BW [°]	... < 120

4.2.2 Sample Design Procedure

Since the sample design procedure is conducted for illustrative purposes, the geometrical shape of the considered sample transducer is kept as simple as possible without overlooking the characteristic properties of the Tonpilz-type transducers. For instance, all the transducer parts except the head mass have geometries of either a full cylinder or a hollow cylinder. Also, an axisymmetric transducer is considered due to its simplicity and ease of applicability to all of the models introduced in Chapter 2. A few common parts for Tonpilz-type transducers such as insulators, rubber coating on the active surface of the head mass, isolation materials around the transducer, electrodes etc. are also not considered for the sake of simplicity. The axisymmetric cross-sectional view of the Tonpilz-type transducer that is assumed throughout the sample design procedure is shown in Figure 4.2 with the corresponding dimensional design parameters.

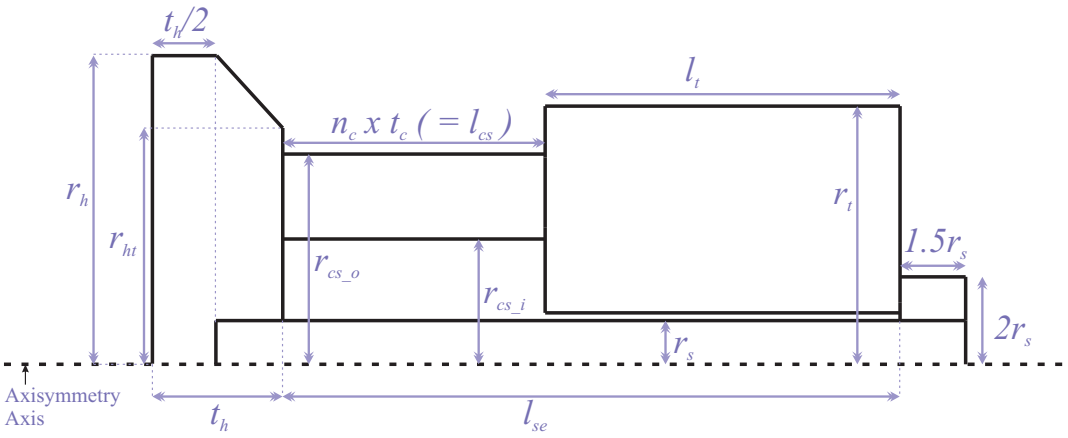

Figure 4.2: The axisymmetric cross-sectional view of the Tonpilz-Type transducer assumed throughout the sample design procedure

As seen in Figure 4.2, independent dimensional design parameters are kept to a minimum by defining many dimensions in terms of a few key characteristic dimensions. For instance, in order not to complicate the sample design procedure further, the dimensions regarding the nut are defined to be dependent on the radius of the stud, r_s. Also, the gap between the stud and tail mass is defined to be one-tenth of r_s. The effective length of the stud, l_{se}, which corresponds to the portion of the stud considered in the stiffness calculations in the Lumped-Parameter Electrical Equivalent Circuit Model, equals to the sum of the lengths of the piezoceramic stack and tail mass. Also, the stud is cut right after the end of the nut on one end and put into

the head mass with a depth of half the thickness of the head mass on the other end. The term r_{ht} is related with the truncation of the head mass to have a semi-conical shape, which is only used in the FE Model and up to an extent in the Matrix Model. Briefly, r_h, t_h, t_c, r_{cs_o}, r_{cs_i}, r_s, r_t, and l_t are the only independent parameters considered throughout the design procedure.

For the transducer parts, exactly the same materials are considered as in the Bayliss' 50 kHz Tonpilz due to their common use in Tonpilz-type transducers. Hence, the material properties used in the models throughout the sample design procedure are taken from Appendix B.

Since SL is the main concern in the design criteria, evaluation of the candidate designs constituted with different dimensional parameters is mainly based on the SL results in each stage of the design procedure. The SL responses are investigated for a frequency range of [10, 20] kHz since the desired peak frequency is 15 kHz and it is not necessary to look for a wider range of frequencies. When calculating the SL results with the models, all limitations except electrical are neglected for the sake of simplicity. However, in an actual design procedure one should also consider the cavitational, thermal, and mechanical limitations. The electrical limitation is related with the maximum applied electrical field to the piezoceramic rings and it is taken as 200 V/mm, which is reported to be a fairly conservative limit to avoid electrical breakdown and usually is the critical limiting factor for piezoelectric transducers [20].

While searching for better parameter sets with respect to the design criteria iteratively using all the models except the Simple Lumped-Parameter Model in the sample design procedure, an optimization algorithm is not considered for the sake of simplicity. Instead, the dimensional parameters are swept within the defined range with a defined number of evaluation points in each model. Although parameter sweep is easier to perform, it takes significantly more time to reach the same results when compared with optimization algorithms. Therefore, the number of parameters and their evaluations points with the parameter sweeps conducted in the sample design procedure are limited as much as possible.

The sample design procedure, which corresponds to the Initial Design and Design Optimization Stages in the Design Methodology in Figure 4.1, is separated into 4 stages to make it easier to follow. In each stage, a different modeling technique is used. The sample design procedure starts with the Simple Lumped-Parameter Model in Stage I and ends with the FE Model in Stage IV. The other modeling techniques are considered with respect to their orders shown in Figure 4.1 in the intermediate stages.

4.2.2.1 Stage I

Stage I starts with determining the radius of the active surface of the head mass. The determination is based on the assumption of uniform oscillation velocity for the head mass of the transducer which is also assumed to be running in a rigid baffle. Under these assumptions, the beam width requirement is considered first in order to find the lower limit for the active surface radius, r_h. With respect to Equation 2.17, BW can be formulated as follows [4]:

$$BW = \arcsin\left(\frac{3.2}{kr_h}\right) \tag{4.1}$$

Using Equation 4.1, the lower limit for the active surface radius is determined as 29.4 mm in order to provide a beam width narrower than 120° with respect to the aimed resonance frequency. The selection is based on having a maximum for the radiation resistance shown in Figure A.1. Hence, the active surface radius is determined as $r_h = 40.9\ mm$. Knowing the value of the radiation resistance and selecting the tail-to-head ratio introduced in Equation 2.16 as $\kappa_{th} = 4$, the masses of the head mass and tail mass, and the stiffness of the piezoceramic stack is determined as $M_h = 0.23\ kg$, $M_t = 0.91\ kg$, and $K_e = 1.62 \times 10^9\ N/m$, respectively, by simultaneous solution of Equations 2.14 - 2.16. However, the thickness of the head mass, t_h, determined with respect to M_h and r_h using Equation 2.18 is detected as not being thick enough after checking Equation 2.19, as the first flexural mode of the head mass occurs at 23.6 kHz which would be a risk for a transducer running at 15 kHz with a bandwidth of 5 kHz. Therefore, the procedure is repeated by decreasing the active surface radius in a controlled manner with the aim of pushing the flexural mode to 30 kHz. Accordingly, the parameters are determined as $r_h = 35.8\ mm$, $t_h = 15.5\ mm$, $M_h = 0.17\ kg$, $M_t = 0.68\ kg$, and $K_e = 1.21 \times 10^9\ N/m$ with respect to the Simple Lumped-Parameter Model.

Therefore, the other dimensions of the transducer parts can now be determined. First, the cross-sectional area of the piezoceramic stack is determined as $A_{cs} = 805\,mm^2$ with respect to Equation 2.21. Second, the length of the piezoceramic stack is determined as $l_{cs} = 43.1\ mm$ using Equation 2.20. Then, the inner and outer radii of the piezoceramic stack are determined as $r_{cs\_i} = 14.3\,mm$ and $r_{cs\_o} = 21.5\,mm$, respectively, using Equations 2.22 - 2.25. Finally, the radius and length of the tail mass are determined using Equation 2.26, with the aim of having their values as small as possible while being smaller than $\lambda/4$ in the corresponding material of the tail mass, as $r_t = 24.1\ mm$ and $l_t = 48.2\ mm$, respectively.

For clarity, all the dimensions determined in this stage of the design procedure using the Simple Lumped-Parameter Model are presented in Table 4.2. It should be noted that all the dimensions obey the assumption of the Simple Lumped-Parameter Model that no dimension of the transducer part should be more than $\lambda/4$ for the corresponding part's material.

Table 4.2: The Transducer Dimensions Obtained in Stage I of the Design Procedure

Dimensions [mm]	r_h	t_h	r_{cs_i}	r_{cs_o}	l_{cs}	r_t	l_t
Stage I	35.8	15.5	14.3	21.5	43.1	24.1	48.2

4.2.2.2 Stage II

Stage II of the design procedure starts with evaluating the dimensions determined in Stage I using the Lumped-Parameter Electrical Equivalent Circuit Model. Therefore, the parameters used in the electrical equivalent circuit shown in Figure 2.6 are calculated with respect to the dimensions presented in Table 4.2. Additionally, the masses of the head mass and tail mass are directly taken from Stage I as $M_h = 0.17\ kg$ and $M_t = 0.68\ kg$, respectively, since their dimensions are not involved directly in the model. On the other hand, in order to determine the clamped capacitance, C_0, the number and thickness of the piezoceramic rings must be known. Since the use of piezoceramic rings which have thicknesses more than 10 mm are not common due to difficulties in the polarization process [20], the number of the piezoceramic rings is selected to be 6 which leads to a thickness of $7.2mm$ for each ring. The reasons to have an even number of rings are to have positive electrodes at the inner portions of the piezoceramic stack and also to provide symmetry in the driving section of the transducer. Hence, the clamped capacitance is calculated as $C_0 = 3.96 \times 10^{-9}\ F$ by combining Equations 2.28 - 2.29. The stiffness of the piezoceramic stack is taken directly from Stage I as $K_{cs} = K_e = 1.21 \times 10^9\ N/m$ and the mass of the piezoceramic stack is calculated as $M_{cs} = 0.26\ kg$. The stiffness of the stud, K_s, is selected to have a value one-tenth of K_{cs} as is reasonable and practical [20]. Since an illustrative design procedure is being conducted and glue is not included in the design, the term K_g shown in Figure 2.6 is dropped from the model. Lastly, the radiation impedance terms, R_r and M_r are determined within the model in terms of frequency by using Equation A.2 with respect to the radius of active surface determined in Stage I. Hence, according to these parameters, the peak frequency and bandwith with respect to the SL result obtained

from the model are determined as $f_{SL} = 13.0\ kHz$ and $\Delta f_{SL} = 2.9\ kHz$, respectively. As a result, with respect to the design criteria, the dimensions determined with the Simple Lumped-Parameter Model in Stage I provides absolute percent relative errors of 13.3% and 42% for the peak frequency and bandwidth, respectively, when compared with the results of the Lumped-Parameter Electrical Equivalent Circuit Model. The thickness of piezoceramic rings, t_c, and the masses of the tail mass, M_t, and head mass, M_h, are subject to change to improve the accuracies of f_{SL} and Δf_{SL} with respect to the design criteria using the Lumped-Parameter Electrical Equivalent Circuit Model. As an example, a simple illustration of parameter sweep based on values taken from Stage I is shown in Table 4.3.

Table 4.3: The Peak Frequency, Bandwidth, and SL Obtained with Various Parameter Sets

Design Parameters	t_c $[mm]$	M_t $[kg]$	M_h $[kg]$	SL_p $[dB]$	Δf_{SL} $[kHz]$	f_{SL} $[kHz]$
Set #01	5.4	0.51	0.13	213.1	5.0	18.2
Set #02	5.4	0.51	0.17	212.8	3.7	16.7
Set #03	5.4	0.51	0.21	212.8	2.8	15.6
Set #04	5.4	0.68	0.13	212.1	5.5	17.4
Set #05	5.4	0.68	0.17	211.9	3.9	15.9
Set #06	5.4	0.68	0.21	211.9	2.9	14.8
Set #07	5.4	0.85	0.13	211.5	5.8	16.9
Set #08	5.4	0.85	0.17	211.2	4.1	15.3
Set #09	5.4	0.85	0.21	211.2	3.0	14.3
Set #10	7.2	0.51	0.13	211.9	4.1	14.7
Set #11	7.2	0.51	0.17	212.1	2.9	13.7
Set #12	7.2	0.51	0.21	211.4	2.2	13.0
Set #13	7.2	0.68	0.13	211.2	4.2	14.0
Set #14	7.2	0.68	0.17	211.4	2.9	13.0
Set #15	7.2	0.68	0.21	211.6	2.2	12.3
Set #16	7.2	0.85	0.13	210.7	4.2	13.5
Set #17	7.2	0.85	0.17	210.8	2.9	12.6
Set #18	7.2	0.85	0.21	211.1	2.2	11.9
Set #19	9	0.51	0.13	211.7	3.0	12.5
Set #20	9	0.51	0.17	212.1	2.2	11.8
Set #21	9	0.51	0.21	212.5	1.7	11.3
Set #22	9	0.68	0.13	211.1	2.9	11.9
Set #23	9	0.68	0.17	211.5	2.1	11.2
Set #24	9	0.68	0.21	211.8	1.7	10.7
Set #25	9	0.85	0.13	210.7	2.9	11.5
Set #26	9	0.85	0.17	211.1	2.1	10.8
Set #27	9	0.85	0.21	211.4	1.6	10.3

The base case value for each parameter is that from Stage I and three values of each parameter are explored: 1) 25% less than the base case value; 2) base case value; and, 3) 25% greater than the base case value. Hence, Table 4.3 presents every combination of these parameter values. The results are calculated for the frequency range of [5, 25] kHz with a step size of 0.05 kHz. The table, whose data were generated in just 8 seconds, is presented to illustrate the dependency of the performance metrics to these parameters. For simplicity in communicating the design methodology, the number of values swept for each parameter is limited to 3. However, in the actual design procedure, the parameter sweep is extended in a way that the span around the base values is increased to 50% and the number of evaluation points for each parameter is increased to 21. The reason to cover such a wide range with such high detail is related with the extreme economy of the model in terms of computation time. It is also related with the aim of not missing any probable better parameter sets which may not be close to the base values of the parameters swept. Due to the simplicity of the model, only t_c, M_h, and M_t are swept. As a result, the selected 3 parameters cover almost every probable solution that can be generated with the Lumped-Parameter Electrical Equivalent Circuit Model.

In the actual design procedure, t_c, M_h, and M_t are swept within the ranges [3.6, 10.8] mm, [0.17, 0.34] kg, and [0.34, 1.02] kg, respectively. As can be noted, the range for M_h is shifted since its base value, 0.17 kg, corresponds to the lower limit for the thickness when the flexural mode of the head mass is considered. The responses of a total of 9261 parameter sets are investigated for the frequency range of [10, 20] kHz with a step size of 0.1 kHz with the Lumped-Parameter Electrical Equivalent Circuit Model. Out of these 9261 parameter sets, the required peak frequency of 15 kHz is provided by 34 parameter sets with different bandwidths. Five of these parameter sets, which lead to results closest to the aimed bandwith of 5000 kHz, are presented in Table 4.4.

Table 4.4: The Best 5 Parameter Sets with respect to the Bandwidth Requirement determined by Parameter Sweep in the Lumped-Parameter Electrical Equivalent Circuit Model

Parameters Swept	t_c [mm]	M_t [kg]	M_h [kg]	SL_p [dB]	Δf_{SL} [kHz]
Set #1	5.4	0.88	0.18	211.1	3.9
Set #2	5.0	1.02	0.20	210.9	3.7
Set #3	5.0	0.92	0.20	211.2	3.4
Set #4	4.7	0.99	0.23	211.2	3.2
Set #5	5.4	0.68	0.20	212.1	3.1

From the 5 parameter sets presented in Table 4.4, *Set #1* is selected since it provides a bandwidth closest to 5 kHz. The dimensions of the transducer parts which are determined with respect to these parameters are presented in Table 4.5 along with the values obtained in the Stage I. Although the length and radius of the stud are not determined in Stage I, the corresponding values for them must be determined in Stage II to run the model. The SL results obtained with the Lumped-Parameter Electrical Equivalent Circuit Model for the dimensions determined in Stage I and Stage II are shown in Figure 4.3 in order to better illustrate the improvement. Hence, fixing the new dimensions based on tuning of the dimensions obtained in Stage I with respect to the design criteria by the Lumped-Parameter Electrical Equivalent Circuit Model concludes Stage II.

Table 4.5: The Transducer Dimensions Obtained in Stage I and Stage II of the Sample Design Procedure

Dimensions [mm]	r_h	t_h	r_{cs_i}	r_{cs_o}	l_{cs}	r_t	l_t	r_s	l_{se}
Stage I	35.8	15.5	14.3	21.5	43.1	24.1	48.2	4.3	91.3
Stage II	35.8	16.5	14.3	21.5	32.4	26.3	52.6	4.7	85.0

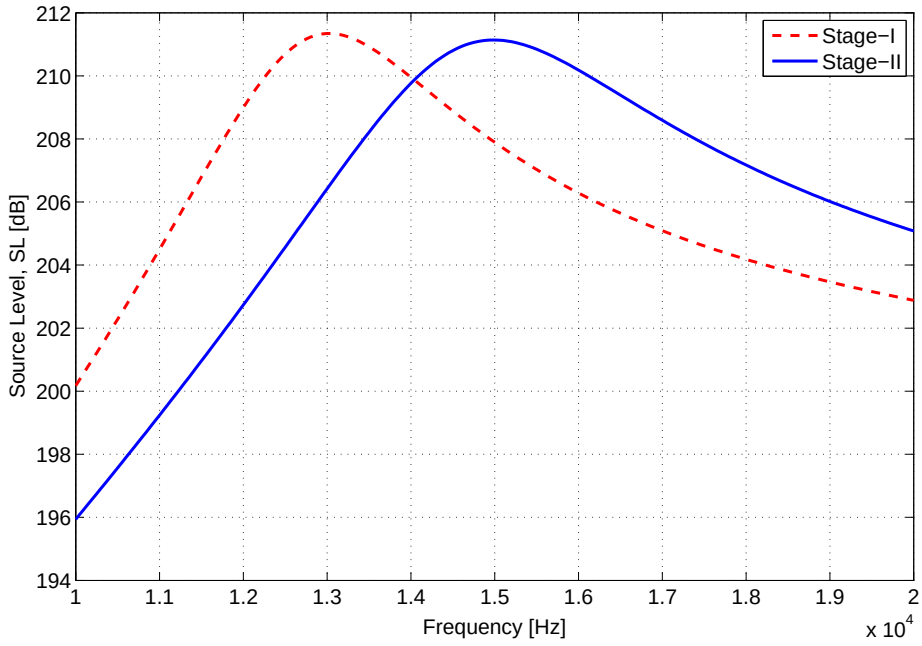

Figure 4.3: The source level results obtained with the Lumped-Parameter Electrical Equivalent Circuit Model with respect to the dimensions determined in Stage I and Stage II

4.2.2.3 Stage III

The Matrix Model introduced in Section 2.3 and validated in Section 3.3 is used throughout Stage III. As a result of the capabilities of the Matrix Model regarding the radial dimensions, the head mass of the modeled transducer is represented as a serial connection of a full cylinder and a hollow cylinder with a reduced diameter in order to approximate the characteristic conical shape of the head mass. The radius of the hollow cylinder, which has a formulation as $r_{ht\_m} = (r_h + r_{r\_ht})/2$ with respect to the dimensional parameters shown in Figure 4.2, is considered as one of the parameters to be swept in Stage III while searching for a better parameter set with respect to the design criteria than the one obtained in Stage II. The cross-sectional view of the transducer being modeled is shown in Figure 4.4 with identifying numbers on each of the network elements used to build the Matrix Model. A total of 14 network elements are connected to each other with respect to their relative positions shown in Figure 4.4 with the same approach used in Section 3.3 for modeling the Bayliss' 50 kHz Tonpilz.

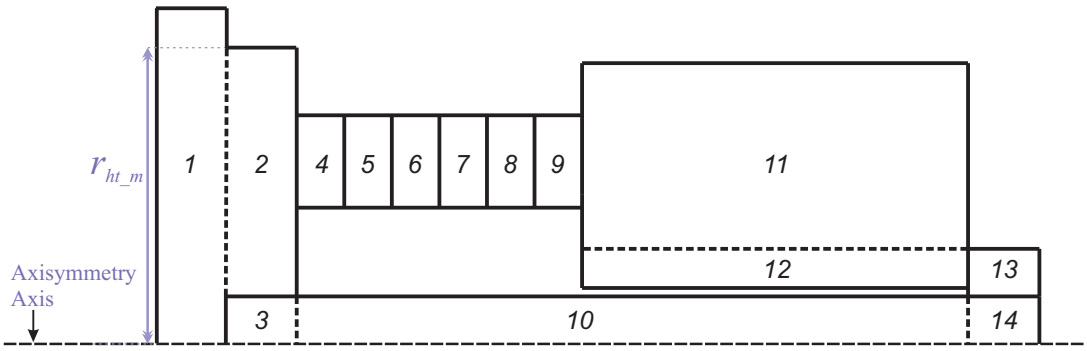

Figure 4.4: The axisymmetric cross-sectional view of the transducer, which is separated into network elements as numbered, and modeled with the Matrix Model in Stage III of the Sample Design Procedure

When the dimensions obtained in Stage II are applied to the Matrix Model, the peak frequency and bandwidth with respect to SL result are determined as $f_{SL} = 14.3\ kHz$ and $\Delta f_{SL} = 3.2$ kHz. Hence, the accuracies of the peak frequency and bandwidth of the transducer having these dimensions are 4.7% and 36%, respectively, when evaluated with the Matrix Model. Since the results are as expected, these dimensions can be used as the base values for the parameter sweep which is conducted to search for a better parameter set with respect to the design criteria using the Matrix Model.

The dimensional parameters t_h, r_{ht_m}, r_{cs_i}, t_c, r_t, l_t, r_s shown in Figures 4.2 and 4.4 are swept for three values: 1) 12.5% less than base; 2) base; and, 3) 12.5% greater than base. The span is reduced for t_h in order to eliminate values below 15.5 mm which is determined as the limit for avoiding the flexural mode of the head mass in Stage I. The base values of r_{ht_m} and r_{cs_i} are shifted to avoid exceeding the physical limitation, r_h, with respect to the geometry and not having a radial thickness for the piezoceramic rings less than 3 mm which is practically unreasonable, respectively. The reasons to keep the number of swept values for each parameter as small as 3 are related with the expense of the Matrix Model when compared with the other models used in the previous stages, the large number of parameters considered for the parameter sweep and the illustrative purposes considered for the sample design.

A total of 2187 different parameter sets required 2.8 hours of calculation time for the Matrix Model with respect to their SL results in the frequency range of [10, 20] kHz with a step size of 0.1 kHz. Since the peak frequency and bandwidth with respect to SL are the primary and secondary objectives in the design criteria, the best 5 parameter sets with respect to the bandwidth requirement out of 42 parameter sets that provided a peak frequency of 15 kHz are listed in Table 4.6 with their corresponding bandwidth and peak SL values.

Table 4.6: The Best 5 Parameter Sets with respect to the Bandwidth Requirement Determined By Parameter Sweep in the Matrix Model

Parameters Swept	t_h $[mm]$	r_{ht_m} $[mm]$	r_{cs_i} $[mm]$	t_c $[mm]$	r_t $[mm]$	l_t $[mm]$	r_s $[mm]$	SL_p $[dB]$	Δf_{SL} $[kHz]$
Set #1	15.5	31.3	16.1	4.7	26.3	46.0	4.7	209.2	4.4
Set #2	15.5	31.3	16.1	4.7	23.0	59.2	4.1	209.1	4.4
Set #3	15.5	31.3	14.3	5.4	26.3	52.6	4.1	211.1	4.0
Set #4	15.5	33.6	16.1	4.7	23.0	52.6	4.1	209.5	3.9
Set #5	16.5	35.8	14.3	4.7	29.6	59.2	5.3	210.7	3.8

According to the results in Table 4.6, *Set #1* is selected as the output parameter set of Stage III since it provides a bandwidth closest to 5 kHz and a slightly better peak SL value than *Set #2*. The dimensions of the transducer parts determined with respect to *Set #1* are presented in Table 4.7 with the ones obtained in Stage II. In order to show the improvement with respect to the design criteria better, the SL results obtained with the Matrix Model for the dimensions determined in Stage II and Stage III are shown in Figure 4.5. Hence, using the Matrix Model to fix the dimensions for Stage IV concludes Stage III.

Table 4.7: The Transducer Dimensions Obtained in Stage II and Stage III of the Sample Design Procedure

Dims. [mm]	r_h	t_h	r_{ht_m}	r_{cs_i}	r_{cs_o}	l_{cs}	r_t	l_t	r_s	l_{se}
Stage II	35.8	16.5	35.8	14.3	21.5	32.4	26.3	52.6	4.7	85.0
Stage III	35.8	15.5	31.3	16.1	21.5	28.2	26.3	46.0	4.1	74.2

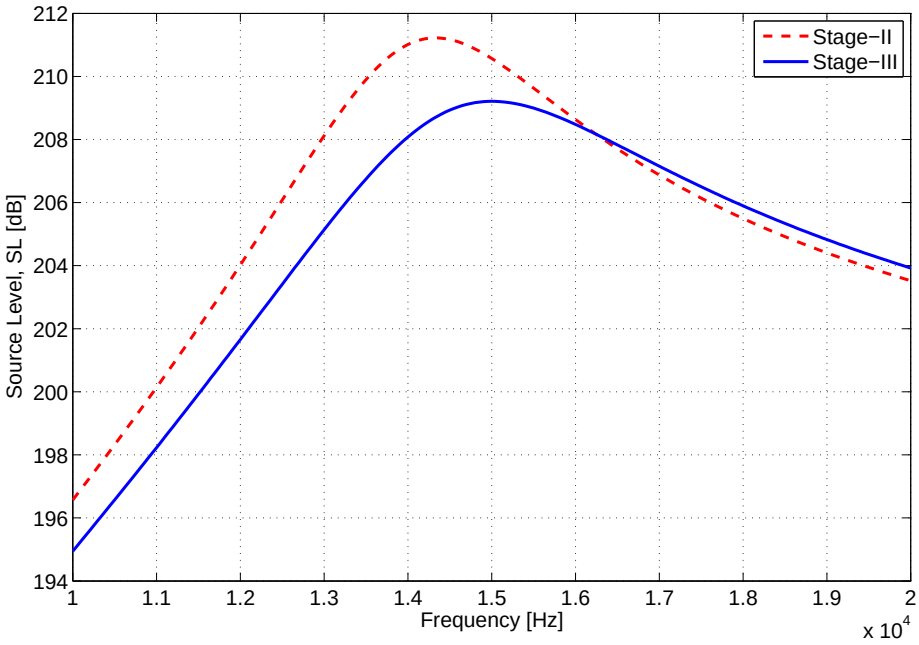

Figure 4.5: The source level results obtained with the Matrix Model with respect to the dimensions determined in Stage II and Stage III

4.2.2.4 Stage IV

In this stage, the sample design procedure is finalized by using the FE Model introduced in Section 2.4. As the first step, the performance metrics of interest for the transducer which has dimensions obtained in Stage III is evaluated with the FE Model. The model used for this evaluation and for the other simulations conducted throughout Stage IV is shown in Figure 4.6. All the details regarding the FE Model and its application are available in Sections 2.4 and 3.4, respectively. The peak frequency and bandwidth are determined as $f_{SL} = 13.9\,kHz$ and $\Delta f_{SL} = 5.7$ kHz. Hence, the accuracies of the peak frequency and bandwidth of the transducer obtained in Stage III are 7.3% and 14%, respectively, when evaluated with the FE Model. As was the case while analyzing the Bayliss' 50 kHz Tonpilz in Chapter 3, the

bandwidth estimated with the Matrix Model is less than it should be. In general, the result is as expected and close to the performance metrics needed. Therefore, better parameter sets can be searched by sweeping the dimensional parameters around the values obtained in Stage III. On the other hand, the flexural mode of the transducer is seen around 21 kHz which could not be seen with the Matrix Model. Since this is not very close to the peak frequency of interest it does not affect the performance adversely but instead helps to widen the bandwidth of the transducer and is a technique used for this purpose in the literature [30].

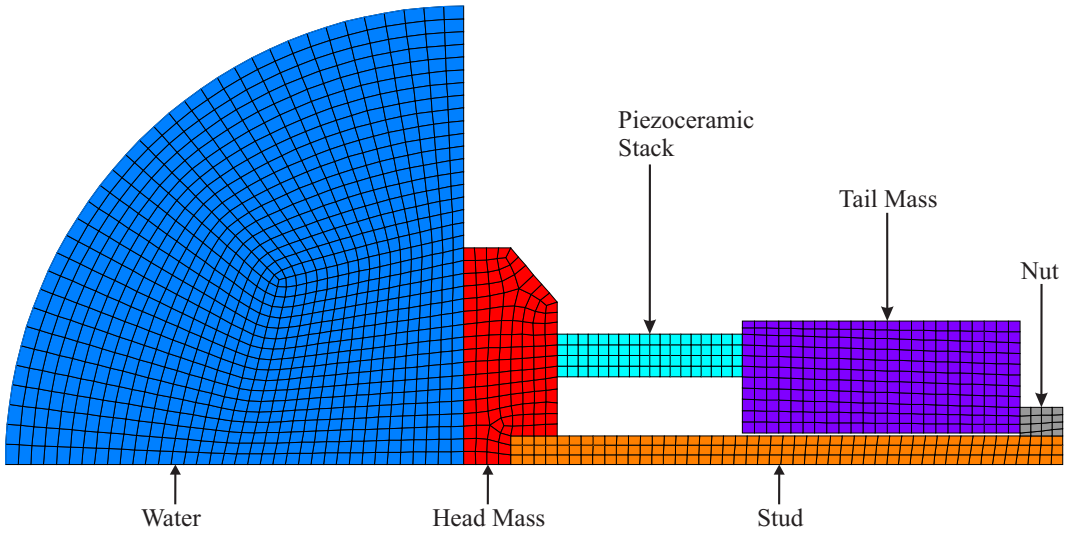

Figure 4.6: The FE Model used in Stage IV of the sample design procedure

In order to obtain a better parameter set with respect to the design criteria, the dimensional parameters r_{ht}, r_s, r_{cs_i}, t_c, and r_t are swept using the FE Model around the base values obtained in the Stage III with a span of 10% using 3 points for each parameter. Since the FE solutions are the most computationally expensive when compared with the other models introduced in Chapter 2, the number of parameters and the values for each parameter swept are kept at a limited level while still being sufficient to illustrate the sample design procedure. Hence, a total of 243 different parameter sets were analyzed within 3.1 hours using the FE Model with respect to their SL results in the frequency range of [10, 20] kHz with a step size of 0.1 kHz. Out of 243 parameter sets, only 5 lead to a peak frequency of 15 kHz. These parameter sets are presented in Table 4.8 with the corresponding bandwidth and peak SL values.

Table 4.8: The Best 5 Parameter Sets with respect to the Bandwidth Requirement Determined By Parameter Sweep in the FE Model

Parameters Swept	r_{ht} $[mm]$	r_s $[mm]$	r_{cs_i} $[mm]$	t_c $[mm]$	r_t $[mm]$	SL_p $[dB]$	Δf_{SL} $[kHz]$
Set #1	26.8	4.7	14.5	5.1	23.7	208.0	5.1
Set #2	24.2	5.1	14.5	5.1	26.3	207.7	7.4
Set #3	26.8	4.3	16.1	4.3	23.7	205.8	7.6
Set #4	24.2	4.3	16.1	4.3	26.3	205.5	7.9
Set #5	26.8	4.3	14.5	4.7	28.9	207.1	8.2

According to the results in Table 4.8, *Set #1* is selected as the final parameter set of Stage IV and the sample design procedure since it provides the bandwidth requirement and offers a better peak SL value than the other parameter sets. Also, *Set #2*, which offers a much wider bandwidth with a slight reduction in the SL, would also be a wise selection. The SL results obtained with the FE Model for the dimensions determined in both Stage III and Stage IV are shown in Figure 4.5 for an extended frequency range up to 25 kHz in order to cover the flexural mode of the head mass. Also, the dimensions obtained with respect to *Set #1* are presented in Table 4.9 with the results obtained in Stage III.

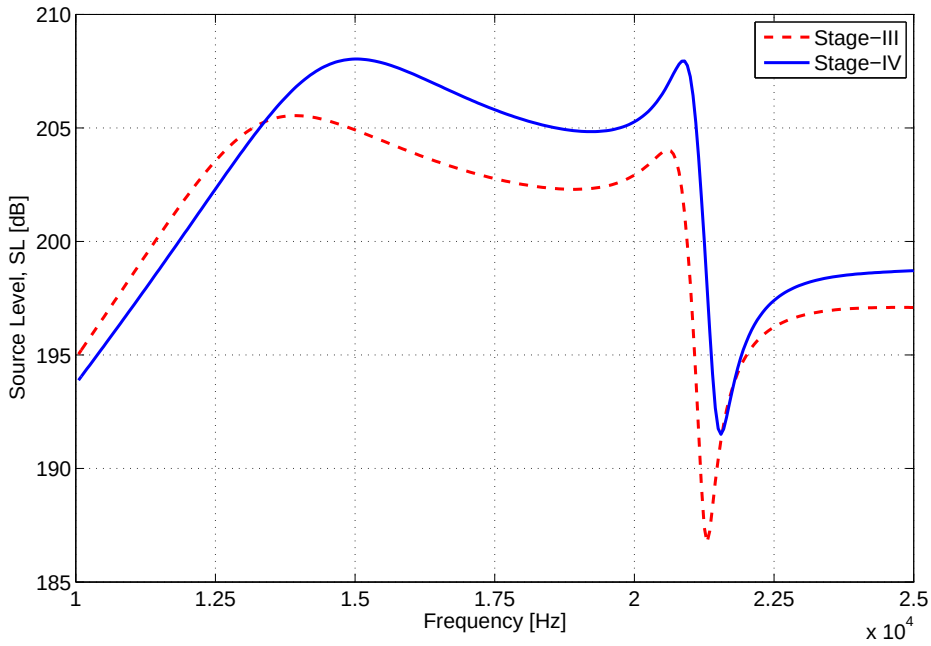

Figure 4.7: The source level results obtained with the FE Model with respect to the dimensions determined in Stage III and Stage IV

Table 4.9: The Transducer Dimensions Obtained in Stage III and Stage IV of the Sample Design Procedure

Dims. [mm]	r_h	t_h	r_{ht}	r_{cs_i}	r_{cs_o}	l_{cs}	r_t	l_t	r_s	l_{se}
Stage III	35.8	15.5	26.8	16.1	21.5	28.2	26.3	46.0	4.1	74.2
Stage IV	35.8	15.5	26.8	14.5	21.5	30.6	23.7	46.0	4.7	76.6

Hence, the physical dimensions of the Tonpilz-type transducer which provides the most important performance requirements of the design criteria are obtained with respect to the corresponding materials used for the transducer parts. As also experienced in Chapter 3 while validating the modeling results with respect to the measurements, a higher bandwidth and a lower peak SL is expected for the transducer having these dimensions. Assuming an accuracy better than 1% with the FE Model for the peak frequency fulfills the peak frequency requirement. Also, assuming an electroacoustic efficiency of 50% at the peak frequency leads to a 3 dB reduction in the peak SL which still fulfills the required peak SL of 204 dB. In addition to these, the beam width requirement in the design criteria is also checked. The beam pattern of the transducer, which is determined by correlating the pressure amplitudes read at the outermost nodes of the acoustic medium in the FE Model, is shown in Figure 4.8. Hence, the transducer is found to have a beam width of 103° which fulfills the design criteria since it is narrower than 120° as expected regarding the calculations made in Stage I.

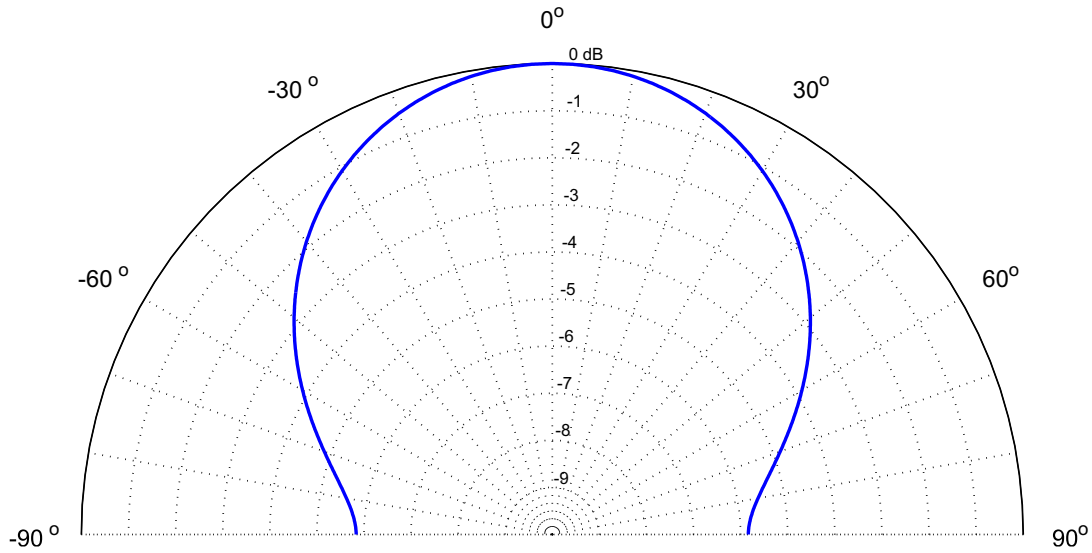

Figure 4.8: Beam pattern of the transducer with the dimensions obtained in the Stage IV of the sample design procedure determined with the FE Model

4.2.3 Comparison of the Performance Metrics of the Transducers with Dimensions Obtained in Different Stages of the Sample Design Procedure

In the sample design procedure, a total of 4 transducer designs are obtained using different modeling techniques in different stages with respect to the design criteria. In order to have a quick comparison between the outputs of the different models for the same design criteria, the physical dimensions of the transducer parts obtained in different stages of the sample design procedure are summarized in Table 4.10. As can be seen in the table, a few dimensions are kept constant across all the stages for simplicity. In an actual design procedure in which the most optimum solution set with respect to the design criteria is aimed, all the dimensional parameters should be subject to change to maximize the possibility of obtaining better parameter sets. However, changing only a limited number of them, while also considering the corresponding possible effects, is sufficient to reach reasonable results in such a sample design procedure aimed to illustrate the effectiveness of the proposed design methodology.

Since the FE Model provides the most accurate results, especially in terms of the peak frequency, as verified in Chapter 3, the accuracies of the other models used in different stages of the sample design procedure can be evaluated with the FE Model. Although some transducer parts do not exist in some of the models, reasonable values are generated for them to be used in the FE Model with respect to the existing parts. For instance, although the stud does not exist in the Simple Lumped-Parameter Model, its effective length is determined as the sum of the lengths of the piezoceramic stack and tail mass. Also, its radius is determined with respect to the practical ratio considered between the stiffnesses of the stud and piezoceramic stack. Hence, the SL results obtained with the FE Model for the parameters shown in Table 4.10 are presented in Figure 4.9.

Table 4.10: The Dimensions regarding the Transducer Parts obtained in Different Stages of the Sample Design Procedure

Dims. [mm]	r_h	t_h	r_{ht}	r_{cs_i}	r_{cs_o}	l_{cs}	r_t	l_t	r_s	l_{se}
Stage I	35.8	15.5	35.8	14.3	21.5	43.1	24.1	48.2	4.3	91.3
Stage II	35.8	16.5	35.8	14.3	21.5	32.4	26.3	52.6	4.7	85.0
Stage III	35.8	15.5	26.8	16.1	21.5	28.2	26.3	46.0	4.1	74.2
Stage IV	35.8	15.5	26.8	14.5	21.5	30.6	23.7	46.0	4.7	76.6

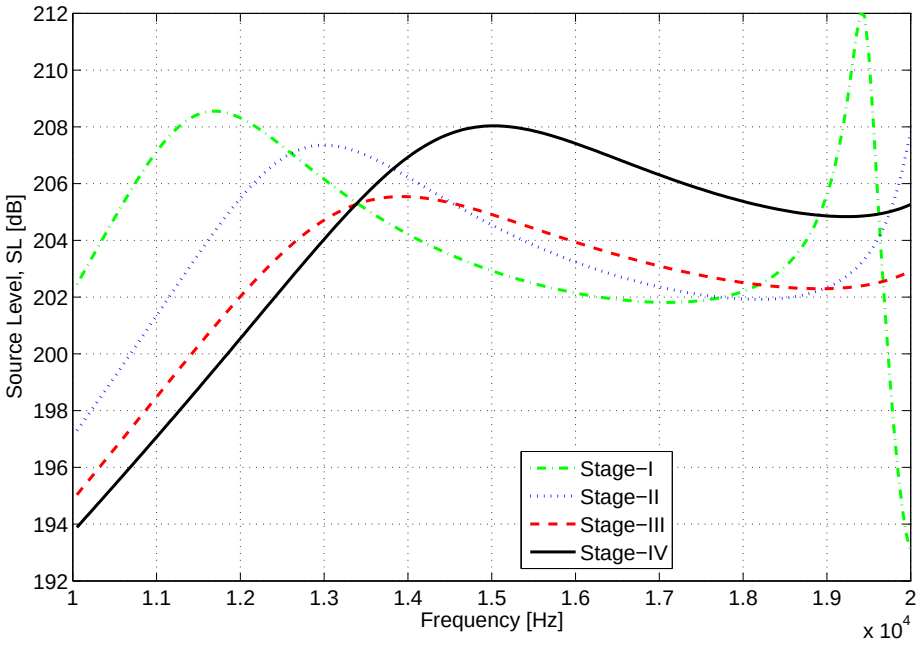

Figure 4.9: The SL results obtained with the FE Model for the transducers having physical dimensions as shown in Table 4.10

The peak frequencies of the SL results shown in Figure 4.9 are presented in Table 4.11 with their absolute percent relative errors with respect to the aimed peak frequency, 15 kHz. In addition, the number of parameter sets in each stage and computational time required for them are also presented. As expected and also being the main basis for the proposed design methodology, the accuracy of the peak frequency improves as the level of detail increases with the model considered in each corresponding stage. However, the same statement is also applicable for the time required to reach these better accuracies. Therefore, it is reasonable to use the more accurate but costly methods to refine a design obtained from the relatively quicker but less accurate methods as is done in the sample design procedure.

Table 4.11: The Peak Frequencies of the SL Results shown in Figure 4.9 with Absolute Percent Relative Errors with respect to 15 kHz and the Number of Parameter Sets with the Computational Times encountered in the corresponding Stages of the Sample Design

	Peak Freq. [kHz]	Rel. Error [%]	# of Par. Sets	Comp. Time [hrs]
Stage I	11.7	22.0	1	-
Stage II	13.0	13.3	9261	0.8
Stage III	13.9	7.3	2187	2.8
Stage IV	15.0	-	243	3.1

CHAPTER 5

CONCLUSION

In this study, a methodology for designing Tonpilz-type transducers is presented. The methodology is based on four different models which can reflect various performance characteristics of the transducer with different accuracies. Before introducing the methodology, all the models are introduced and then benchmarked with respect to the same measurement results obtained for a Tonpilz-type transducer whose dimensions and material properties are known. As expected, the models which involve higher levels of detail achieved better accuracies with respect to the measurements but also have higher computational costs. Leveraging the relative accuracies and computational costs of the different models constitutes the main idea behind the proposed methodology. Briefly, the methodology is based on the consecutive use of all these models in order of increasing accuracy and computational cost. Such an approach avoids spending excessive time in the infinite domains of design which would occur if the detailed models are used directly. Instead, the methodology uses the less detailed but fast models to provide fairly reasonable initial design points for the more detailed and slow models, which allows the more detailed models to reach the design goals much quicker through the accurate optimization iterations. After the introduction of the methodology, the methodology is illustrated with a sample design procedure in which the design criteria is effectively achieved through the straightforward use of the methodology.

The main advantage of using the introduced methodology is to save a significant amount of time while designing Tonpilz-type transducers. As shown in Table 4.11, a total of 11449 design iterations are checked in 3.6 hours with all the models except the most detailed one. However, it took almost as much time, 3.1 hours, to check far fewer design iterations, 243, with the most detailed model to reach the design goals. As an alternative to the proposed methodology, if the intermediate models between the least and most detailed models were not

considered in the design procedure, the absolute percent relative error for the initial design point when compared with the final design would be 22% instead of 7.3% which resulted with the use of the methodology. Hence, substantially more computation time would be required by the most detailed model to reach the design goals. Also, it should be noted that an axisymmetric transducer is considered in the sample design procedure. For geometries which cannot be modeled axisymmetrically, such as the transducers with a square-shaped active surface which are commonly used in sonar arrays, the most detailed model, the FE model, has to be prepared in 3-D instead of 2-D which in turn would require far more computation time for the same accuracy. Significantly, such complex geometries cannot be represented with the Matrix Model, which is the second most detailed model, but modeling 3-D complex shapes with their 2-D axisymmetric approximates would not lead to any problem since the final design is not obtained by the Matrix Model.

Another advantage of the methodology is the diversity brought to the design procedure which would not be possible otherwise. Again, as an alternative to the proposed methodology, if the intermediate models are not considered in a design procedure, there will only be a single design set available for optimization with the most detailed model. However, numerous design sets corresponding to various transducer performances are available with the use of the intermediate models and this diversity can easily be turned into a benefit by changing the final design set obtained with any intermediate model according to the feedback taken from the subsequent model. For instance, the final design set obtained with the Matrix Model, which satisfy both the resonance frequency and source level requirements when evaluated with the Matrix Model, may turn out to show a 1 kHz shift in the resonance frequency and 2 dB deficit in the source level when evaluated with the FE Model as expected due to the less accurate nature of the Matrix Model. Then, instead of using this design set, another design set which possibly would tolerate the 1 kHz shift and 2 dB deficit can be picked among the design sets obtained with the Matrix Model and most probably a better initial result will be obtained with the FE Model. Reiteration of the same procedure with respect to the existing results regarding the previously considered 2 design sets will result with picking an even better design set from the Matrix Model for the optimization in FE Model. Such manual manipulations may shorten the design procedure even more. However, the time spent for such manipulations should be kept at a minimum in order not to consume more time than is saved.

Yet another advantage with the proposed methodology is the use of the Simple Lumped-

Parameter Model introduced in Section 2.1. All the other models require transducer dimensions and lead to performance metrics, accordingly. However, the Simple Lumped-Parameter Model requires the desired performance metrics and leads to the transducers dimensions needed for the requirements. Therefore, even though the Simple Lumped-Parameter Model is less accurate than the other models, its use is important as it explicitly provides a reasonable initial design which cannot be provided by the more advanced models.

Apart from being part of the larger methodology, the intermediate models can also be useful for other purposes where computation time has more importance than accuracy. The analysis of sonar arrays can be given as an example of such purposes. As mentioned in Section 1.2, a sonar array may require up to 1000 or more transducers to be formed. Therefore, a single analysis of such an array through a FE model may take weeks or months even with the most powerful computers available today. Hence, the intermediate models can be useful for the analysis of such arrays in reasonable computation times with a relatively worse accuracy.

A possible weakness of the methodology is the risk of facing meaningless results while evaluating the final design set obtained from a model with the subsequent more advanced model. Such situations should actually be expected sometimes since everything considered in the subsequent more advanced model are not considered in the less detailed model. The solutions for such situations is also available within the methodology which is the feedback mechanism.

The presented methodology is an initial attempt to fill a gap in the literature and offers room for improvements. The Matrix and FE Models involved in the methodology can be updated in the future with respect to the advancements in the literature. The Simple Lumped-Parameter Model can be improved even today by considering more cases, such as avoiding undesirable modes of motion within the frequency range of interest, and using different practical assumptions. As a future work, the Simple-Lumped Parameter Model can be implemented to software such as MATLAB to have a simple interface which allows the designer to obtain the outputs of the model automatically after entering the inputs. On the other hand, suitable optimization algorithms can be implemented for each model to decrease the time required for design. Also, the manual feedback mechanism can be automated for a fully computerized design procedure. The methodology can be adapted to magnetostrictive Tonpilz-type transducers by changing the models accordingly as well as to other transducer types if such models with different accuracies are applicable to them.

REFERENCES

[1] *History of Underwater Acoustics*, Last accessed July 23, 2011, http://www.dosits.org/people/history/.

[2] Urick, R. J., 1983, *Principles of Underwater Sound*, Peninsula Publishing, Los Alton, California.

[3] Burdic, W. S., 1984, *Underwater Acoustic System Analysis*, Prentice-Hall, New Jersey.

[4] Sherman, C. H., Butler, J. L., 2007, *Transducers and Arrays for Underwater Sound*, Springer, New York.

[5] Lasky, M., 1976, "Review of Undersea Acoustics to 1950," Journal of the Acoustical Society of America, 61(2), pp. 283-297.

[6] Hunt, F. V., 1954, *Electroacoustics*, John Wiley and Sons, New York.

[7] Albers, V. M., 1965, Underwater Acoustics Handbook - II, The Pennsylvania State University Press.

[8] Raichel, D. R., 2006, *The Science and Application of Acoustics*, Second Edition, Springer, New York.

[9] Jacobsen, F., Poulsen, T., Rindel, J. H., Gade, A. C., and Ohlrich, M., 2008, *Fundamentals of Acoustics and Noise Control*, Lyngby: Technical University of Denmark.

[10] Kinsler, L. E., Frey, A. R., Coppens, A. B., and Sanders, J. V., 2000, *Fundamentals of Acoustics*, Fourth Edition, John Wiley and Sons.

[11] Marshall, W. J., 1999, "Underwater Sonar Projectors," Wiley Encyclopedia of Electrical and Electronics Engineering.

[12] Harper, D., *Online Etymology Dictionary*, Last accessed July 27, 2011, http://www.etymonline.com/index.php?search=piezoelectric.

[13] Hankel, W. G., 1881, "Über die Aktino- und piezoelektrischen Eigenschaften des Bergkrystalles und ihre Beziehung zu den thermoelektrischen," Abh. Sächs, 12, pp. 457-548.

[14] Curie, J., and Curie P., 1880, "Développement, par pression, de l'électricité polaire dans les cristaux hémièdres à faces inclinées," C. R. Acad. Sci. Paris, 91, pp. 294-295.

[15] Tichý, J., Erhart, J., Kittinger, E., and Přívratská, J., 2010, Fundamentals of Piezoelectric Sensorics, Springer.

[16] Haertling, G. H., 1999, "Ferroelectric Ceramics: History and Technology," Journal of the American Ceramic Society, 82(4), pp. 797-818.

[17] *History of Piezoelectricity*, Piezo Systems, Inc., Last accessed July 27, 2011, http://www.dosits.org/people/history/.

[18] Arnau, A., 2008, *Piezoelectric Transducers and Applications*, Springer.

[19] Kholkin, A. L., Pertsev, N. A., and Goltsev, A. V., 2008, "Piezoelectricity and Crystal Symmetry," ed. by Safari, A., and Akdoğan, E. K., *Piezoelectric and Acoustic Materials for Transducer Applications*, Chapter 2, Springer.

[20] Stansfield, D., 1991, *Underwater Electroacoustic Transducers*, Peninsula Publishing, California.

[21] Trolier-McKinstry, S., 2008, "Crystal Chemistry of Piezoelectric Materials," ed. by Safari, A., and Akdoğan, E. K., *Piezoelectric and Acoustic Materials for Transducer Applications*, Chapter 3, Springer.

[22] Doğan, A., and Uzgur, E., 2008, "Piezoelectric Actuator Design," ed. by Safari, A., and Akdoğan, E. K., *Piezoelectric and Acoustic Materials for Transducer Applications*, Chapter 17, Springer.

[23] Tressler, J. F., 2008, "Piezoelectric Transducer Design for Sonar Applications," ed. by Safari, A., and Akdoğan, E. K., *Piezoelectric and Acoustic Materials for Transducer Applications*, Chapter 11, Springer.

[24] Fujishima, S., 2000, "The History of Ceramic Filters," IEEE Transactions on Ultrasonics, Ferroelectrics, and Frequency Control, 47(1), pp. 1-7.

[25] Damjanovic, D., 2008, "Lead-Based Piezoelectric Materials," ed. by Safari, A., and Akdoğan, E. K., *Piezoelectric and Acoustic Materials for Transducer Applications*, Chapter 11, Springer.

[26] U. S. Government, 1995, "Military Standard - Piezoelectric Ceramic Material and Measurements Guidelines for Sonar Transducers," MIL-STD-1376B(SH).

[27] Berlincourt, D. A., Curran, D. R., and Jaffe, H., 1964, "Piezoelectric and piezomagnetic materials and their functions in transducer," Physical Acoustics, 1(Part A).

[28] Miller, H. B., 1989, "Origin of the 33-driven ceramic ring-stack transducer," Journal of the Acoustical Society of America, 86(4), pp. 1602-1603.

[29] Brosnan, K. H., and Messing, G. L., 2009, "Comparison of the properties of tonpilz transducers fabricated with ¡001¿ fiber-textured lead magnesium niobate-lead titanate ceramic and single crystals," Journal of the Acoustical Society of America, 126(5), pp. 2257-2265.

[30] Yao, Q., and Bjørnø, L., 1997, "Broadband Tonpilz Underwater Acoustic Transducers Based on Multimode Optimization," IEEE Transactions on Ultrasonics, Ferroelectrics, and Frequency Control, 44(5), pp. 1060-1066.

[31] Xiping, H., and Jing, H., 2009, "Study on the broadband tonpilz transducer with a single hole," Ultrasonics, 49, pp. 419-423.

[32] Desilets, C., Wojcik, G., Nikodym, L., and Masterton, K., 1999, "Analyses and Measurements of Acoustically Matched, Air-Coupled Tonpilz Transducers," IEEE Ultrasonics Symposium, pp. 1045-1048.

[33] McCammon, D. F., and Thompson, J. W., 1980, “The design of Tonpilz piezoelectric transducers using nonlinearg oal programmin,” Journal of the Acoustical Society of America, 68(3), pp. 754-757.

[34] Saijyou, K., and Okuyama, T., 2011, “Estimation of frequency characteristics of the Tonpilz piezoelectric transducer with a bending piezoelectric disk,” Applied Acoustics, 72, pp. 915-922.

[35] Chhith, S., and Roh, Y., 2009, “Wideband Tonpilz Transducer with a Cavity Inside a Head Mass,” Japanese Journal of Applied Physics, 49, pp. 07HG08-1-5.

[36] Dhilsha, K. R., Markandeyulu, G., Rao, B. V. P. S., and Rao, K. V. S. R., 1997, “Design and fabrication of a low frequency giant magnetostrictive transducer,” Journal of Alloys and Compounds, 258, pp. 53-55.

[37] Chen, Y., and Wu, S., 2002, “A Design Approach of Tonpiltz Transducer,” Japanese Journal of Applied Physics, 41, pp. 3866-3877.

[38] Miller, H. B., 1963, “Origin of the mechanical bias for transducers,” Journal of the Acoustical Society of America, 35, p. 1455.

[39] Bodholt H., 1995, “Pre-stressing a Tonpilz transducer,” Journal of the Acoustical Society of America, 98(2), pp. 1225-1227.

[40] Roh, Y., and Lu, X., 2006, “Design of an underwater Tonpilz transducer with 2-2 mode piezocomposite materials,” Journal of the Acoustical Society of America, 119(6), pp. 3734-3740.

[41] Pei, D. L., and Roh, Y., 2008, “Design of an Underwater Tonpilz Transducer with 1-3 Piezocomposite Materials,” Japanese Journal of Applied Physics, 47(5), pp. 4003-4006.

[42] Hawkins, D. W., and Gough, P. T., 1996, “Multiresonance Design of a Tonpilz Transducer Using the Finite Element Method,” IEEE Transactions on Ultrasonics, Ferroelectrics, and Frequency Control, 43(5), pp. 782-790.

[43] Rajapan, D., 2002, “Performance of a low-frequency, multi-resonant broadband Tonpilz transducer,” Journal of the Acoustical Society of America, 111(4), pp. 1692-1694.

[44] Crombrugge, M. V., and Thompson, J. W., 1985, “Optimization of the transmitting characteristics of a Tonpilz-type transducer by proper choice of impedance matching layers,” Journal of the Acoustical Society of America, 77(2), pp. 747-752.

[45] Kim, J., and Kim, H. S., 2009, “Finite element analysis of piezoelectric underwater transducers for acoustic characteristics,” Journal of Mechanical Science and Technology, 23, pp. 452-460.

[46] Mančić, D. D., and Stančič G. Z., 2009, “New Three-dimensional Matrix Models of the Ultrasonic Sandwich Transducers,” Journal of Sandwich Structures and Materials, 0, pp. 1-18.

[47] Iula, A., Carotenuto, R., and Pappalardo, M., 2002, “An approximated 3-D model of the Langevin transducer and its experimental validation,” Journal of the Acoustical Society of America, 111(6), pp. 2675-2680.

[48] Teng, D., Chen, H., Zhu, N., Zhu, G., and Gou, Y., 2008, "Comparison About Design Methods of Tonpilz Type Transducer," *Global Design to Gain a Competitive Edge*, Springer, pp. 81-89.

[49] Piersol, A. G., and Paez, T. L., 2009, *Harris' Shock and Vibration Handbook*, McGraw-Hill Professional.

[50] Mason, W. P., 1938, *Electromechanical Transducers and Wave Filters*, Van Nostrand, New York.

[51] Krimholtz, R., Leedom, D. A., and Matthaei, G. L., 1970, "New Equivalent Circuits for Elementary Piezoelectric Transducers," Electronic Letters, 6(13), pp. 398-399.

[52] Chubachi, N., and Kamata, H., 1996, "Various Equivalent Circuits for Thickness Mode Piezoelectric Transducers," Electronics and Communications in Japan, Part 2, 79(6), pp. 50-59.

[53] Tilmans, H. A. C., 1996, "Equivalent circuit representation of electromechanical transducers: I. Lumped-parameter systems," Journal of Micromechanics and Microengineering, 6, pp. 157-176.

[54] Wilson, O. B., 1988, *Introduction to Theory and Design of Sonar Transducers*, Peninsula Publishing.

[55] Malecki, I., 1969, *Physical Foundations of Technical Acoustics*, Pergamon Press, Oxford.

[56] Radmanović, M. D., and Mančić, D. D., 2004, *Design and Modelling of the Power Ultrasonic Transducers*, Faculty of Electronics in Nis.

[57] Lin, S., 1994, "The three-dimensional equivalent circuit and the natural frequencies of rectangular piezoelectric ceramic resonators," Journal of the Acoustical Society of America, 96(3), pp. 1620-1626.

[58] Lin, S., 2000, "Analysis of the Equivalent Circuit of Piezoelectric Ceramic Disk Resonators in Coupled Vibration," Journal of Sound and Vibration, 231(2), pp. 277-290.

[59] Lin, S., 2004, "Study on the equivalent circuit and coupled vibration for the longitudinally polarized piezoelectric ceramic hollow cylinders," Journal of Sound and Vibration, 275, pp. 859-875.

[60] Feng F., Shen J., and Deng J., 2006, "A 2D equivalent circuit of piezoelectric ceramic ring for transducer design," Ultrasonics, 44, p. e723-e726.

[61] Iula, A., Carotenuto, R., and Pappalardo, M., 1997, "A 3-D Model of the Classical Langevin Transducer," IEEE Ultrasonics Symposium, pp. 987-990.

[62] Iula, A., Lamberti, N., and Pappalardo, M., 1998, "An Approximated 3-D Model of Cylinder-Shaped Piezoceramic Elements for Transducer Design," IEEE Transactions on Ultrasonics, Ferroelectrics, and Frequency Control, 45(4), pp. 1056-1064.

[63] Mančić, D. D., and Radmanović, M. D., 2002, "Piezoceramic ring loaded on each face: a three-dimensional approach," Electronic Journal Technical Acoustics, 2, pp. 1-7.

[64] Turner, M. J., Clough, R. W., Martin, H. C., and Topp, L. J., 1956, "Stiffness and Deflection Analysis of Complex Structures," Journal of the Aeronautical Sciences, 23, pp. 805-823.

[65] Madenci, E., and Guven, I., 2006, *The Finite Element Method and Applications in Engineering Using ANSYS*, Springer.

[66] Zienkiewicz, O. C., and Taylor, R. L., 2000, *The Finite Element Method Volume 1: The Basis*, Fifth Edition, Butterworth-Heinemann.

[67] Lidwell, W., Holden, K., and Butler, J., 2010, *Universel Principles of Design: 125 ways to enhance usability, influence perception, increase appeal, make better design decisions, and teach through design*, Rockport Publishers.

[68] Hutton D. V., 2004, Fundamentals of Finite Element Analysis, McGraw-Hill, New York.

[69] Qi, W., and Cao, W., 1997, "Finite Element Analysis of Periodic and Random 2-2 Piezocomposite Transducers with Finite Dimensions," IEEE Transactions on Ultrasonics, Ferroelectrics, and Frequency Control, 44(5), pp. 1168-1171.

[70] Kang, K., 2003, "Optimization of structural variables of a flextensional transducer by the statistical multiple regression analysis method," Journal of the Acoustical Society of America, 114(3), pp. 1454-1461.

[71] Decarpigny, J. N., and Debus, J. C., 1985, "In-air analysis of piezoelectric Tonpilz transducers in a wide frequency band using a mixed finite element-plane wave method," Journal of the Acoustical Society of America, 78(5), pp. 1499-1507.

[72] Jalihal, P., Vishveshwar, S., and Prasad, A. M., 2005, "Finite Element Analysis of a Tonpilz Transducer," Advances in Structural Dynamics and Design, pp. 31-37.

[73] Lee, S., Pei, D. L., and Roh, Y., 2006, "Optimal Design of a 1-3 Piezocomposite Tonpilz Transducer by means of the Finite Element Method," IEEE Ultrasonics Symposium, pp. 1521-1524.

[74] Rao, S. S., 2004, *The Finite Element Method in Engineering*, Elsevier Science & Technnology Books.

[75] Bayliss, C., 1998, "Application and Development of Finite Element Techniques for Transducer Design and Analysis," PhD Thesis, The University of Birmingham, Birmingham, UK.

[76] Dunn J. R., 1987, "Some Aspects of Transducer Design by Finite Element Techniques," ed. by Merklinger, H. M., *Progress in Underwater Acoustics*, p. 639-645, Plenum Press.

[77] "Engauge Digitizer," Mitchell, M., Last accessed August 16, 2011, http://digitizer.sourceforge.net/

[78] Butler, J. L., Cipolla, J. R., and Brown, W. D., 1981, "Radiating head flexure and its effect on transducer performance," Journal of the Acoustical Society of America, 70(2), pp. 500-503.

[79] Aarts R. M., and Janssen A. J. E. M., 2003, "Approximation of the Struve function H_1 occurring in impedance calculations," Journal of the Acoustical Society of America, 113(5), pp. 2635-2637.

[80] 2010, *Release 13.0 Documentation for ANSYS*, ANSYS Inc.

APPENDIX A

VALIDATION OF THE ACOUSTIC FIELD IN THE FINITE ELEMENT MODELS

A.1 Definition of Radiation Impedance

Radiation impedance of a vibrating surface can basically be defined as the ratio of the force exerted on the medium from the vibrating surface to the normal velocity of the vibrating surface. In this definition, radiation impedance, being a mechanical concept, may be shown analogous to electrical impedance which is the ratio of voltage to current. Radiation impedance is one of the most important characteristics of acoustic transducers. It is directly related with the near field of the transducer as it is found by multiplication of pressure and velocity over the active surface of the transducer. Radiation resistance is an indication of the power that the transducer can transmit to the medium at a certain velocity. It has critical importance as it affects the efficiency and the effective bandwidth of the transducers. Due to its effect on resonance frequency and bandwidth of a transducer, radiation reactance also has significant importance. The main factors affecting radiation impedance can be listed as the size and shape of the radiating surface, and also the properties of its surroundings [4, 20]. Radiation impedance can be expressed as follows:

$$Z_r = \frac{F}{u} \qquad\qquad Z_r = R_r + jX_r \tag{A.1}$$

where Z_r represents radiation impedance, F represents the force exerted by the vibrating surface to the medium, and u represents the normal velocity of the vibrating surface to the medium. As shown in Equation (A.1), radiation resistance, R_r, is the real part of radiation impedance, whereas radiation reactance, X_r, is the imaginary part.

A.2 Analytical Representation of Radiation Impedance for a Circular Piston in a Rigid Baffle

Different analytical models for radiation impedance are available in the literature for different geometries and boundary conditions. In this section, radiation impedance of a circular piston in a rigid baffle is introduced. In its derivation, pressure across the vibrating surface of the piston is found by integrating infinitesimal contributions due to the motion of the piston over the surface. Then, this integral is divided by the average velocity of the vibratory motion. Therefore, velocity is assumed to be uniform over the entire surface in this analytical model, which certainly is not the case in reality. The formulation is as follows [4]:

$$Z_r = \rho c A \left[\left(1 - \frac{J_1(2ka)}{ka} \right) + j \frac{H_1(2ka)}{ka} \right] \qquad k = \frac{2\pi}{\lambda} = \frac{2\pi f}{c} \tag{A.2}$$

where ρ is the density of the acoustic medium, c is the speed of sound in the acoustic medium, A is the area of the vibrating surface, ka is the Helmholtz number, a is the radius of the vibrating surface, k is the wave number, λ is the wavelength in the acoustic medium, f is the frequency of vibration, J_1 is the Bessel function of first kind of order 1, and H_1 is the Struve function of first kind of order 1. Within this formulation, the Struve function is not commonly found in computer languages nor commercial programs such as MATLAB. Although several accurate approximations are available in the literature for the Struve function, they require different considerations for small and large Helmholtz numbers. Therefore, the following expression, which is applicable for all Helmholtz numbers, by R. M. Aarts [79] is considered while calculating Z_r through Equation (A.2):

$$H_1 \approx \frac{2}{\pi} - J_0(ka) + \left(\frac{16}{\pi} - 5\right)\frac{\sin(ka)}{ka} + \left(12 - \frac{36}{\pi}\right)\frac{1 - \cos(ka)}{(ka)^2} \tag{A.3}$$

where J_0 is the Bessel function of first kind of order 0. The results for radiation resistance and radiation reactance obtained with Equation (A.2) are shown in Figure A.1. The results are normalized in order to obtain unitless values and be independent of acoustic medium properties as well as vibrating surface dimensions. These results can be compared with results obtained from the finite element model introduced in Section A.3 to test the validity of the numerical approach.

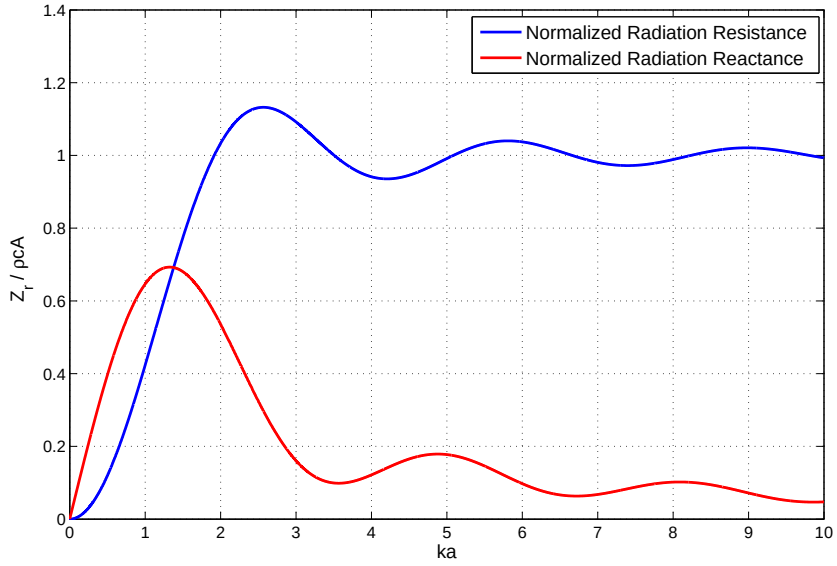

Figure A.1: Analytical results for normalized radiation impedance of a circular piston in a rigid baffle with respect to Helmholtz number

A.3 Numerical Representation of Radiation Impedance for a Circular Piston in a Rigid Baffle

A finite element model consisting of an acoustic medium and a circular vibrating surface is built parametrically in order to calculate the radiation impedance numerically for different conditions. Since the vibrating surface is circular, a 2D axisymmetric model is used to represent the actual 3D case. A geometrical representation of the model is shown in Figure A.2. Vibration of the surface is simulated by introducing a sinusoidal displacement normal to the acoustic medium ranging between $[-\lambda^*/10^6, \lambda^*/10^6]$ for frequencies ranging between $ka = 0$ and $ka = 10$. The model is built with the simulation software ANSYS.

In order to run the finite element model, several constants have to be defined. First, the acoustic medium is assumed to have a density of 1000 kg/m^2 and a sonic speed of 1500 m/s, which are the typical values for water. In the finite element model, parameters such as mesh density and radius of the acoustic medium are defined dependent on frequency. Actually, it is best to define these parameters for every frequency of interest and run the model accordingly. However, this practically means redefining and solving the whole model for each frequency of interest. Instead, it is far less time consuming to define a single model with respect to a certain

reference frequency, and solve it for the whole frequency range of interest. The benefit is significant reduction in the solution time and eliminating possible meshing problems but at the cost of sacrificing some accuracy for frequencies away from the selected reference frequency. This method is also very applicable for analyzing a specific transducer as it is reasonable to select the transducer's resonance frequency as the reference frequency for defining other parameters in the model. The reference frequency, which is used to define the necessary parameters for the model, is selected to be 50 kHz. So, the reference wavelength, λ^*, for the corresponding medium is automatically defined as 30 mm. Also, the diameter of the circular piston has to be known before modeling. It is reasonable to define it with respect to the reference wavelength. Hence, the diameter is selected to be half the reference wavelength, which makes $a = \lambda^*/4$.

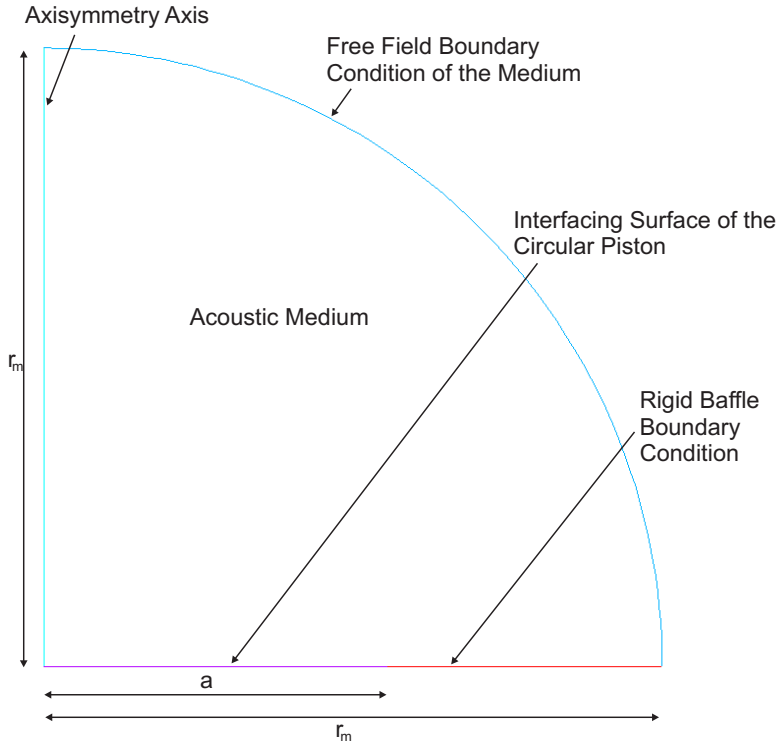

Figure A.2: Geometrical representation of the finite element model build for radiation impedance analysis

The remaining parameters required for the model are the radius of the acoustic medium that can provide a free field boundary condition, r_m, and the maximum distance between two connected nodes in the mesh, x_m. The formulations for these parameters are as follows:

$$r_m = \frac{\lambda}{n_m} + a \tag{A.4}$$

$$x_m = \frac{\lambda}{y} \tag{A.5}$$

where n_m is a constant assumed to be 5 [80], and y is a constant, assumed to be more than 10 [4], referring to the mesh density, as advised in the literature. 2D and 3D views of a sample finite element model built for radiation impedance calculations is shown in Figure A.3. In the figure, elements which are colored light blue are the interface elements. All nodes in the model have a pressure DOF. Nodes located at the horizontal edge of the interface elements also have displacement degrees-of-freedom. Hence, the excitation required for the radiation impedance calculations are implied from these nodes, which actually resemble the surface of the vibrating circular piston as a whole. In ANSYS, FLUID29 and FLUID129 element types are used for the acoustic medium and its free field boundary condition, respectively.

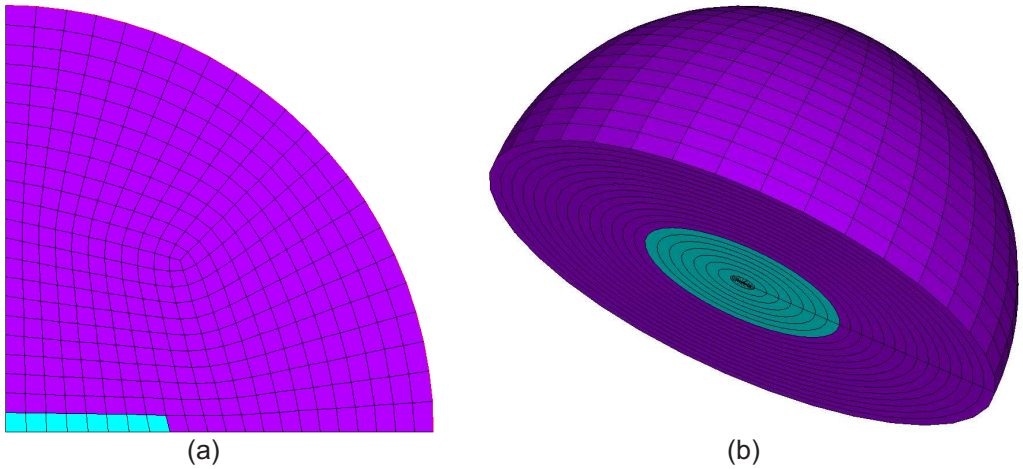

Figure A.3: 2D (a) and 3D (b) views of a sample finite element model which is built for radiation impedance calculations

A harmonic response analysis is conducted to see the steady-state response of the system under harmonic excitation within the frequency band of interest, which covers the range between $ka = 0$ and $ka = 10$. While calculating the radiation resistance and reactance, for each swept frequency steady-state pressure and velocity values of the nodes, which resemble the surface, are modeled through the following formulations [4]:

$$R_r = Re(Z_r) = \frac{1}{uu^*} \int\int Re(pu^*) dS \tag{A.6}$$

$$X_r = Im(Z_r) = \frac{1}{uu^*} \int\int Im(pu^*) dS \tag{A.7}$$

where p is the pressure, u is the velocity and u^* is the complex conjugate of the velocity. Normalized radiation impedance results obtained numerically with $n_m = 5$ and $y = 10$, are shown with the analytical results in Figure A.4.

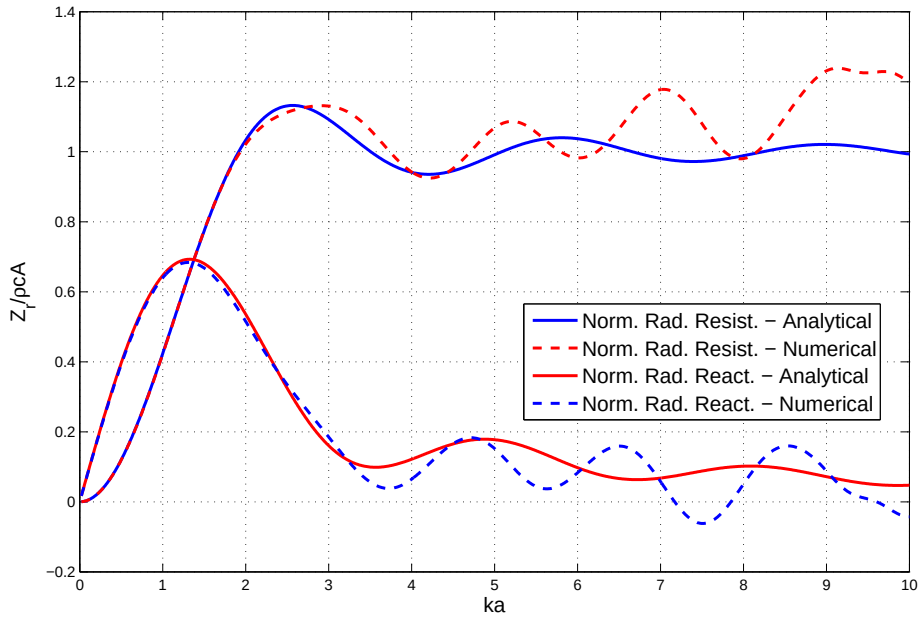

Figure A.4: Analytical and numerical ($n_m = 5$ & $y = 10$) results for normalized radiation resistance and reactance between $ka = 0$ and $ka = 10$

As shown in Figure A.4, the error of the numerical analysis increases periodically with increasing Helmholtz number, ka. However, it should be noted that the parameters in the numerical model are determined with respect to a certain reference frequency, piston radius and acoustic medium. When analyzing a certain transducer, the piston radius and acoustic medium are fixed and one would like to see a transducer's response over a certain frequency range. Therefore, frequency may be considered as the only independent variable while analysing a certain transducer under certain conditions. Typically the frequency range of interest is around the resonance frequency of the transducer. Therefore investigating the response of a transducer only up to a certain frequency, for instance two-times its resonance frequency, is usually sufficient. The whole numerical model is built with respect to $ka = \pi/2$, hence it is reasonable to investigate only the Helmholtz numbers from $ka = 0$ up to $ka = \pi$. The absolute percent error of the numerical results with respect to the analytical results for the mentioned range are shown in Figure A.5.

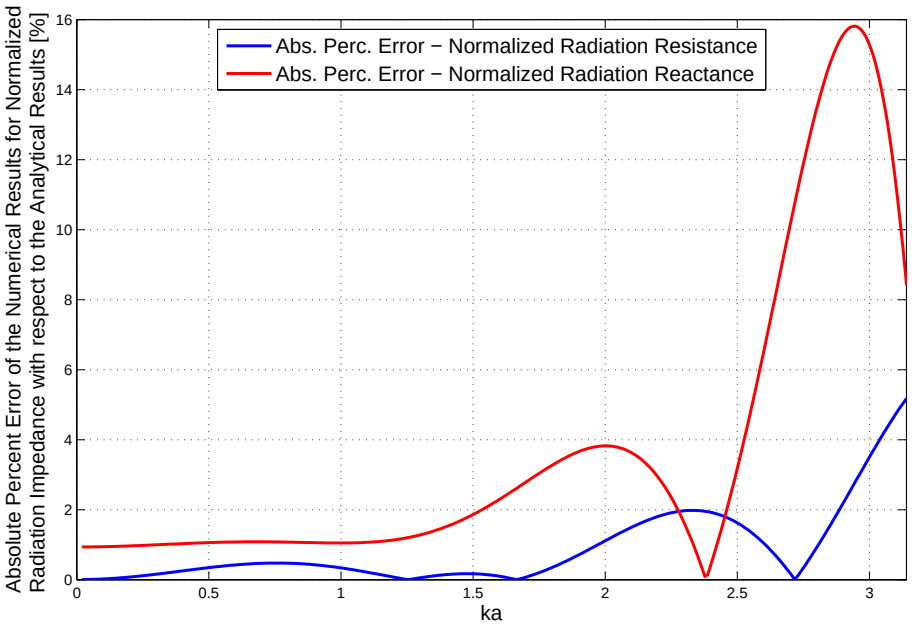

Figure A.5: Absolute percent error of the numerical results for normalized radiation impedance with respect to the analytical results between $ka = 0$ and $ka = \pi$

As can be seen in both Figure A.4 and Figure A.5, the error fluctuates and over certain Helmholtz number ranges increases or decreases are quite sharply. Therefore, in order to quantify the error in the numerical calculations using a single number, the average of the absolute percent error with respect to the analytical results over the interested Helmholtz number range is used. After quantifying the error for each case, a comparison between the cases can be possible. The constants in Equation (A.5) and Equation (A.4), namely n_m and y, are changed to test the accuracy of the finite element model under different conditions. In addition to these changes, two different values of the piston radius, a, which are also dependent on wavelength, are also investigated under several conditions. Average absolute percent errors of radiation resistance, $e_{r.resistance}$, and radiation reactance, $e_{r.reactance}$, are calculated for a total of 24 different cases. Computation times for these cases are also determined. All these results are given in Table A.1. Acoustic medium constants and a reference frequency, which are required to build the numerical model, are kept constant in all the investigated cases. However, the results are applicable for all acoustic mediums and reference frequencies, since they are introduced in unitless forms. However, it should be noted that the error calculations are made over a Helmholtz number range starting from 0 and goes up to two-times the reference Helmholtz number. For instance, the reference Helmholt number equals to π for the cases

where $a = \lambda^*/2$, so only the Helmholtz number range, $ka = [0, 2\pi]$ is considered in the error calculations for these cases. For the sake of showing sample details for the tabulated results, normalized radiation impedance results obtained numerically with $y = 40$, $n_m = 1.25$, and $a = \lambda^*/2$ and the corresponding analytical results are shown in Figure A.6. The improvement in the agreement between the numerical and analytical results is obvious when compared with Figure A.4, but at a cost of the numerical solution being 27 times slower.

Table A.1: Average Absolute Percent Errors and Computation Times of the Numerical Calculations for the Radiation Resistance, $e_{r.resistance}$ and Radiation Reactance, $e_{r.reactance}$ with respect to the Analytical Ones for 24 Different Cases Having a, y, and n_m as Changing Parameters

		$y = 10$	$y = 20$	$y = 30$	$y = 40$	
$e_{r.resistance}$ [%]	$a = \lambda^*/4$	0.877	0.229	0.142	0.101	$n_m = 5$
		0.508	0.185	0.081	0.055	$n_m = 2.5$
		0.764	0.208	0.095	0.055	$n_m = 1.25$
	$a = \lambda^*/2$	0.823	0.331	0.223	0.194	$n_m = 5$
		0.506	0.172	0.107	0.084	$n_m = 2.5$
		0.677	0.173	0.083	0.052	$n_m = 1.25$
$e_{r.reactance}$ [%]	$a = \lambda^*/4$	3.738	0.718	0.357	0.224	$n_m = 5$
		2.132	0.669	0.493	0.388	$n_m = 2.5$
		3.035	0.913	0.545	0.429	$n_m = 1.25$
	$a = \lambda^*/2$	4.544	1.552	0.917	0.763	$n_m = 5$
		4.990	1.517	0.843	0.629	$n_m = 2.5$
		5.055	1.592	0.877	0.616	$n_m = 1.25$
$Comp.Time$ $[s]$	$a = \lambda^*/4$	20.5	33.5	47.9	79.2	$n_m = 5$
		35.3	49.0	100.0	158.4	$n_m = 2.5$
		52.4	179.3	298.4	380.6	$n_m = 1.25$
	$a = \lambda^*/2$	27.6	51.9	128.5	160.1	$n_m = 5$
		33.3	80.0	176.9	298.6	$n_m = 2.5$
		49.7	156.8	332.0	552.6	$n_m = 1.25$

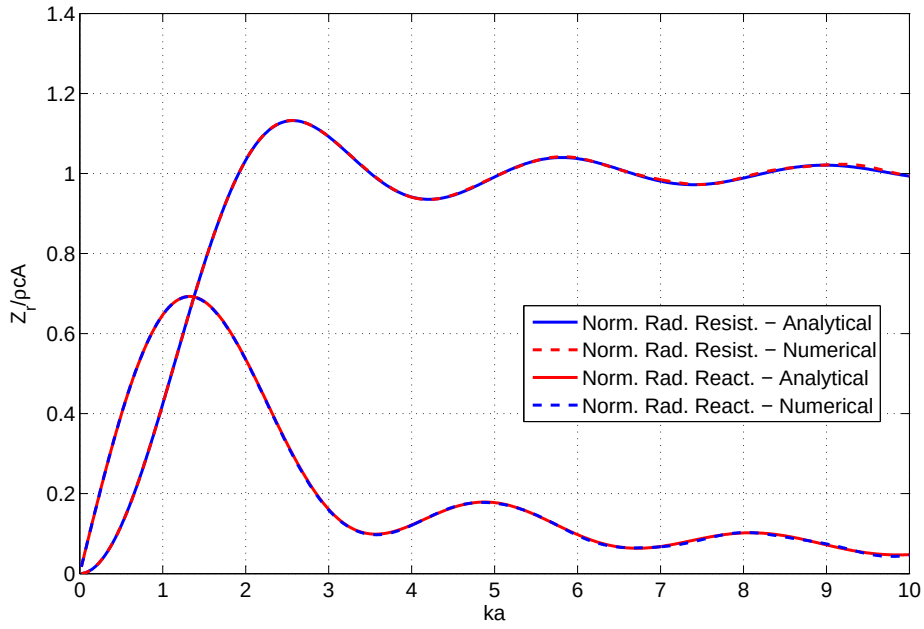

Figure A.6: Analytical and numerical ($n_m = 1.25$ & $y = 40$ & $a = \lambda^*/2$) results for normalized radiation resistance and reactance between $ka = 0$ and $ka = 10$

A.4 Discussions & Conclusion

In this appendix, firstly, the validity of the acoustic field in the finite element models throughout the thesis is verified by comparing radiation impedance results obtained with the numerical approach with the ones obtained analytically under the same conditions. Naturally, the numerical results do not exactly match the analytical results. Therefore, further investigations are made to quantify the accuracy of the numerical results. In order to do that, several parameters important for the finite element representation of the acoustic medium are varied in order to generate different cases, and average absolute percent errors with respect to the analytical results are found and tabulated for each case. Also, economic aspects of the accuracy are considered by presenting the computation times for all the cases. Hence, while modeling a similar acoustic field in a finite element analysis, one may use Table A.1 to define some of the parameters of his/her model in order to achieve a certain accuracy, at least up to an extent.

According to the results shown in Table A.1, an increase in the mesh density, n_m always affects the accuracy in a positive manner. However, the same situation is not true for the radius of the acoustic medium. For instance, for the cases with $a = \lambda^*/4$ and $y = 40$, while the radius of

the acoustic medium increases (n_m decreases), accuracy does not improve, rather it degrades. In general, it may be possible to say that mesh density has a stronger influence on accuracy than radius of the acoustic medium, at least for the investigated, practically reasonable cases. Therefore, instead of increasing the volume of the acoustic medium, one may consider increasing the mesh density for better accuracy. The conflict about n_m may be explained as follows: increasing the acoustic medium volume may strengthen the free field boundary condition but it also leads to more nodes, which increases the accumulated numerical errors in the results.

On the other hand, investigating the cases with different piston radii, a, also has a meaning of investigating the effects of the reference Helmholtz number to the results. In other words, changing the value of a from $\lambda^*/4$ to $\lambda^*/2$ while keeping the reference wavelength constant effectively means changing the reference Helmholtz number from $\pi/2$ to π, which results in doubling the Helmholtz number range considered for the average error calculations. Also, that manipulation can be considered as keeping the radius of the piston as $a = \lambda^*/4$, while doubling/halving the reference frequency/wavelength, which also means doubling the values of y and n_m. The reason to express the difference in terms of the piston radius is to make Table A.1 more user-friendly, as readers who may use it most likely have a transducer with a certain resonance frequency and piston radius. Regardless, in general, similar average errors with similar trends are obtained for different radii of the circular piston, a. Even for the highest difference, the order in the average errors remains the same when the other parameters are kept constant. Lastly, while selecting the parameters for the finite element model, computation times should also be considered. In some cases, a change in a parameter may have a small impact on accuracy, but a large impact on computation time.

APPENDIX B

MATERIAL CONSTANTS USED IN THE MODELS

The material properties presented in the tables below are mainly taken from Bayliss' PhD dissertation [75]. The properties of the materials used in transducer modeling except that for the piezoceramics are shown in Table B.1. The properties of Navy Type I (PZT) piezoceramics used in transducer modeling are shown in Table B.2. Note that several properties in Table B.2 are taken from a different source [4], which also offers the same values for the other properties as in Bayliss' PhD dissertation. In addition to these properties, the density and sonic speed of the water used in the models are taken as 1000 kg/m^3 and 1500 m/s, respectively. Also, the vacuum permittivity, ε_0, is taken as 8.842×10^{-12} C/mV.

Table B.1: The Properties of the Materials Used in Transducer Modeling Except the Piezoceramics [75]

Material	Density $[kg/m^3]$	Young's Modulus $[GPa]$	Poisson's Ratio [–]
Aluminium	2710	68.9	0.30
Mild Steel	7700	195.0	0.28
Stainless Steel	7960	193.0	0.31
Glue	1180	6.5	0.40

Table B.2: The Properties of Navy Type I (PZT-4) Piezoceramics [4, 75]

	s_{11}^E	s_{12}^E	s_{13}^E	s_{33}^E	s_{44}^E	s_{66}^E
$[pm^2/N]$	12.3	-4.05	-5.31	15.5	39.0	32.7
	s_{11}^D	s_{12}^D	s_{13}^D	s_{33}^D	s_{44}^D	s_{66}^D
$[pm^2/N]$	10.9	-5.42	-2.10	7.90	19.3	32.6
	c_{11}^E	c_{12}^E	c_{13}^E	c_{33}^E	c_{44}^E	c_{66}^E
$[GPa]$	13.9	7.78	7.43	11.5	2.56	3.06
	c_{11}^D	c_{12}^D	c_{13}^D	c_{33}^D	c_{44}^D	c_{66}^D
$[GPa]$	145	83.9	60.9	159	51.8	3.07
	$\varepsilon_{11}^T/\varepsilon_0$	$\varepsilon_{11}^S/\varepsilon_0$	$\varepsilon_{33}^T/\varepsilon_0$	$\varepsilon_{33}^S/\varepsilon_0$		
$[-]$	1475	730	1300	635		
	d_{31}	d_{33}	d_{15}			
$[pC/N]$	-123	289	495			
	ρ					
$[kg/m^3]$	7500					

APPENDIX C

PHYSICAL DIMENSIONS OF THE TRANSDUCER USED FOR BENCHMARKING THE MODELS

As stated in Bayliss' PhD dissertation [75], the design of the 50 kHz Tonpilz-type transducer modeled actually belongs to J. R. Dunn [76]. The off-the-shelf transducer, based on Dunn's design, is used by Bayliss in various operational measurements. In the present work, the dimensions of the parts that constitute the transducer are taken from Bayliss' dissertation. Several simplifications for the ease of modeling are also made in the mathematical representation of the actual design. Therefore, the technical drawings presented in this section belong to the finite element model, not the actual transducer.

In addition to the head mass (Figure C.2), the tail mass (Figure C.3), the stud (Figure C.4), the piezoceramic ring (Figure C.5), and the nut (Figure C.6), the glue between the two piezoceramic rings is also modeled. It is modeled as having the same geometry and dimensions as the piezoceramic ring, except the thickness is 0.12mm. A technical drawing of the transducer assembly, which includes all the modeled parts, is shown in (Figure C.1).

For the sake of simplicity, the outer circumference of the nut is modeled as a cylinder with an approximate diameter instead of a hexagon. Also, the threads of both the nut and the stud are not modeled.

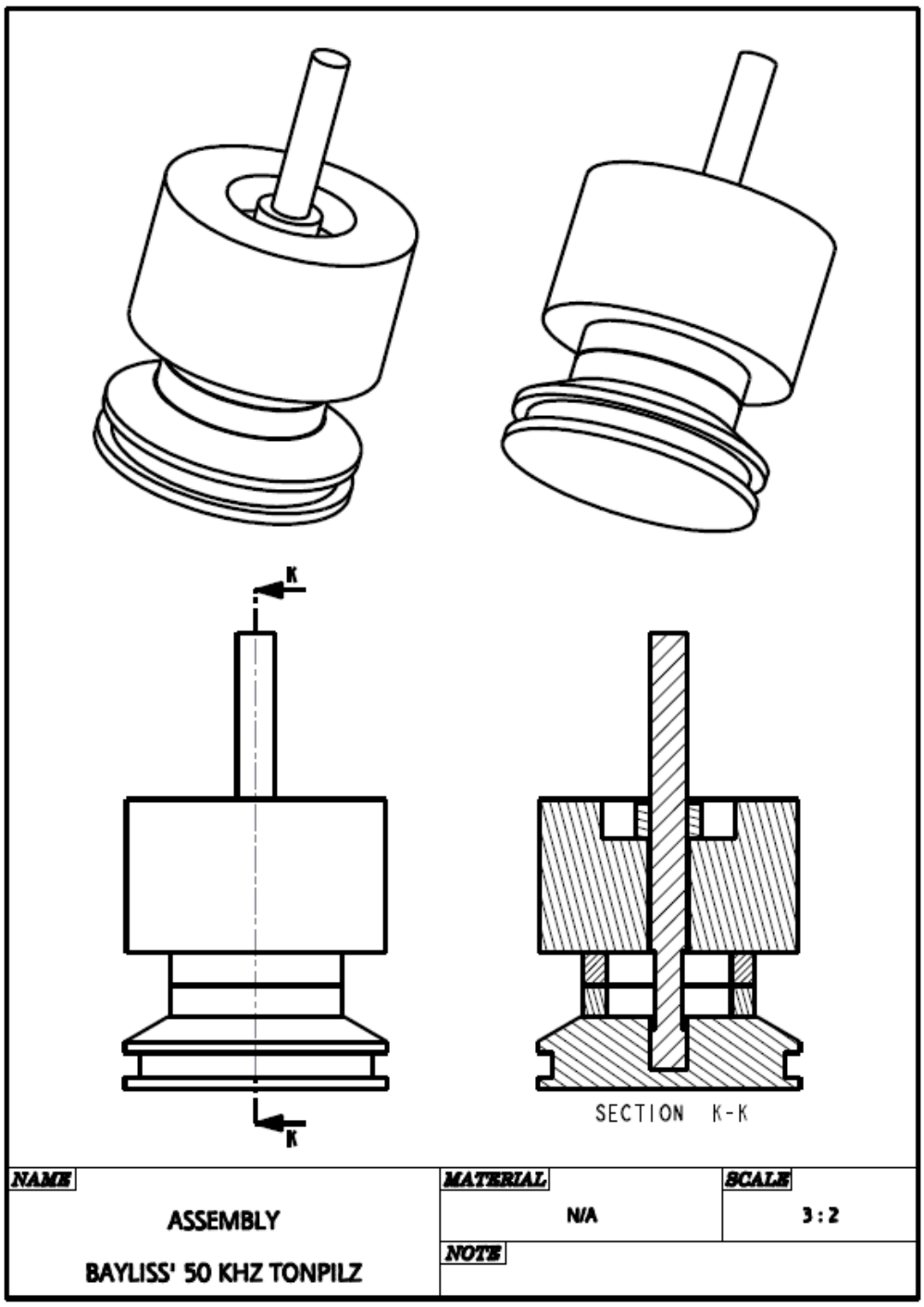

Figure C.1: Technical drawing of Bayliss' 50 kHz Tonpilz's assembly (Adapted from [75])

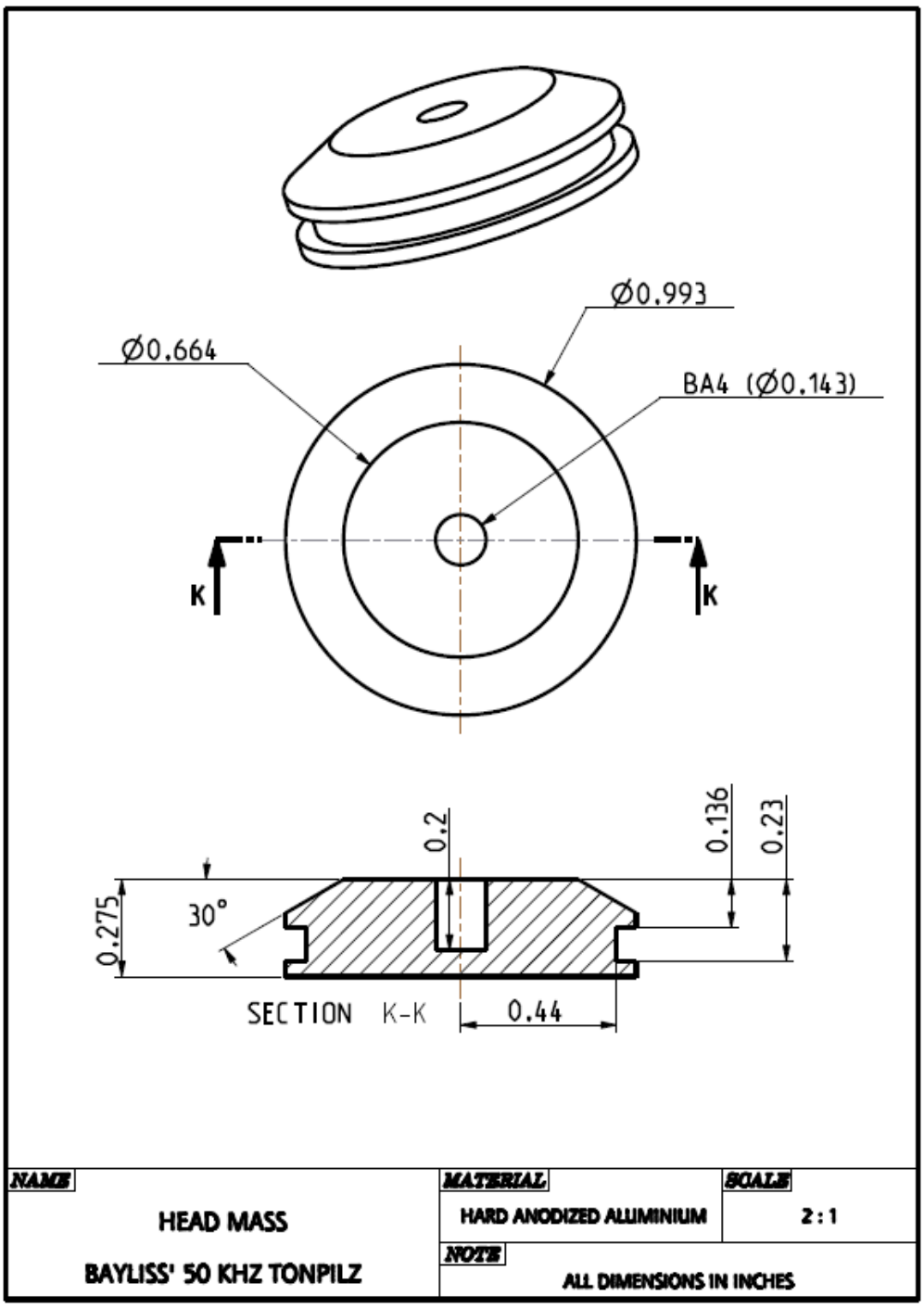

Figure C.2: Technical drawing of Bayliss' 50 kHz Tonpilz's head mass (Adapted from [75])

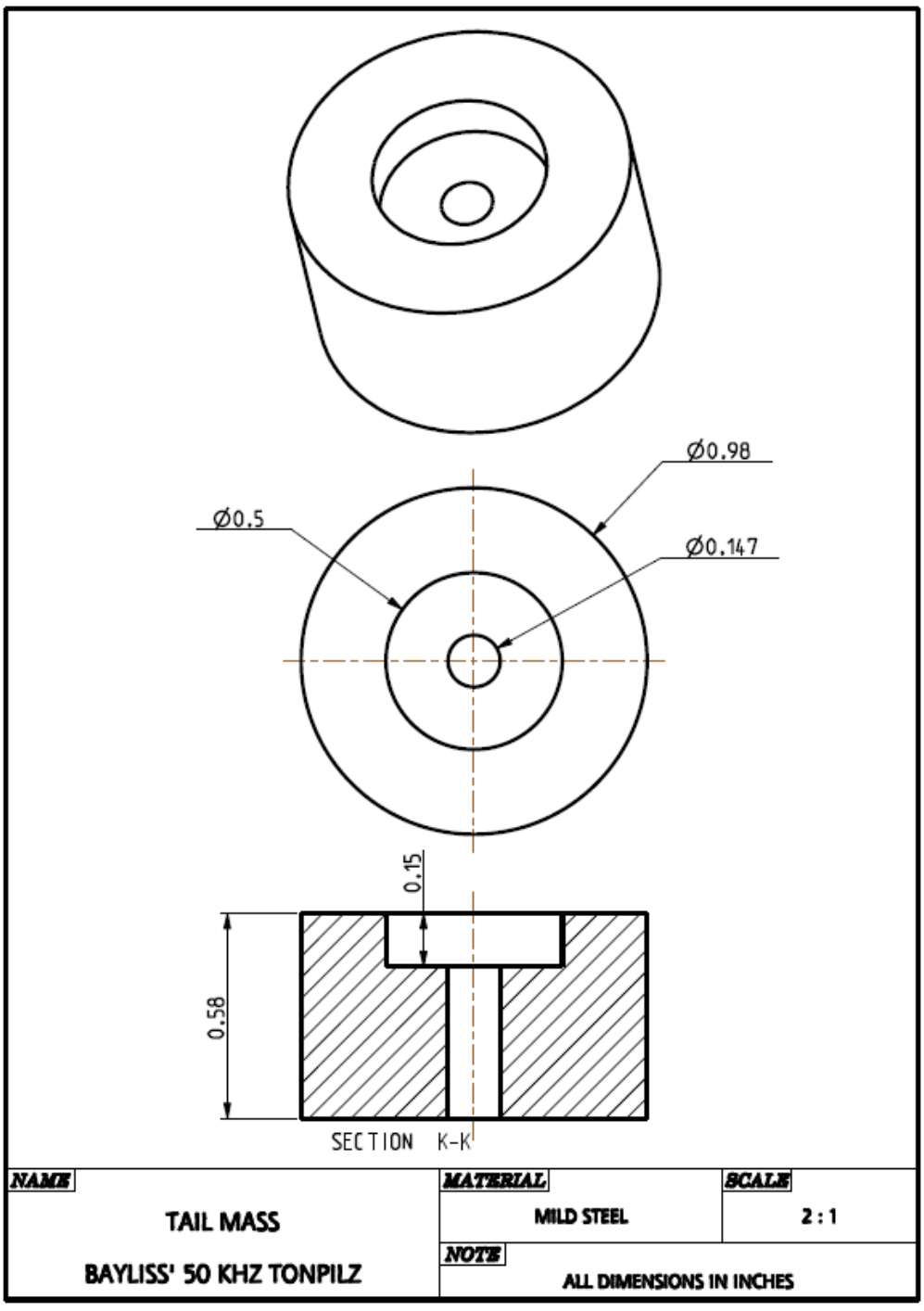

Figure C.3: Technical drawing of Bayliss' 50 kHz Tonpilz's tail mass (Adapted from [75])

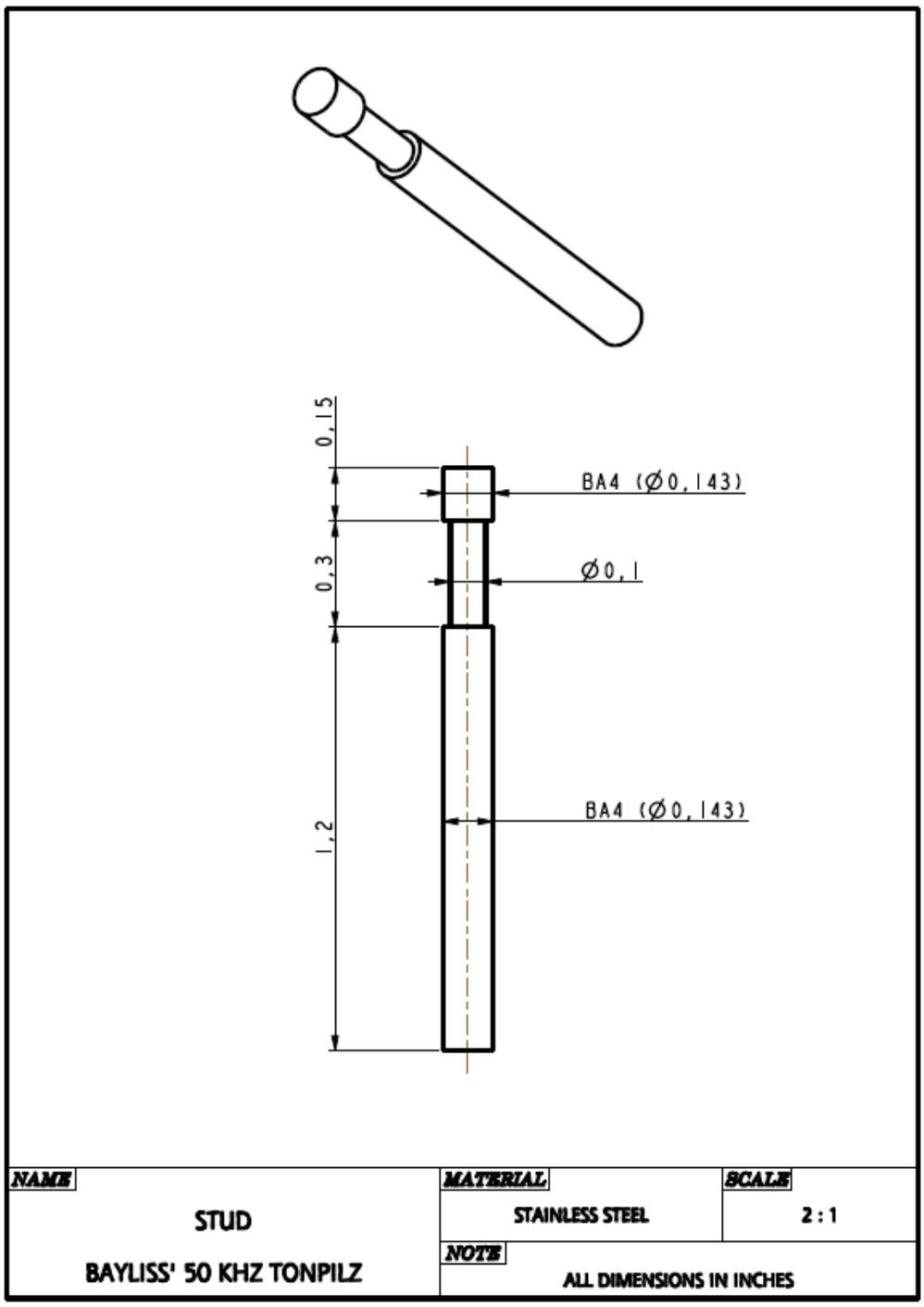

Figure C.4: Technical drawing of Bayliss' 50 kHz Tonpilz's stud (Adapted from [75])

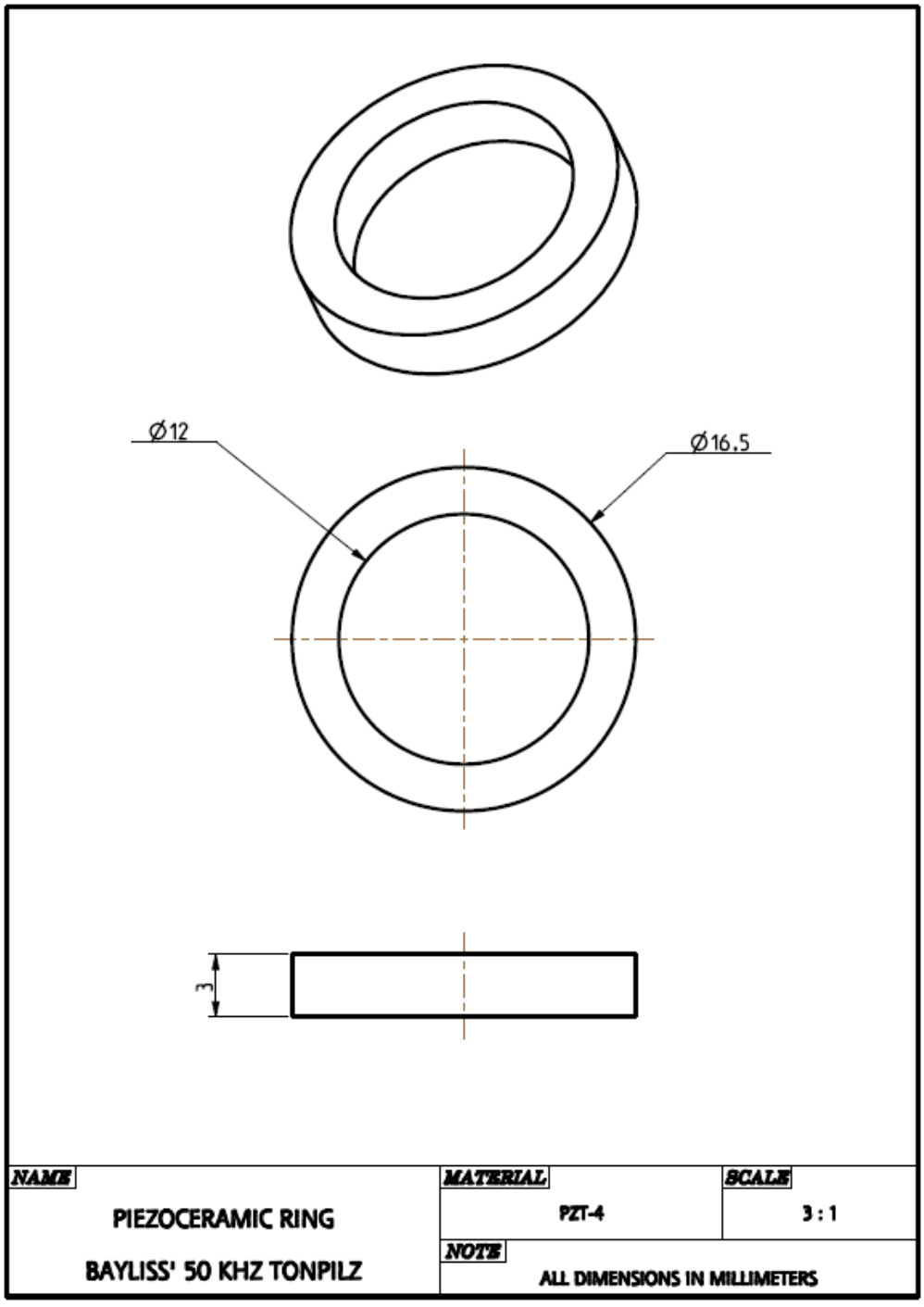

Figure C.5: Technical drawing of Bayliss' 50 kHz Tonpilz's piezoceramic ring (Adapted from [75])

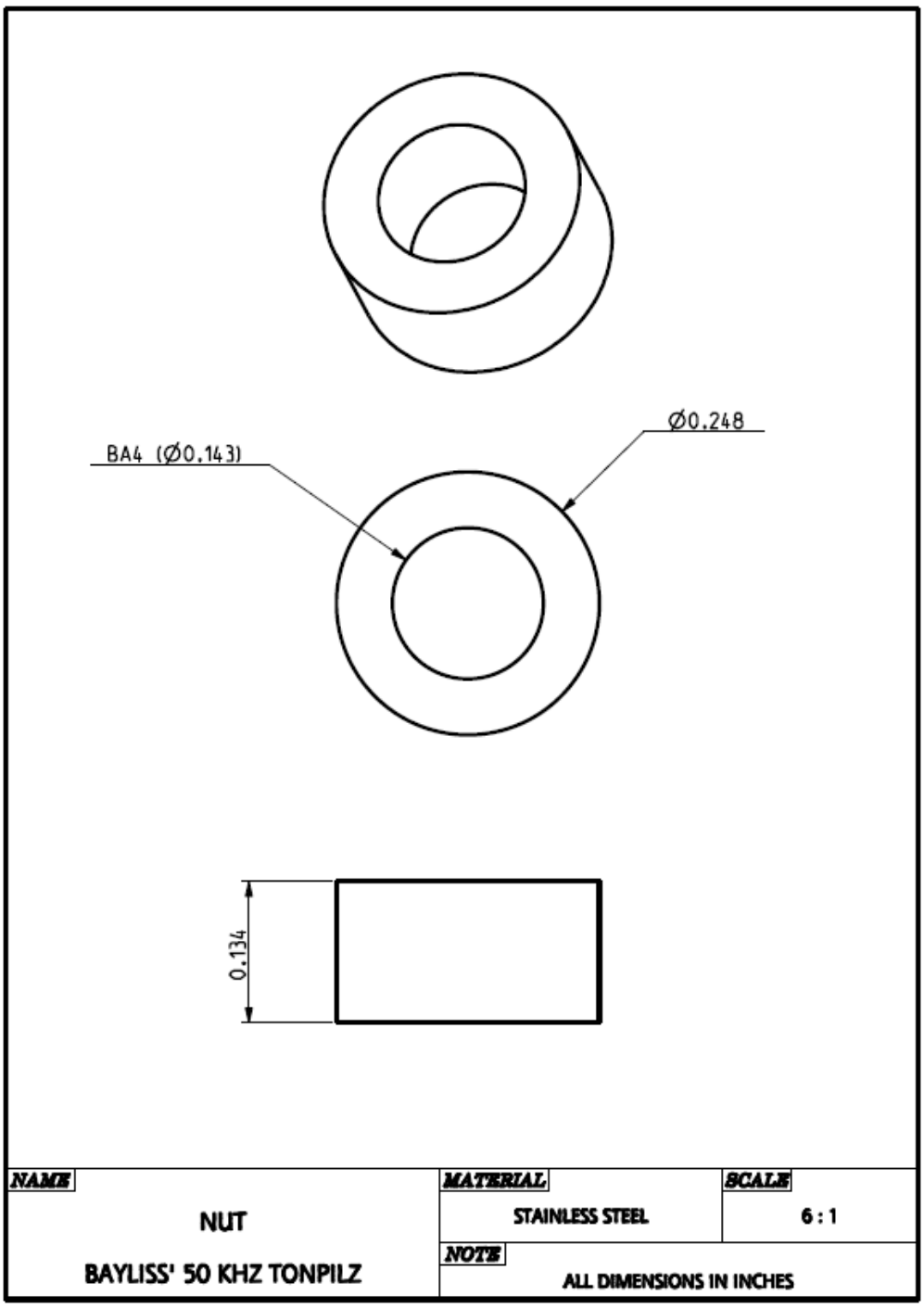

Figure C.6: Technical drawing of Bayliss' 50 kHz Tonpilz's nut (Adapted from [75])